Epigenetic and transcriptional control of the microglial inflammatory response: potential insights into neuro-inflammaging

By

Sandra E Muroy

A dissertation submitted in partial satisfaction of the

requirements for the degree of

Doctor of Philosophy

in

Molecular and Cell Biology

in the

Graduate Division

of the

University of California, Berkeley

Committee in charge:

Professor Kaoru Saijo, Chair
Professor Ellen Robey
Professor Andreas Stahl
Professor David Schaffer

Fall 2019

Abstract

Epigenetic and transcriptional control of the microglial inflammatory response: potential insights into neuro-inflammaging

by

Sandra E Muroy

Doctor of Philosophy in Molecular and Cell Biology

University of California, Berkeley

Professor Kaoru Saijo, Chair

Inflammation is an evolutionarily conserved host defense response during infection or injury that seeks to remove the causal agent that led to its initiation, repair the damaged tissue(s) and restore homeostasis. Thus, transient inflammation in response to an adequate threat with a quick return to a basal resting state is beneficial. However, when inflammation becomes inappropriately increased or prolonged it can have severe pathophysiological consequences.

During aging, the immune system shifts to a proinflammatory state characterized by low-grade, chronic, sterile inflammation that has been termed 'inflammaging'. The proinflammatory state largely results from chronic activation of the innate immune system and includes elevated circulating levels of inflammatory mediators including the immune cell signaling molecules (cytokines) Interleukin (IL)-1, IL-6, IL-8, IL-13, IL-18, tumor necrosis factor (TNFα) and antivirals (the type I interferons (IFN-I). Numerous factors are thought to contribute to inflammaging and amongst potential mechanisms high fat feeding/obesity and associated increases in gut permeability to bacterial endotoxins, as well as, cellular senescence have emerged as key contributors. Importantly, inflammaging is tightly correlated to global indicators of poor health status, multimorbidity, impairment in day-to-day living activities and is thought to underlie or accelerate most age-dependent chronic diseases (e.g. cardiovascular disease, diabetes, cancer, as well as, neurodegenerative conditions like Parkinson's disease (PD) and Alzheimer's disease (AD)).

While mechanisms driving peripheral inflammaging are beginning to be understood, the etiology of neuro-inflammaging is a crucially unresolved issue. An important source of inflammation in the brain are the non-neuronal cell populations (glia) which provide structural, trophic, and other physiological support for neurons, and especially, the activity of microglia–the brain's own resident innate immune cells. Microglia are essential for brain development, maintenance and protection throughout

the life of an organism. As innate immune cells, however, they can also mount a full inflammatory response to infection or environmental challenge to restore brain health.

Environmental factors, for example, changes in peripheral levels of fatty acids, bacterial endotoxins or proinflammatory mediators resulting from high fat feeding or gut permeabilization can cause microglia to undergo changes that signal activation. Most importantly, microglia lose their homeostatic function during aging, becoming less neuroprotective and increasingly neurotoxic. Microglia-mediated inflammation, for example, is strongly linked to age-induced cognitive impairment, is a common hallmark of both PD and AD, and is believed to be mechanistically important in driving pathogenesis. Thus, there is great interest in discovering factors that regulate age-related changes in microglial inflammatory function.

Although inflammation is a complex and multicomponent response, a key point of its control occurs at the level of gene transcription and involves several classes of transcription factors, transcriptional co-regulators and chromatin modifications. A recent 2017 study by Soreq et al., identified a relatively unknown gene, PHD finger protein 15 (*PHF15*) as one of the top 25 differentially expressed genes in microglia during non-pathological aging in humans, with *PHF15* levels increasing with age. Sequence and structural similarity to other members of the PHF family suggest that PHF15 might function as a putative chromatin-mediated gene regulator.

I first sought to determine whether PHF15 could repress inflammatory function in microglia. If so, I wanted to investigate whether factors known to be causal in inflammaging (e.g. high fat feeding/obesity or cellular senescence) lead to age-dependent cognitive impairment via modulation of microglial PHF15. A major hallmark of senescent cells is the secretion of inflammatory mediators including various cytokines (IL-6, IL-1β, IL-8), chemoattractant cytokines (chemokines; for example C-X-C motif chemokine 10 (CXCL10), C-C motif chemokine ligand (CCL-) 5 (CCL5) and CCL20), antivirals (IFN-I), growth factors and extracellular matrix proteases termed the senescence-associated secretory phenotype (SASP). Secretion of the SASP is partially controlled by the Cyclic GMP-AMP (cGAMP) synthase (cGAS)-Stimulator of interferon genes (STING) (cGAS-STING) cytosolic DNA sensing pathway at the molecular level. Thus, peripheral changes induced by high fat feeding/obesity or the SASP could lead to increased neuroinflammation via inhibition of microglial PHF15.

I show that *Phf15* significantly represses proinflammatory gene expression in mouse microglia, modulating both the magnitude and duration of the inflammatory response. Importantly, *Phf15* regulates both basal expression and signal-dependent upregulation of proinflammatory genes—which constitute different phases of the transcriptional inflammatory response and are controlled by distinct molecular mechanisms. Global transcriptional changes after *Phf15* knockout in a microglial cell line further revealed that *Phf15* may specifically regulate the antiviral response, as well as, proinflammatory factor production and secretion. Interestingly, loss of *Phf15* resulted in increased IFN-I-dependent and inflammatory gene expression profiles that closely mimic transcriptional changes in aged microglia. Together, my data indicate that *Phf15* is an important novel repressor of microglial inflammatory function which might counteract age-induced inflammation in the healthy, aging brain.

Interestingly, I found decreased expression levels of *Il-6*, a key proinflammatory cytokine expressed by senescent cells in the hippocampus–an area which mediates various memory-related process–of aged (27-month old) STING-deficient mice. However, this decrease did not translate to improved working memory or differences in *Phf15* mRNA expression in the brain, suggesting that expression of SASP-related inflammatory factors by the cGAS-STING pathway does not proceed via inhibition of *Phf15*. Similarly, prolonged treatment with a high fat diet/obesity did not affect working memory or levels of *Phf15* in the mouse brain, suggesting that brain inflammation resulting from a HFD or obesity is likewise not a result of *Phf15* downregulation.

Overall, my results suggest that *Phf15* could function as an immune regulatory checkpoint, restraining the transition from a homeostatic phenotype towards the chronic, proinflammatory, IFN-I responsive state seen in microglia in the aged brain. Further understanding of its exact mechanism of action could lend insight into possible future therapeutic intervention.

Dedication

In pursuit of higher education, a journey that took much longer than I imagined when I first set out, I have been separated from my family and those important to me, twice now. Each time with uncertainty and sadness as to when I might be able to see them again. I wish to dedicate this to them and to my friends and allies on this journey.

To Maya and Valentina, my two bright little stars. You will shine with your own light.
To my best friend, my *sine qua non* (without which it could not be) Dushka Hernández who has been there with me through everything. *Every step of the way*.
To my brother from another mother, Matthew Goff, thank you for letting me be a part of the pack and taking care of my 3 girls.
To my parents, Elvira and Rafael Muroy, who never gave up. In anything.
To my brother, Rafael Muroy, I hope to one day be as helpful and reliable as you.
To my sister, Romy Muroy, you've had your own tough struggle and are coming out on top.
To my aunts, Makío, Mamali, Matami, Muy and Tía Juany, thank you for being my second mothers.
To my grandmother Tita, you were denied an education past elementary school but made absolutely sure that your daughters were able to have it.
To my dear friend Jane Reynolds, thank you for being a part of my family and for making us feel safe and loved.
To my friend and mentor, Daniela Kaufer, you are such a source of comfort and joy.
To my current mentor, Kaoru Saijo, this would absolutely not have been possible without you.
To my allies, Abby Rincón, Oscar Dubón, Liliana Iglesias, Meng So, Father Rigo Calocarivas and the Multicultural Institute, thank you for having my back.
To my UndocuGrads, not explicitly named to protect their identities, thank you for walking this road by my side.
And to all those who face the fight in pursuit of the dream of higher education

This is for you.

Table of Contents

Acknowledgements

This work was supported by the Berkeley Fellowship for Graduate Study. I would like to thank Hector Nolla and Alma Valeros of the Cancer Research Laboratory (LSA Flow Cytometry Facility) for their kind assistance with cell sorting and the UC Berkeley Office of Laboratory Animal Care for animal husbandry support.

Chapter 1: Introduction

Section 1.1: The inflammatory response

Inflammation is an evolutionarily selected defense response of body tissues to harmful stimuli such as infection, injury or damaged cells produced by acute cellular stress [1]. It consists of a complex biological response that involves, at its core, cells of the innate immune system–largely macrophages, monocytes, neutrophils and dendritic cells–the vasculature, and various molecular mediators, for example, cytokines and chemokines which mediate immune cell communication and chemotaxis, respectively. The function of inflammation is to remove the causal agent that led to its initiation, clear out damaged cells and initiate repair of the wounded tissue(s) [2]. Inflammation thus has a beneficial role in health when it is transiently activated, that is, when the inflammatory response is activated quickly in response to adequate threat and resolves to a basal resting state in a timely fashion. However, when inflammation becomes excessive, inappropriate or sustained, it can lead to severe pathophysiological consequences.

Section 1.2: Aging and inflammation

Aging is associated with immune dysregulation which is characterized by high circulating levels of proinflammatory mediators in the absence of adequate immune triggers, as well as, a decreased capacity to effectively mount an inflammatory response when faced with pathogenic and noxious immune challenge [3,4] . The proinflammatory state results largely from a chronic activation of the innate immune system and includes elevated circulating levels of inflammatory mediators including the cytokines Interleukin (IL)-1, IL-1 receptor antagonist protein (IL-1RN), IL-6, IL-8, IL-18, tumor necrosis factor (TNFα) and its receptors (TNF receptor superfamily members 1A and 1B), antivirals (the type I interferons (IFN-I) including IFNα and IFNβ), transforming growth factor β (TGFβ) and serum amyloid A (SSA) [2]. This state of sterile, chronic, low-grade inflammation has been termed ‘inflammaging’ [3] and contributes to the pathogenesis of many age-dependent chronic diseases including diabetes, cardiovascular disease, cancer, osteoporosis, depression, as well as, neurodegenerative conditions like Parkinson’s disease (PD), Alzheimer’s disease (AD) and dementia [2,5–10]. It is also tightly correlated to global indicators of poor health status, for example, multimorbidity, disability in day-to-day living activities, frailty, and premature death [2,11–13].

Section 1.3: Causes of inflammaging

Numerous factors are thought to contribute to inflammaging and potential mechanisms include genetic predisposition, cellular senescence, obesity, increased gut permeability, dysbiosis (changes in composition of the host microbiota), mitochondrial dysfunction, defects in autophagy, immune cell dysregulation, and chronic infections (for review see [2]).

High fat feeding and obesity

One of the most pathologically relevant mechanisms due to its high and increasing prevalence is diet-induced obesity (DIO) [14]. DIO generally results from ingestion of a calorically-rich and high fat diet (HFD) [15] resulting in significantly increased body weight, chronic, low-grade systemic inflammation [16–18], metabolic impairment [18] and cognitive deficits [19,20]. Increased dietary fatty acid (FA) intake, for example, induces immune activation and inflammatory responses in many metabolic organs including adipose tissue, pancreas, liver, muscle, and brain [18,21]. FA's can directly stimulate immune cells and adipocytes by binding to specialized receptors (i.e., Toll-like receptor 4 (TLR4), a sensor for pathogen detection) [22,23] and activate transcription factors like Nuclear factor kappa-light-chain-enhancer of activated B cells (NF-κB) and Activator Protein 1 (AP-1), which upregulate expression of proinflammatory cytokines (e.g. *IL-1β*, *TNFα* and *IL-6*) and other proinflammatory mediators.

Importantly, consumption of a HFD can also lead to increased gut permeability, increasing the concentration of bacterial products, like the endotoxin lipopolysaccharide (LPS), a component of gram-negative bacterial cell walls, in the bloodstream. For example, the HFD itself can aid in solubilizing bacterial products easing their transport into systemic circulation [24–26]. Furthermore, HFD consumption leads to changes in the composition of gut microbiota populations. Reductions of beneficial commensal microbes which control the growth of pathogenic commensals and maintain intestinal barrier integrity via production of mucus and metabolites [27,28] leads to dysbiosis as well as permeabilization of the gut barrier [29] allowing passage of bacterial endotoxins into circulation. Increased levels of LPS in the bloodstream, for example, can then activate inflammatory responses in immune and other cells via direct binding to TLR4.

In the brain, DIO can lead to changes in blood brain barrier (BBB) permeability which can alter brain homeostasis by allowing entry of substances (including pathogens) normally restricted to peripheral circulation. For example, mice fed a HFD (60% kcal from fat) for 14 weeks showed decreased protein levels of tight and adherens junction proteins claudin-5 and occludin [30]. Similarly, 16 weeks of HFD treatment (60% kcal from fat) led to increased Evans Blue dye extravasation, a functional measure of BBB permeability, into the central nervous system (CNS) in mice [31]. Importantly, chronic inflammation resulting from DIO was specifically identified as being linked to impaired cognitive function [32]. For example, in humans, obesity is associated with neuroinflammation and architectural changes in grey and white matter [33–36] Similarly,

increased plasma levels of Il-6 and C-reactive protein (CRP), which are markers of peripheral inflammation, were associated with changes in brain morphology, e.g. decreased hippocampal volume and cortical surface area, as well as, impaired learning and memory [37]. In rodents, a HFD (60% kcal from fat) administered for 20-21 weeks, resulted in deterioration of spatial memory and spatial learning, measured using behavioral assays such as the Y-maze [38], Morris water maze [39,40] and the T-maze [41]. These changes were accompanied by increased levels of *Tnfa*, *Il-6*, the chemoattractant cytokine (chemokine) *Ccl2* and Nitric oxide synthase, inducible (*Nos2*, which synthesizes the reactive nitrogen species NO), as well as, non-neuronal brain cell (glial cell) activation.

In addition to its direct contribution to systemic inflammation, DIO can lead to further metabolic dysfunction and accumulated evidence shows that consuming a HFD induces a low grade but sustained inflammation in macrophages that triggers insulin resistance and is important for the pathogenesis of Type 2 diabetes mellitus (T2DM) [17,18,42]. Importantly, T2DM is associated with cognitive impairment [43,44] and alongside aging, is one of the most critical risk factors for neurodegenerative diseases such as AD [45], which is characterized by progressive cognitive decline and brain inflammation [46,47] (among other hallmarks).

Cellular senescence

A second mechanisms posited to underlie inflammaging that is gaining strong traction is cellular senescence [48], which is characterized by terminal cell cycle arrest of aged or damaged cells [49,50]. Senescent cells display phenotypic changes resulting from altered metabolism, organization of chromatin and transcriptional activity [51]. A major hallmark of senescent cells is the secretion of inflammatory mediators including various cytokines (IL-6, IL-1β, IL-8), chemokines (e.g. CCL5, CCL20, CXCL10), antivirals (IFN-I), growth factors and extracellular matrix proteases termed the senescence-associated secretory phenotype (SASP) [51,52]. The SASP is thought to have evolved as a way for senescent cells to communicate with the immune system in order to drive senescent cell clearance and activate tissue repair via stimulation of progenitor cells [53]. However, chronic exposure to the inflammatory response driven by the SASP is thought to underlie many of the senescence-associated adverse effects on aging-dependent diseases [54,55]. Through the SASP, senescent cells can also transmit senescence to neighboring cells in a paracrine fashion [51].

At the molecular level, an important regulator of SASP gene expression is the Cyclic GMP-AMP (cGAMP) synthase (cGAS)-Stimulator of interferon genes (STING) (cGAS-STING) cytosolic DNA sensing pathway [56]. cGAS-STING is part of the innate immune pattern recognition receptor network and its central function is the secretion of inflammatory and antiviral cytokines and chemokines in response to infection [57,58]. However, the cGAS-STING pathway can also sense endogenous DNA ligands, for example, cytosolic DNA fragments resulting from aging or other stress-induced damage that can trigger its activation [51,59].

Recent studies suggest that senescent cells are detectable in the brain, with senescence likely occurring in glial cells (astrocytes, microglia, oligodendrocytes) which are replication-competent [60,61]. Glial cells, especially microglia and astrocytes, normally provide metabolic, trophic and structural support to neurons but could contribute to sustained neuroinflammatory and neurodegenerative processes via secretion of SASP-related factors including proinflammatory cytokines and matrix metalloproteinases (MMPs) which disrupt cell-cell contacts necessary for structural and functional neuronal-glial and inter-glial interactions that maintain metabolic and ion homeostasis in neurons [62,63]. In the aged brain, chronic inflammation is associated with pathological cellular and tissue changes, for example significant decreases in certain neuronal populations, axonal and dendritic arborizations, number of dendritic spines, synapses and brain volume [64] which result in cognitive impairment, memory loss and loss of motor coordination.

Section 1.4: The role of microglia

While the mechanisms driving peripheral inflammaging are beginning to be understood, the etiology of neuro-inflammaging is a critically unresolved issue. As previously mentioned, an important source of neuroinflammation in the aging brain are the replication-competent glia and especially the activity of microglia, the brain's own specialized resident innate immune cells. Microglia are essential for brain development, protection, maintenance and repair and throughout the life of an organism, carry out a number of routine functions necessary for brain homeostasis including shaping of neuronal circuitry, synaptic pruning, production of trophic factors, and removal of debris and dead cells [65–69]. As immune cells, however, microglia are also capable of mounting a full inflammatory response to infection or environmental challenge [67,70–73]. Microglia express pattern recognition receptors including TLRs to sense environmental changes, such as invasion by pathogens or neuronal damage, and respond by releasing proinflammatory mediators to clear threats and restore brain health [71,73,74].

Environmental factors, for example, changes in peripheral levels of FAs, LPS and cytokines resulting from high fat feeding or gut permeabilization can cause microglia to undergo changes that signal activation, leading to increased expression of proinflammatory factors and reactive oxygen species (ROS) [75] that can damage the surrounding healthy tissue [76]. For example, studies in the mouse microglial cell line BV-2 showed that FA-activated BV-2 cell culture medium was cytotoxic to neurons [77].

Most importantly, microglia lose their homeostatic function during aging and adopt a proinflammatory phenotype, becoming prone to dysfunctional reactions [78]. This microglial aging phenotype is complex, characterized by impairment of their neuroprotective functions and at the same time, increases in their neurotoxic responses [79,80]. For example, aged microglia upregulate specific markers associated with increased antigen presentation [81,82], lysosomal functioning [83,84], and pathogen recognition (including TLR expression) [85] and increase production and release of

proinflammatory cytokines [86–89], changes which are associated with immune reactivity. At the same time, aged microglia become less competent to respond efficiently to immune challenge [90,91].

Importantly, microglial inflammatory activation has been strongly linked to both cognitive deficits and neurodegenerative diseases [79]. Microglia-mediated neuroinflammation, for example, is a common hallmark of both Parkinson's disease and Alzheimer's disease and is believed to be mechanistically important in driving pathogenesis [92–96].

Section 1.5: Transcriptional control of the microglial inflammatory response

Due to their central role in mediating neuroinflammatory processes and their contribution to the pathophysiology of neurodegenerative diseases, there is great interest in discovering factors that regulate age-related changes in microglial function, specifically, repressors of microglial inflammatory output. Although the inflammatory response is a complex and multicomponent process, a crucial control point occurs at the level of gene transcription, and is regulated by several classes of transcription factors, transcriptional co-regulators and chromatin modifications (for review see [97–99]).

A recent study by Soreq et al., [100] which compared transcriptional profiles of different brain cell types and regions throughout healthy human aging found microglial gene expression profiles as being one of the most predictive markers of biological age in the brain. The same study identified a relatively unknown gene, PHD finger protein 15 (*PHF15*) among the top 25 differentially expressed genes in microglia during non-pathological aging, with *PHF15* levels increasing with age. I hypothesized that *PHF15* might function as a chromatin-mediated gene regulator based on several lines of evidence. First, PHF15 (JADE2) is a member of the PHF/JADE family of proteins, which includes PHF17 (JADE1) and PHF16 (JADE3) paralogs. All 3 JADE family proteins bear two mid-molecule PHD-finger domains [101] a motif commonly found in transcriptional co-activators and chromatin remodeling factors (e.g. Autoimmune regulator, AIRE; EP300 or E1A binding protein p300, p300; Creb-binding protein, CBP; and Polycomb-like protein, PCL) [102–105]. Second, a study by Han et al., [106] found that PHF15 associates with Lysine-specific demethylase 1 (LSD1), a key demethylase of histone 3 lysine 4 [107] in mouse embryonic stem cells. LSD1 is a member of the CoREST co-repressor complex (a chromatin remodeling complex) [106,108,109] and is required for transcriptional repression of inflammation in microglia [110]. Third, PHF15 and other PHF family proteins have also been found as members of the Human acetylase binding to ORC1 (HBO1) histone acetyltransferase complex [111,112] –a chromatin modifying complex. An additional member of the HBO1 complex, Inhibitor of growth 4 (ING4) has been shown to negatively regulate the transcription factor NF-κB in immune precursor cells, tying HBO1 complex function to negative regulation of inflammatory signaling [113]. Fourth, PHF17 (JADE1) is a known epigenetic regulator [101] and structural and sequence similarity

between PHF17 and PHF15 led me to believe that this might be the case for PHF15 as well.

Based on its putative function as a chromatin-mediated gene regulator, I sought to determine whether PHF15 might regulate inflammation in microglia, and specifically, whether it might repress aging-related inflammatory gene expression. Given that *PHF15* expression levels increased in the *healthy*, aging human brain [100], putatively it might function as a transcriptional repressor helping to counteract the age-dependent microglial inflammatory phenotype. If so, I hypothesized that factors thought to be causal in inflammaging and linked to cognitive dysfunction might affect brain function via modulation of microglial PHF15. For example, prolonged consumption of a HFD or obesity might lead to decreased levels of PHF15 and increased microglial inflammatory output leading to neuroinflammation and cognitive deficits. Similarly, factors involved in mediating SASP-related inflammatory gene expression, i.e., the cGAS-STING pathway might regulate expression of the SASP via interactions with PHF15..

Chapter 2: *Phf15*—a novel transcriptional repressor regulating inflammation in mouse microglia

Section 2.1: Abstract

Aim: Excessive microglial inflammation has emerged as a key player in mediating the effects of aging and neurodegeneration on brain dysfunction. Thus, there is great interest in discovering transcriptional repressors that can control this process. We aimed to examine whether *PHF15*— one of the top differentially expressed genes in microglia during aging in humans—could regulate transcription of proinflammatory mediators in microglia.

Methods: RT-qPCR was used to assess *Phf15* mRNA expression in mouse brain during aging. Loss-of-function (shRNA-mediated knockdown (KD) and CRISPR/Cas9-mediated knockout (KO) of *Phf15*) and gain-of-function (retroviral overexpression (OE) of murine *Phf15* cDNA) studies in a murine microglial cell line (SIM-A9) followed by immune activation with lipopolysaccharide (LPS) were used to determine the effect of *Phf15* on proinflammatory factor (*Tnfα, Il-1β, Nos2*) mRNA expression. RNA-sequencing was used to determine global transcriptional changes after *Phf15* knockout under basal conditions and after LPS stimulation.

Results: *Phf15* expression increases in mouse brain during aging, similar to humans. KD, KO and OE studies determined that *Phf15* represses mRNA expression levels of proinflammatory mediators such as *Tnfα*, *Il-1β* and *Nos2*. Global transcriptional changes after *Phf15* KO showed that *Phf15* specifically represses genes related to the antiviral (type I interferon) response and cytokine production in microglia.

Conclusion: We provide the first evidence that *Phf15* is an important transcriptional repressor of microglial inflammation, regulating the antiviral response and proinflammatory cytokine production. Importantly, *Phf15* regulates both basal and signal-dependent activation and controls the magnitude and duration of the microglial inflammatory response.

Keywords: *Phf15*, microglia, transcriptional repression, neuroinflammation.

Section 2.2: Introduction

Microglia are the resident myeloid-lineage cells of the brain. They actively provide homeostatic surveillance of the brain parenchyma playing critical roles during development, maintenance and repair throughout the life of an organism. As innate immune cells, however, microglia are also capable of mounting a full inflammatory response to environmental challenge in order to clear threats and restore homeostasis [65,67,70–73]. Microglia express pattern recognition receptors including Toll-like receptors (TLRs) to sense changes in their environment, such as infection by pathogens or endogenous danger signals. They can then respond by releasing proinflammatory mediators such as Tumor necrosis factor alpha (TNFα), Interleukin 1 beta (IL-1β), Interleukin 6 (IL-6), reactive oxygen species (ROS) and reactive nitrogen species (RNS) including nitric oxide (NO) to protect against threats [71,73,74].

Although beneficial when their production is tightly controlled, deregulated or sustained microglial production of inflammatory mediators can lead to collateral damage of surrounding neurons and other cells [73,74,110]. Thus, the transition to an activated state, as well as, timely resolution of the inflammatory response, must be tightly regulated. Increasing evidence suggests that during aging, microglia lose homeostatic function and acquire a proinflammatory phenotype that exacerbates aging-related brain dysfunction [8]. Indeed, aberrant microglia activation has been found in many types of age-related neurodegenerative conditions for example, Parkinson's disease (PD) and Alzheimer's disease (AD) which are marked by inflammatory processes involving glia, and microglia in particular [8,114,115].

Since excessive production of proinflammatory mediators is neurotoxic [110,116–118], various molecular mechanisms exist to regulate transcriptional repression of inflammatory gene expression. For example, basal state repression, that is, before the arrival of an activating signal, is generally carried out via recruitment of co-repressor complexes that prevent initiation of inflammatory gene transcription. After stimulation by an activating signal, additional mechanisms can maintain quiescence by restraining active transcription. Finally, numerous mechanisms mediate the timely resolution of the inflammatory response at the transcriptional level, including transrepression mechanisms that can remove transcription factors from inflammatory gene promoters [97–99,110,119].

Studies have also highlighted an important role for chromatin modifications in the transcriptional control of inflammatory gene expression [120,121]. A recent study by Soreq et al., [100] which compared transcriptional profiles of different brain cell types and regions throughout healthy human aging found microglial gene expression profiles as being one of the most predictive markers of biological age in the brain. The same study identified a relatively unknown gene, PHD finger protein 15 (*PHF15*) among the top 25 differentially expressed genes in microglia during aging. Work in embryonic stem cells, and

sequence and structural similarity to other members of the PHF family, indicate that PHF15 is a putative chromatin-mediated gene regulator [106].

Given that aging skews microglia towards a proinflammatory phenotype, and that *PHF15* was found to be highly upregulated during non-pathological aging, we sought to determine whether *Phf15* might regulate microglial inflammatory function. We found that *Phf15* strongly represses proinflammatory gene expression, regulating both basal and signal-dependent activation and modulating the magnitude and duration of the mouse microglial inflammatory response. Importantly, *Phf15* seems to regulate proinflammatory and Interferon type I (IFN-I)-dependent gene expression. Increased IFN-I tone and proinflammatory cytokine expression are both hallmarks of the aging brain [122–125]. Our findings suggest that *Phf15* is an important novel repressor of microglial inflammatory function that might work to counteract age-induced inflammation in the healthy, aging brain.

Section 2.3: Results

Aging increases *Phf15* expression in mouse brain.

To investigate whether *Phf15* increases in mouse brains similar to humans [100], we measured *Phf15* mRNA expression in mouse frontal cortical brain areas across age. We were interested in frontal cortical regions because of their involvement in mediating various aspects of cognitive function and because they are selectively affected in several aging-related neurodegenerative conditions like PD, AD and frontotemporal dementia (FTD) [126,127].

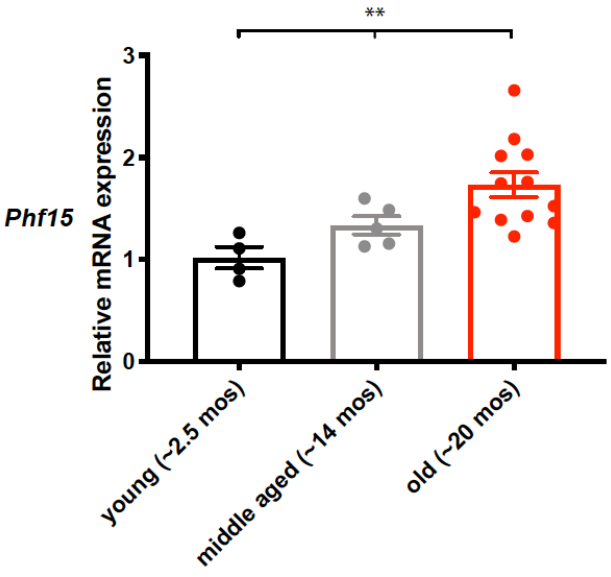

Figure 2.1. *Phf15* expression increases in aged mouse frontal cortical areas. *Phf15* expression was significantly elevated in frontal cortical areas of old (~20-month-old; red bar)

mice compared to young (~2.5 month old; black bar) mice. Data are mean ± SEM (n = 4 young, n = 5 middle aged, n = 12 old). One-way ANOVA with Tukey's post hoc comparisons between age groups: $^{**}p<0.01$.

We found that compared to young (~2.5-month-old) mice, old (~20-month-old) mice had significantly elevated *Phf15* mRNA levels in frontal cortical areas (Figure 2.1). Middle-aged (~14-month-old) mice showed a trend towards increased *Phf15* mRNA expression that did not reach statistical significance. Our data suggest that *Phf15* expression increases in mouse frontal cortical regions upon normal aging, similar to what was previously reported in humans [100].

Knockdown of *Phf15* increases the magnitude of the microglial inflammatory response.

To determine whether *Phf15* regulates microglial inflammatory function, we performed loss-of function studies via shRNA-mediated knockdown (KD) in a murine microglial cell line, SIM-A9, followed by immune activation with lipopolysaccharide (LPS), a component of gram-negative bacterial cell walls and Toll-like receptor 4 (TLR4) agonist. We chose LPS because 1) Intraperitoneal and/or intracranial administration of LPS in mice led to increased microglial activation, neuroinflammation, neuronal loss including loss of dopaminergic neurons in the substantia nigra in a mouse model of PD [110], as well as, cognitive and neurological deficits [128], 2) Aged individuals show increased systemic levels of LPS in the bloodstream [129] which are associated with increased inflammation and microglial activation [130] and 3) In humans, TLR4 activation is linked to age-related pathologies like PD and AD [131–133]. Thus, LPS serves as a relevant aging-related physiological immune stimulant.

KD of *Phf15* resulted in a significant reduction in *Phf15* mRNA transcript levels of 52% or 60% for cell lines sh*Phf15*-1 or sh*Phf15*-2, respectively (Figure 2.2A), as well as, significantly increased mRNA expression of *Tnfα*, a proinflammatory cytokine, after KD with sh*Phf15*-2 at 0, 1, 6 and 12 hours after LPS stimulation (Figure 2.2B). Similarly, mRNA levels of *Nos2*, the enzyme that catalyzes the production of NO, were significantly elevated at 1, 6 and 12 hours post stimulation for sh*Phf15*-2 and 0, 6 and 12 hours for sh*Phf15*-1 (Figure 2.2D). Overall, our experiments show that ~50-60% KD, the equivalent of a "heterozygous" condition, results in increased expression of proinflammatory mediators over a 12 hour time course that resolves and falls below control levels by 24 hours after immune stimulation. Importantly, microglial inflammatory function was elevated in the absence of immune stimulation (0 hour time point, Figures 2.2B, D and No stimulation condition, Figures 2.2C, E), suggesting a loss of repressive mechanisms that inhibit basal state inflammatory gene transcription.

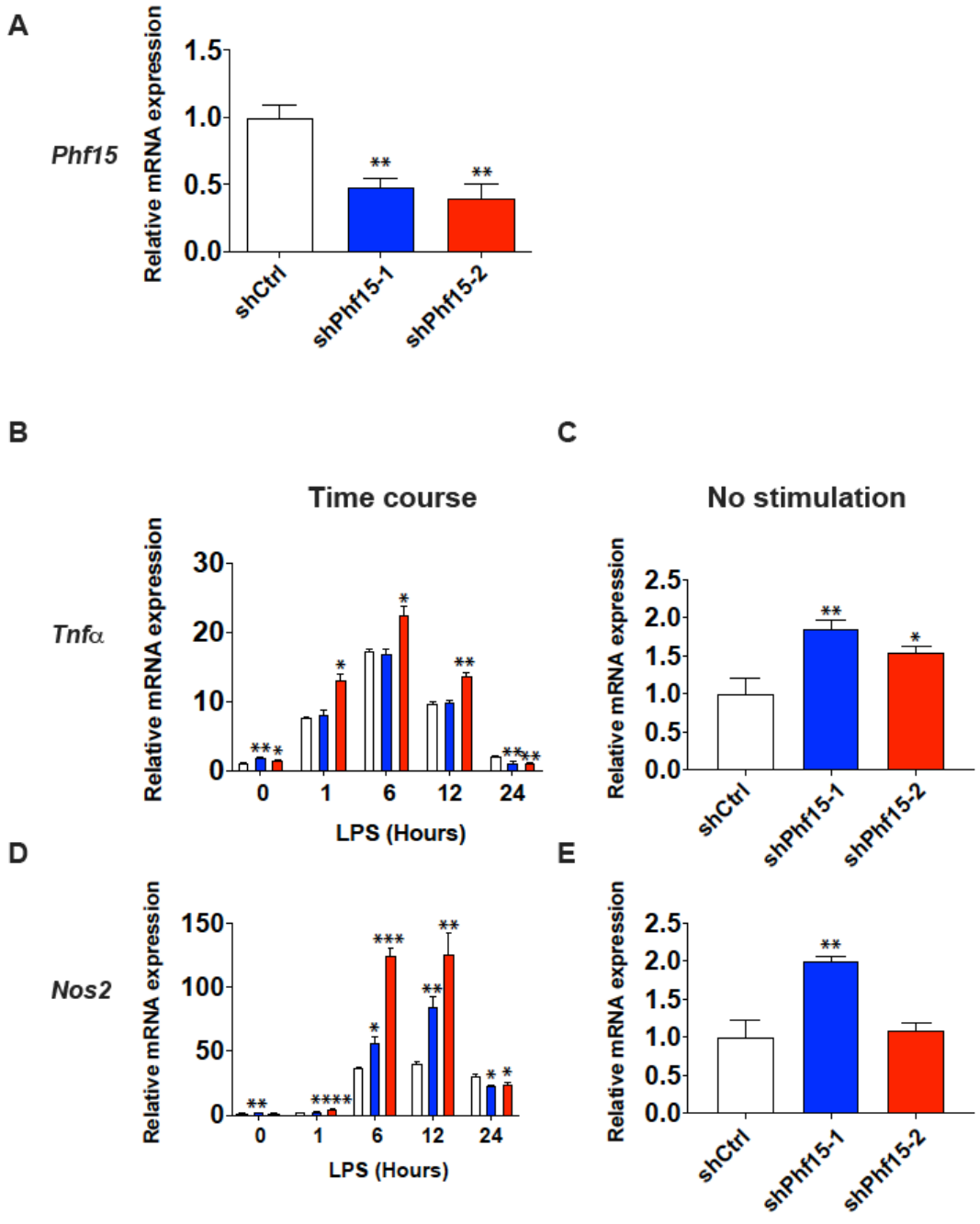

Figure 2.2. Knockdown of *Phf15* increases the magnitude of the microglial response. (**A**) Knockdown efficiency for anti-*Phf15* shRNAs sh*Phf15-1* (blue bar, 52% knockdown) and sh*Phf15-2* (red bar, 60% knockdown) Data are mean ± SEM (n = 3 per condition). Unpaired t-tests between *shPhf15-1* or *shPhf15-2* and shCtrl (control scrambled shRNA) cells: asterisks indicate $^{**}p<0.01$. 24-hour time course experiments showing relative mRNA expression levels of *Tnfα* (**B**) and *Nos2* (**D**) after LPS stimulation of shRNAs sh*Phf15-1* and sh*Phf15-2* compared to shCtrl. "No stimulation" 0 hr time point is shown for *Tnfα* (**C**) and *Nos2* (**E**). Data are mean ± SEM (n = 3 per condition). Unpaired t-tests for *shPhf15-1* or *shPhf15-2* and shCtrl cells for individual timepoints: asterisks indicate

*p<0.05, **p<0.01, ***p<0.001, ****p<0.0001.
LPS, lipopolysaccharide; *Tnfα*, Tumor necrosis factor alpha; *Nos2*, Nitric oxide synthase, inducible.

We repeated the immune activation time course experiments in *Phf15* KD cells using two separate immune stimulants specific to two distinct TLRs to test the pathway specificity of the inflammatory response. CpG Oligodeoxynucleotide (CpG ODN), a synthetic bacterial and viral DNA mimic targets TLR9 and Polyinosinic:polycytidylic acid (Poly(I:C)), a synthetic viral dsRNA mimic targets TLR3. Although TLR4 uses both the Myeloid differentiation primary response 88 (MyD88) and TIR-domain-containing adapter-inducing interferon-*β* (TRIF) downstream adapters to transduce its inflammatory cascade, TLR9 and TLR3 utilize MyD88 *or* TRIF respectively (Supplementary Figure 2.1) [134,135].

Immune stimulation with CpG ODN and Poly(I:C) both yielded similar results to those obtained with LPS stimulation (Supplementary Figures 2.2 and 2.3, respectively) denoting no adapter selectivity and confirming that *Phf15* antagonizes inflammatory gene expression downstream of *both* the MyD88 and TRIF signaling pathways.

Genetic deletion of *Phf15* increases the magnitude *and* prolongs the duration of the microglial inflammatory response.

Since our KD strategy resulted in ~50% reduction in *Phf15* mRNA expression, we next performed CRISPR/Cas9-mediated genetic deletion of *Phf15* in SIM-A9 microglial cells followed by immune activation with LPS. Knockout (KO) of *Phf15* (Figure 2.3A) resulted in significantly increased LPS-induced expression of *Tnfα* (Figure 2.3B), *Il-1β* (Figure 2.3D) and *Nos2*, albeit to a lesser extent (Figure 2.3F) over a 24-hour time course. Importantly, mRNA levels of both *Tnfα* and *Il-1β* remained elevated at 24 hours compared to control cells, denoting a prolonged inflammatory response and failure to return to steady-state. mRNA expression of *Nos2* showed a significant upregulation over 12 hours (0, 1 and 12 hour timepoints) but had returned to control levels by 24 hours (Figure 2.3F). Notably, basal expression of all 3 genes was significantly elevated, with a 4-fold increase in *Tnfα,* 14-fold increase in *Il-1β* and 32-fold increase in *Nos2* when comparing KO versus control cells Figures 2.3C, E, G).

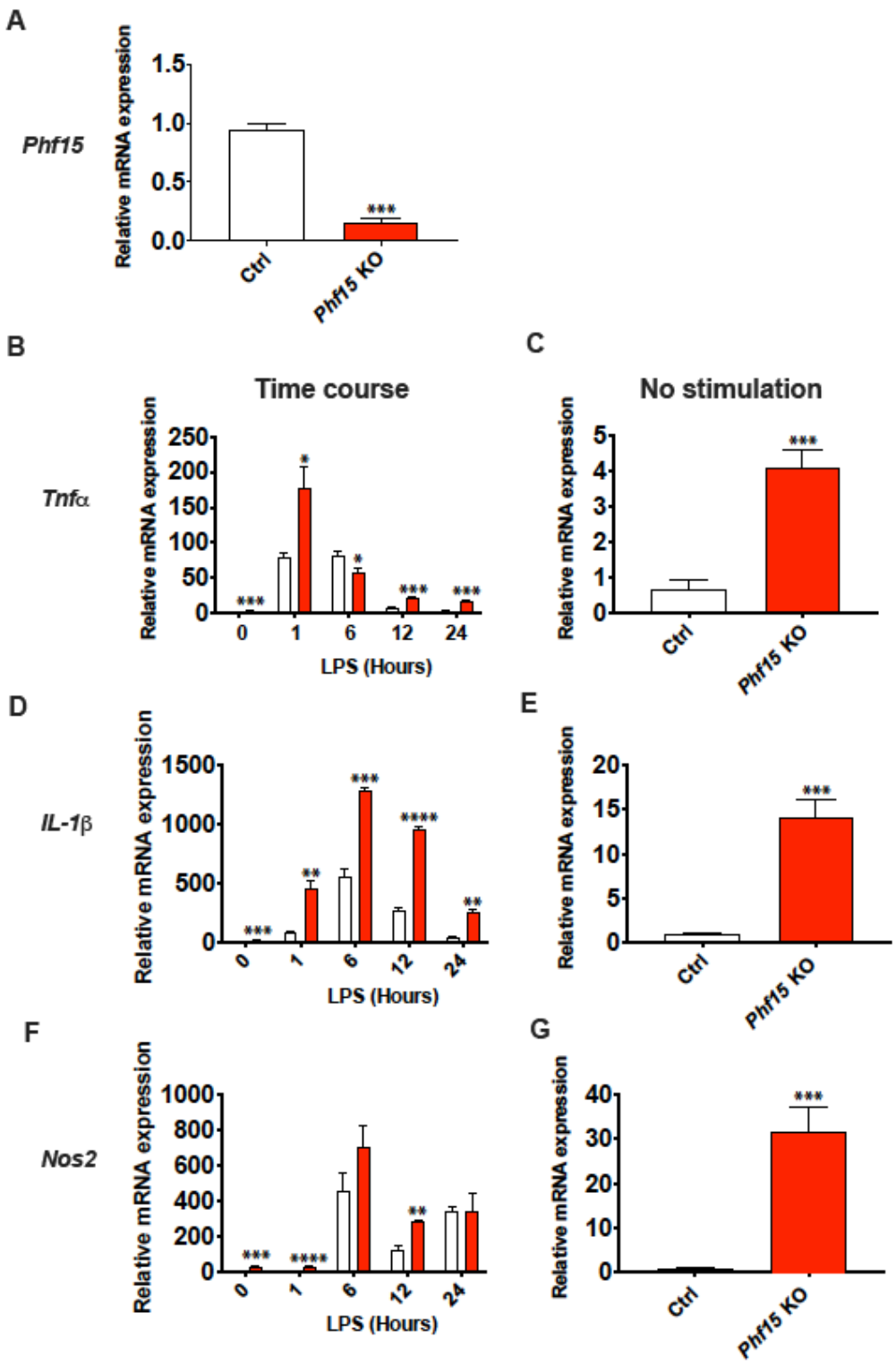

Figure 2.3. Knockout of *Phf15* increases the magnitude and duration of inflammatory expression. (**A**) Percent reduction in *Phf15* transcript expression in *Phf15* knockout SIM-microglia (*Phf15* KO, red bar) compared to control (Ctrl, open bar). 24-hour time course experiments showing relative mRNA expression levels of *Tnfα* (**B**), *Il-1β* (**D**), and *Nos2* (**F**)

after LPS stimulation. No stimulation (0 hr time point or baseline) expression of *Tnfα* (**C**), *Il-1β* (**E**) and *Nos2* (**G**) are also shown. All data are mean ± SEM (n = 3 per condition). Unpaired t-tests between *Phf15* KO and control cells for percent reduction and for individual timepoints: asterisks indicate *p<0.05, **p<0.01, ***p<0.001, ****p<0.0001.
LPS, lipopolysaccharide; *Tnfα*, Tumor necrosis factor alpha; *Il-1β*, Interleukin 1 beta; *Nos2*, Nitric oxide synthase, inducible.

Time course experiments after stimulation of TLR9 with CpG-ODN (Supplementary Figure 2.4) and TLR3 with Poly(I:C) (Supplementary Figure 2.5) in *Phf15* KO cells again yielded similar results to LPS stimulation in *Phf15* KO microglial cells, denoting no difference in downstream adapter selectivity and confirming our prior KD results.

Overall, KO of *Phf15* resulted in a more severe phenotype compared to our KD results, increasing the magnitude and prolonging the duration of the microglial inflammatory response. Taken together, our KD and KO results indicate that *Phf15* functions to restrict microglial inflammatory output, regulating the magnitude and duration, as well as, basal inhibition of the inflammatory response.

Overexpression of *Phf15* in microglia results in a dampened inflammatory response

To further test the role of *Phf15* as a repressor of proinflammatory genes, we carried out gain-of-function studies of *Phf15* in SIM-A9 cells. Overexpression (OE) via retroviral delivery of the full-length murine *Phf15* cDNA (Figure 2.4A) resulted in significantly decreased expression of *Tnfα* at 6 hours (Figure 2.4B), *Il-1β* (0, 6, 12 hours; Figure 2.4D) and *Nos2* (0, 6, 24 hours; Figure 2.4F). Notably, basal levels of both *Il-1β* and *Nos2* were also significantly decreased (Figures 2.4E, G). Time course experiments following stimulation with CpG-ODN (Supplementary Figure 2.6) and Poly(I:C) (Supplementary Figure 2.7) likewise yielded similar results as LPS stimulation of *Phf15* OE microglia, displaying no adapter selectivity.

Taken together, our OE results show a dampened microglial inflammatory response, revealing a reciprocal response phenotype compared to our KD and KO experiments. Collectively these results confirm that *Phf15* functions to repress both basal and stimulus-dependent inflammatory gene expressions in microglia.

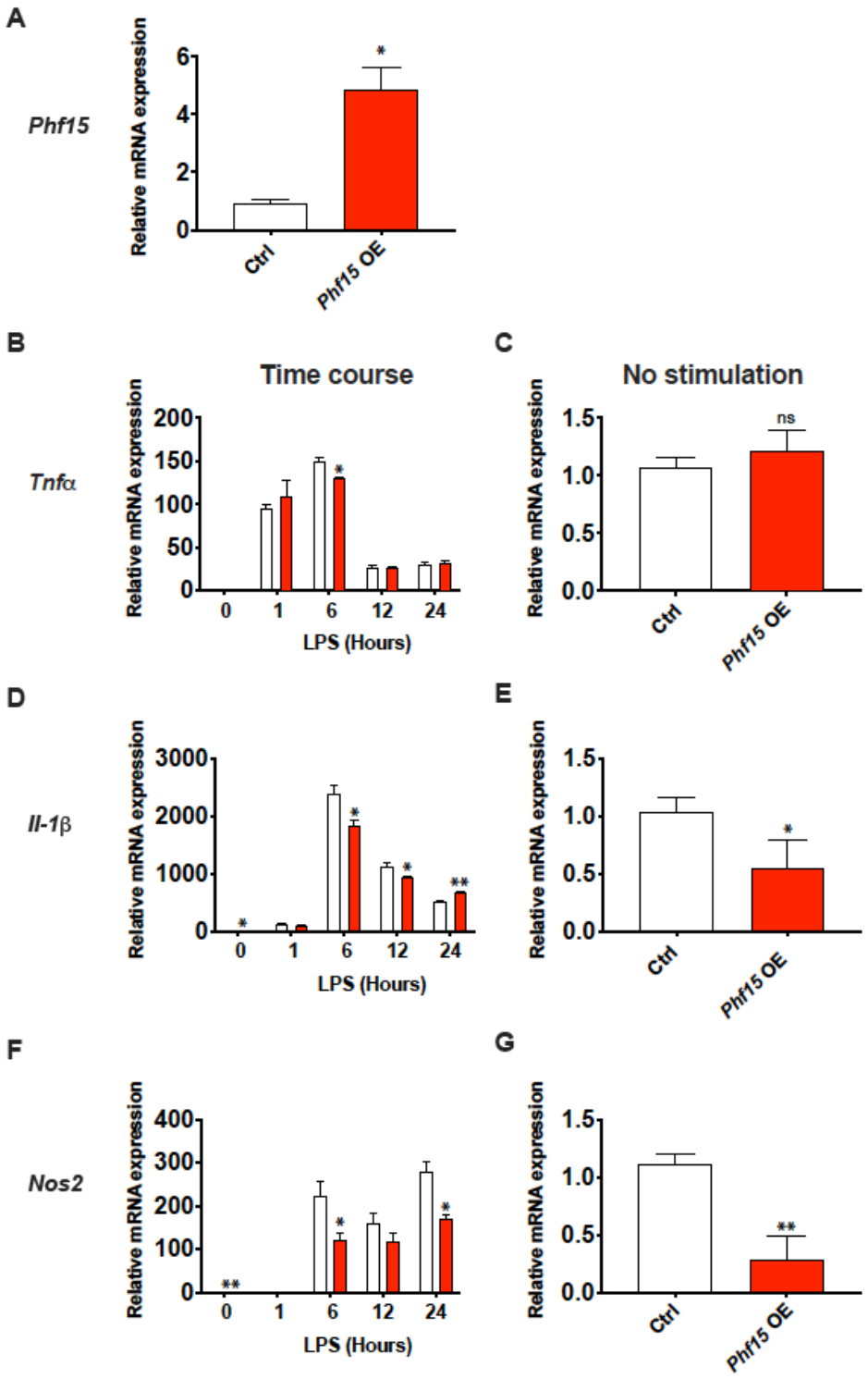

Figure 2.4. *Phf15* overexpression decreases the microglial inflammatory response. overexpression (OE) of *Phf15* in SIM-A9 microglia (red bar) versus control cells (Ctrl, open bar). 24-hour time course experiments showing relative mRNA expression levels of *Tnfa* (**B**), *Il-1β* (**D**), and *Nos2* (**F**) after LPS stimulation. Baseline (0 hour time point, No

stimulation) expression of *Tnfα* (**C**), *Il-1β* (**E**), and *Nos2* (**G**) are displayed separately from time course experiments. All data are mean ± SEM (n = 3 per condition). Unpaired t-tests between *Phf15* OE and control cells for fold-overexpression and for individual time points: asterisks indicate *p<0.05, **p<0.01.
LPS, lipopolysaccharide; *Tnfα*, Tumor necrosis factor alpha; *Il-1β*, Interleukin 1 beta; *Nos2*, Nitric oxide synthase, inducible.

Loss of *Phf15* affects global expression of genes involved in antiviral responses and regulation of inflammatory processes

To examine global transcriptional changes as a result of *Phf15* deletion in microglia, we carried out RNA-sequencing (RNA-seq) on *Phf15* KO SIM-A9 cells under no stimulation conditions and 6 hours post LPS stimulation. We chose to examine the no stimulation condition (0 hour time point) based on our KD and KO time course results which showed that baseline is one of the most consistently and strongly deregulated time points. Importantly, elevated or 'leaky' proinflammatory mediator expression at baseline might result in chronic inflammation leading to neurodegeneration. Similarly, 6 hours after LPS stimulation corresponded to the peak of the transcriptional inflammatory response, with large increases in magnitude for both *Il-1β* and *Nos2*.

Differential gene expression analysis revealed that 466 genes with log2 fold change > 1.5 and *p adj* < 0.01 were up-regulated and 309 genes with log2 fold change < -1.5 and *p adj* < 0.05 were downregulated (Figure 2.5A). Biological theme enrichment analysis using Metascape [136] on the upregulated genes revealed that the most enriched biological process categories under basal conditions were "response to virus" and "cytokine production" (Figure 2.5B, C). Under the "response to virus" category, there was significant upregulation of various interferon-stimulated genes (ISGs), for example *Ifit1*, *Ifit3*, *Irf7*, *Isg15*, *Oas2* and *Oasl2* (Figure 2.5C). The downregulated genes show more variability in the types of pathways affected, largely involving growth, differentiation and glial cell migration processes (Figure 2.5A and Supplementary Figure 2.8A).

A

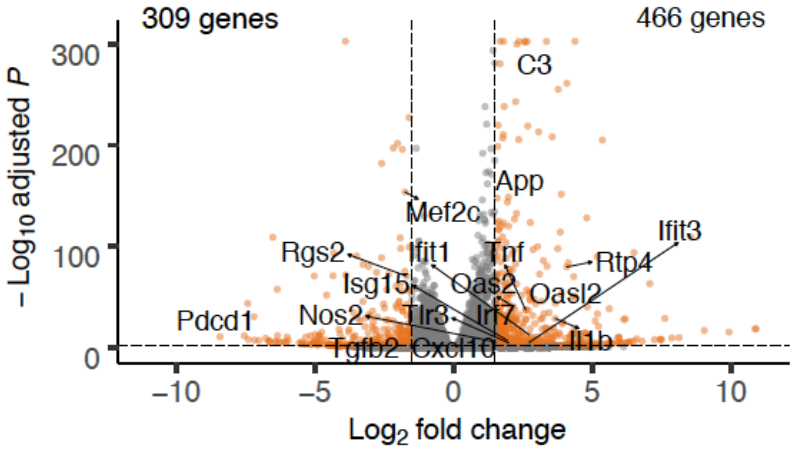

B

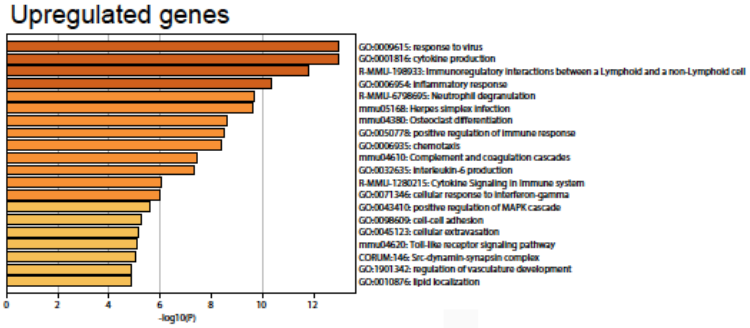

C

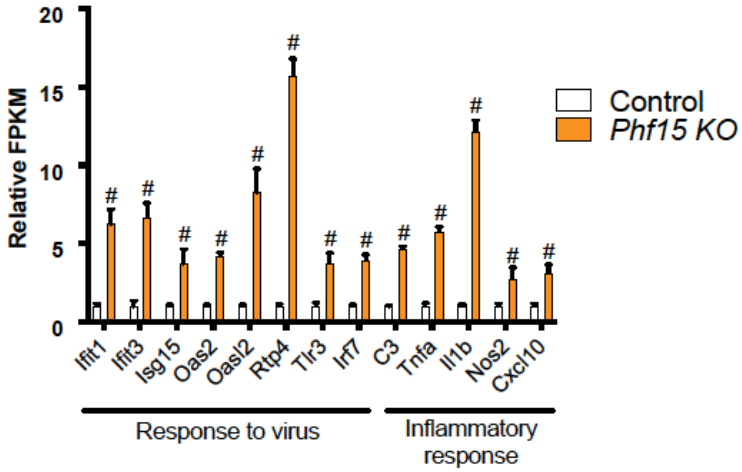

D

Motif	Name	P-value
	IRF	1e-6
	AP-1	1e-5
	IRF3	1e-5
	NFkB-p65	1e-5
	IRF8	1e-5

Figure 2.5. Loss of *Phf15* affects the expression of genes involved in viral response and regulation of inflammatory processes in the absence of immune stimulation

(**A**) Volcano plot representing the RNA-seq results. Orange dots represent differentially expressed genes in *Phf15* knockout microglia compared to control (upregulated genes at a cutoff of log2fold change > 1.5 and *p adj* < 0.01; downregulated genes at a cutoff of log2fold change < -1.5 and *p adj* < 0.05). (**B**) GO analysis for significantly upregulated genes showing biological process categories related to "response to virus" and "inflammatory response". (**C**) Upregulated genes associated with response to virus and inflammatory response in the No stimulation (baseline) condition. Relative FPKM values were obtained by normalizing FPKM values of *Phf15* knockout SIM-A9 microglia to control FPKM values for each gene (n = 3 per condition). Statistics are by DESeq2: #*p*<0.0001. (**D**) Top 5 enriched transcription factor binding motifs for the set of upregulated genes in the No stimulation (baseline) condition.

Motif analysis for transcription factor (TF) binding sites enriched in the promoters of the upregulated genes at baseline revealed consensus motifs for Interferon (IFN) stimulated response element (ISRE, IRF binding motif), and motifs for IFN response factor 3 (IRF3) and IRF8 in the top 5 best matches. Also enriched were Activator protein 1 (AP-1) and Nuclear factor kappa-light-chain-enhancer of activated B cells p65 subunit (NF-κB-p65) motifs. Both can regulate expression of canonical proinflammatory cytokines such as *TNFα* and *IL-1β* [137,138] (Figure 2.5D). Motif enrichment for the set of downregulated genes revealed motifs for Twist-related protein 2 (Twist2) and basic helix–loop–helix (bHLH) MIST1(BHLHA15). Twist2 has been shown to mediate cytokine downregulation after chronic NOD2 (a bacterial peptidoglycan sensor) stimulation [139]. MIST1 has been shown to induce and maintain secretory architecture in cells specialized for secretion [140] (Supplementary Figure 2.8B).

Differential gene expression analysis after 6 hours of LPS stimulation in KO versus control cells revealed 576 up-regulated genes (log2 fold change > 1.5 and *p adj* < 0.01) and 322 down-regulated genes (log2 fold change < -1.5 and *p adj* < 0.05) (Figure 2.6A). Interestingly, by 6 hours after LPS administration, some of the most enriched biological process categories in KO cells were related to "cytokine secretion" and "immunoregulatory interaction" (Figure 2.6B and C), denoting a strong increase in magnitude of expression of genes involved in regulating the secretion of proinflammatory mediators. The downregulated genes at 6 hours after LPS stimulation in KO cells relative to control again displayed more variability, but did show decreases in biological process categories related to "regulation of defense response" and "cytokine production", indicating negative regulation of these processes in *Phf15* KO cells compared to control (Supplementary Figure 2.9A).

A

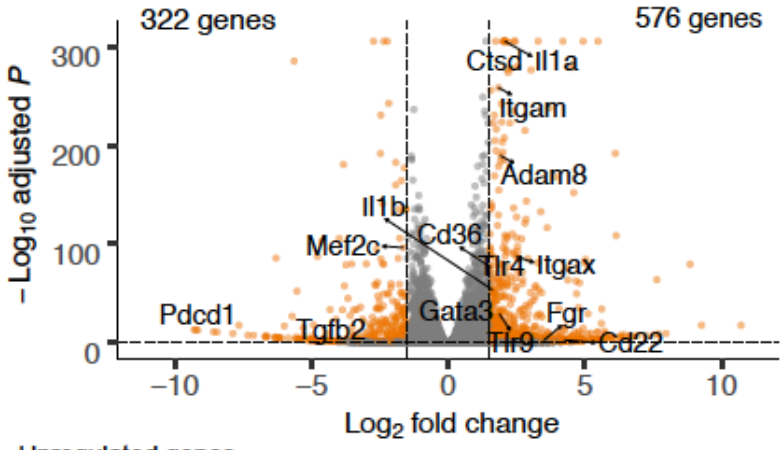
322 genes
576 genes
Ctsd
Il1a
Itgam
Adam8
Il1b
Cd36
Mef2c
Tlr4
Itgax
Pdcd1
Tgfb2
Gata3
Fgr
Tlr9
Cd22
300
200
100
0
−10
−5
0
5
10
– Log10 adjusted P
Log2 fold change

B

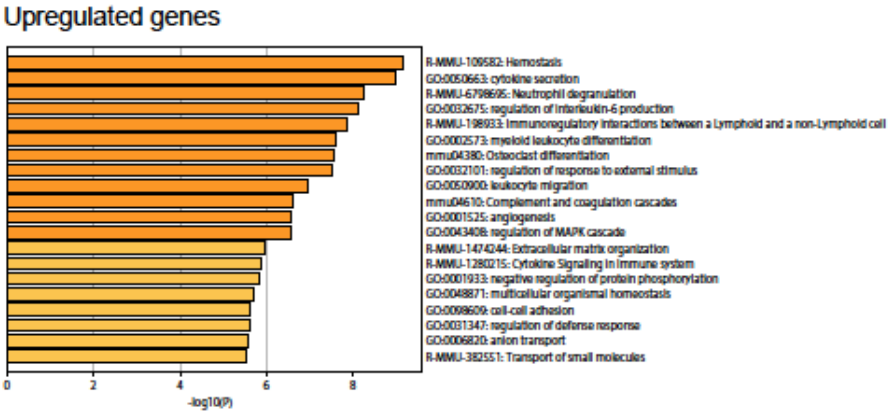
Upregulated genes
R-MMU-109582: Hemostasis
GO:0050663: cytokine secretion
R-MMU-6798695: Neutrophil degranulation
GO:0032675: regulation of interleukin-6 production
R-MMU-198933: Immunoregulatory interactions between a Lymphoid and a non-Lymphoid cell
GO:0002573: myeloid leukocyte differentiation
mmu04380: Osteoclast differentiation
GO:0032101: regulation of response to external stimulus
GO:0050900: leukocyte migration
mmu04610: Complement and coagulation cascades
GO:0001525: angiogenesis
GO:0043408: regulation of MAPK cascade
R-MMU-1474244: Extracellular matrix organization
R-MMU-1280215: Cytokine Signaling in Immune system
GO:0001933: negative regulation of protein phosphorylation
GO:0048871: multicellular organismal homeostasis
GO:0098609: cell-cell adhesion
GO:0031347: regulation of defense response
GO:0006820: anion transport
R-MMU-382551: Transport of small molecules
0
2
4
6
8
-log10(P)

C

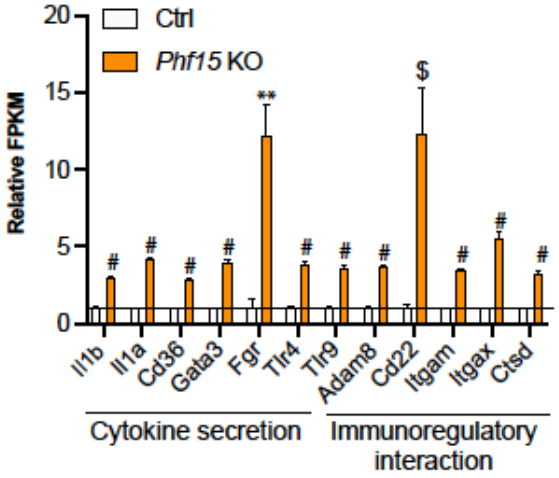
Ctrl
Phf15 KO
Relative FPKM
20
15
10
5
0
**
$
#
Il1b
Il1a
Cd36
Gata3
Fgr
Tlr4
Tlr9
Adam8
Cd22
Itgam
Itgax
Ctsd
Cytokine secretion
Immunoregulatory interaction

D

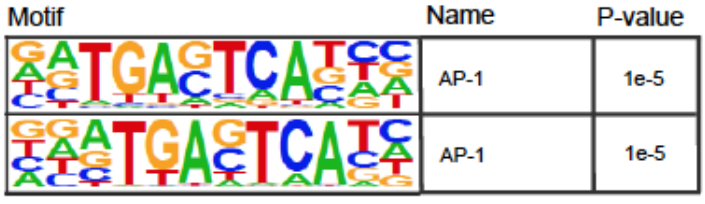
Motif
Name
P-value
AP-1
1e-5
AP-1
1e-5

Figure 2.6. Knockout of *Phf15* affects the expression of genes involved in inflammatory factor secretion and immunoregulatory processes after LPS stimulation

(**A**) Volcano plot representing the RNA-seq results. Orange dots represent differentially expressed genes in *Phf15* knockout microglia 6 hours after LPS administration compared to control (upregulated genes at a cutoff of log2fold change > 1.5 and $p\ adj < 0.01$; downregulated genes at a cutoff of log2fold change < -1.5 and $p\ adj < 0.05$). (**B**) GO analysis for upregulated genes shows biological process categories associated with cytokine secretion and immunoregulatory interaction. (**C**) Upregulated genes associated with cytokine secretion and immunoregulatory interaction biological process categories 6 hours post LPS stimulation. Relative FPKM values were obtained by normalizing FPKM values of *Phf15* knockout SIM-A9 microglia to control FPKM values for each gene (n = 3 wells per condition). Statistics are by DESeq2: $^{**}p<0.01$, $\$p<0.001$, $\#p<0.0001$. (**D**) Transcription factor binding motifs for the set of upregulated genes 6 hours after LPS stimulation are enriched for Activator protein 1 (AP-1).

Motif enrichment analysis for TF binding sites enriched in the promoters of upregulated genes at the 6-hour time point revealed consensus sequences for AP-1, a key regulator of microglia reactivity in inflammation [141] (Figure 2.6D). Motif enrichment for the set of downregulated genes revealed motifs for ISRE (IRF binding motif), IRF1 and IRF3 (Supplementary Figure 2.9B), supporting the observation that there is a negative "regulation of defense response" by 6 hours post stimulation. It is interesting to note that a functional transition from cytokine production to cytokine secretion seems to occur in the 6 hour period after LPS activation.

Taken together, our RNA-seq results confirm that *Phf15* is a repressor of microglial inflammatory gene expression, regulating the antiviral response—specifically, IFN-I-dependent responses—as well as processes related to proinflammatory cytokine production and release.

Section 2.4: Discussion

Our results show that *Phf15* inhibits microglial expression of proinflammatory mediators under basal and signal-dependent activation, regulating both the magnitude and duration of the inflammatory response. Genetic deletion of *PhfF15* in a microglial cell line followed by stimulation with LPS led to an exaggerated proinflammatory response with increased production of *Tnfα*, *Il-1β* and *Nos2* over a time course of 24 hours. Importantly, levels of proinflammatory factors remained elevated at 24 hours demonstrating a sustained and prolonged response. Consistent with our LPS stimulation of TLR4 results, similar results were obtained after TLR9 and TLR3 activation confirming that *Phf15* is a general negative regulator and controls *both* the MyD88 and TRIF downstream signal transduction pathways (Supplementary Figure 2.1). Overexpression of *Phf15* showed a dampened microglial inflammatory response,

highlighting a reciprocal response phenotype that further supports our loss-of-function results.

Prolonged inflammation can damage surrounding healthy tissue, eventually resulting in neuronal degeneration and loss, and negatively affecting brain function. For example, levels of TNFα are seen to rapidly rise in experimental models of PD and are highly toxic to dopaminergic neurons [117,118,142]. Similarly, high levels of TNFα are a hallmark of PD in humans [143–145]. Additionally, both TNFα and IL-1β are involved in maintaining proper synaptic plasticity at physiological levels [146,147] and overproduction of these cytokines can result in neuronal death via excitotoxicity and cognitive dysfunction [148,149].

Our studies further demonstrate that *Phf15* can regulate both basal and signal-dependent microglial inflammatory gene expression. KD and KO of *Phf15* in microglial cell lines resulted in significantly increased levels of proinflammatory cytokine gene expression 1) without stimulation and 2) after immune activation, while OE had the reverse effect. The inflammatory response is a tightly controlled process in immune cells in order to protect against unintended damage to healthy tissue. Even in aged microglia, where production and secretion of proinflammatory mediators is generally increased, this process is dependent upon treatment with immune stimulants [8,87,150]. Increased proinflammatory cytokine gene expression *without* stimulation denotes constitutive or 'leaky' expression of inflammatory mediators, simulating a state of low-grade but constant activation. Similarly, hyperresponsiveness to immune stimuli combined with a lack of resolution of the inflammatory response can lead to a state of chronic inflammation. All three can trigger pathological chronic inflammation in the brain which is detrimental to brain function.

Importantly, distinct molecular mechanisms regulate transcriptional control of different phases ('modules') of the inflammatory response and it is noteworthy that *Phf15* might be involved in regulating several of these. Basal inflammatory function, for example, is generally regulated by co-repressors such as nuclear receptor co-repressor (NCOR), silencing mediator of retinoid and thyroid receptors (SMRT) and REST co-repressor 1, (RCOR1 or CoREST) that block poised promoters from active transcription, preventing 'leaky' expression of primary response genes (e.g., *TNFα*, Type I IFNs, *IL-1β*, etc.) (for review see [97]). Significantly increased inflammatory gene transcription under baseline conditions, as observed in our *Phf15* KD and KO experiments, suggests a loss of this repressive mechanism.

After stimulation by an activating signal, additional mechanisms can maintain quiescence by restraining active transcription. For example, nuclear receptors like peroxisome proliferator-activated receptor-γ (PPARγ), glucocorticoid receptor (GR) and liver X receptors (LXRs) can inhibit the signal-activated exchange of co-repressors for co-activators at poised promoters, inhibiting the initiation of transcription [97,98]. Lastly, several mechanisms regulate resolution of inflammation at the transcriptional level, including transrepression mechanisms that can remove transcription factors like NF-κB, from inflammatory gene promoters, effectively blocking expression of secondary response genes, that is, genes which require chromatin-modification as well as protein synthesis for their induction (for example *Nos2* and ISGs) [97,99,110]. Timely resolution of

an inflammatory response is crucial in order to limit cellular and tissue damage caused by prolonged or chronic inflammation. Our results suggest that *Phf15* may be involved in regulating all three of the abovementioned mechanisms.

But how might *Phf15* be involved in regulating transcriptional repression of the inflammatory response? PHF15 was first described in embryonic stem cells as an E3 ligase that directly targets Lysine-specific demethylase 1 (LSD1, *Kdm1a*)—a key demethylase of histone 3 lysine 4—for degradation [106]. LSD1 has been identified as a member of the CoREST co-repressor complex [108,151] which is required for transcriptional repression of inflammation in microglia [110]. Additionally, our preliminary data showed that *Lsd1* is a potent inhibitor of inflammatory responses in microglia: primary microglia from LSD1 knockout (KO) mice exhibited significantly increased expression of proinflammatory genes after immune stimulation (Supplementary Figure 2.10). We therefore initially hypothesized that increased levels of *Phf15* upon aging might lead to decreased levels of LSD1 and increased microglial inflammatory output. Our results, however, demonstrate that *Phf15 itself* inhibits microglial inflammatory function, thus, its purported mechanism for inhibition is likely not via degradation of LSD1 (Supplementary Figure 2.11).

Interestingly, the global transcriptional changes caused by *Phf15* deletion are highly similar to previously reported age-associated transcriptional changes in microglia [8,152,153]. In particular, a study by Deczkowska et al., [154] found "immune system process" and specifically "response to virus" among the most highly upregulated biological categories for differentially expressed genes in microglia of young (2-month old) versus aged (22-month old) mice, consistent with our results in *Phf15* KO microglia. Notably, a study by Hammond et al., [153] which used single-cell RNAseq to look at microglia profiles throughout the mouse lifespan, found subpopulations in aged (P540) mouse brains which were largely 1) inflammatory, that is, they upregulated *Il-1β*, *Tnfα* and other cytokines or 2) IFN-I-responsive, upregulating ISGs, particularly *Ifit3, Irf7, Isg15, Oasl2, Ifitm3*, and *Rtp4*, compared to younger adult (P100) brains. Similarly, a recent study from the Tabula Muris Consortium [155] which produced a single-cell transcriptomic atlas of 23 tissues and organs across the *Mus musculus* life span, confirmed that microglia in the aged (P540 and P720) brain are enriched for IFN-I-responsive genes and upregulate a similar set of genes including *Ifit3, Irf7, Isg15, Oasl2, Ifitm3*, and *Rtp4*. The genes upregulated by the interferon-responsive microglia clusters in both these studies are highly similar to those upregulated in our *Phf15* KO cells under basal conditions (see Figure 2.5A and C). Because ISGs can modulate inflammation [122] it is possible that interferon-responsive microglia could play a role in contributing to the inflammatory signature found in the aged brain. Interestingly, among the set of downregulated genes in *Phf15* KO cells at baseline and 6 hours after LPS stimulation, is Myocyte Enhancer Factor 2C (*Mef2C*). MEF2C is an important checkpoint inhibitor that restrains microglial activation in response to proinflammatory insults and is lost in brain aging via IFN-I mediated downregulation [154,156]. Thus, an increase in *Phf15* expression in microglia during healthy aging could putatively work to counteract not only microglial activation but increased IFN-I in the aged brain as well.

Notably, a recent study by Readhead et al., [157] found that several virus species are commonly present in the aged human brain. Among them, human herpesvirus 6A and 7 (HHV-6A and HHV-7) were highly upregulated in the brain of AD patients and were found to modulate host genes associated with AD risk, for example, Amyloid precursor protein (*APP*) processing. APP is the precursor molecule whose proteolysis forms amyloid-β (Aβ) and formation of Aβ plaques has long been thought of as the driving force behind Alzheimer's disease [158]. Aβ has more recently been found to have antimicrobial properties, [159] conferring increased resistance against infection from both bacteria and viruses [160]. *App* is among the significantly upregulated genes under basal conditions in our *Phf15* KO cells (log2 fold change =1.492 and $p\ adj < 0.0001$; see Figure 2.5A). Upregulation of *App* due to loss of *Phf15* in mouse microglia is thus consistent with our data showing *Phf15* regulation of the antiviral microglial response.

Altogether, our results show that *Phf15* is a novel repressor of microglial inflammatory gene expression, regulating both the magnitude and time-to-resolution of the inflammatory response. Importantly, *Phf15* also serves to repress baseline inflammatory output in the absence of immune activation. Putatively, increases in *Phf15* during healthy aging could help counteract brain inflammation and protect brain health.

Future studies will determine the mechanism of action of *Phf15*. For example, the identity of its binding partner proteins, its genome-wide binding sites and associated histone marks to determine the specific gene regulatory regions it interacts with (e.g. active enhancers or promoters). Additionally, studies in *Phf15* KO mice will elucidate whether loss of *Phf15*-mediated repression of pro-inflammatory factors is sufficient to induce cognitive decline or exacerbate LPS-induced neurotoxicity of dopaminergic neurons in the substantia nigra.

Section 2.5: Materials and Methods

Animals

Adult male C57Bl6/J mice were purchased from The Jackson Laboratory and maintained on a 12:12-h light–dark cycle (lights on at 0700 hours) with *ad libitum* access to food and water and aged for ~2.5, ~14 or ~20 months. All animal care and procedures were approved by the University of California, Berkeley Animal Care and Use Committee.

shRNA-mediated knockdown of *Phf15* in murine microglial cells

pGIPZ Lentiviral mouse Jade2 shRNA constructs or a control scrambled shRNA were purchased from Dharmacon (Lafayette, CO). Lentivirus was packaged via co-transfection of each pGIPZ-shRNA with pCMV-VSV-G (Addgene plasmid #8454) [161] and pCMV-dR8.2 (Addgene plasmid #8455) [161] into HEK 293T cells using Lipofectamine 3000 reagent (Life Technologies, Carlsbad, CA) according to the manufacturer's

instructions. Viral supernatant was harvested after 48 hours and incubated with SIM-A9 murine microglial cells in SIM-A9 complete medium (DMEM/F12, Life Technologies, Carlsbad, CA), 10% fetal bovine serum (FBS; GE Healthcare Life Sciences, Chicago, IL), 5% horse serum (HS; GE Healthcare Life Sciences, Chicago, IL), 1% Pen-Strep (Life Technologies, Carlsbad, CA)). After 48 hours, GFP+ cells were sorted by FACS on an Aria Fusion (BD Biosciences, San Jose, CA; UC Berkeley Cancer Research Laboratory), expanded and subcultured for immune stimulation experiments. Percent knockdown was determined via RT-qPCR.

Overexpression of *Phf15* in murine microglial cells

A *Phf15* overexpression vector was constructed by cloning the full length *Phf15* cDNA (*Mus musculus* PHD finger protein 15, mRNA cDNA clone MGC:143877 IMAGE:40094330) obtained from Dharmacon (Lafayette, CO) into a pMYs-IRES-GFP retroviral vector (Cell Biolabs Inc, San Diego, CA). Virus expressing the full length *Phf15* cDNA or empty vector control were co-transfected with pCL-10 A1 (Addgene plasmid #15805) [162] in HEK293T cells using Lipofectamine 3000 (Life Technologies, Carlsbad, CA) reagent according to the manufacturer's instructions. SIM-A9 cells were incubated with virus for 24 hrs and then sorted via FACS on an Aria Fusion, expanded and subcultured for immune stimulation experiments. Fold overexpression was verified via RT-qPCR.

Generation of *Phf15* knockout microglia

Phf15 knockout (KO) SIM-A9 cells were generated using the Alt-R CRISPR-Cas9–mediated gene editing system (guide RNA sequence ACTACATCCTGGCGGACCCGTGG) from IDT (Coralville, IA) using CRISPRMAX Lipofectamine reagent (IDT) as per the manufacturer's instructions. ATTO 550+ cells were single-cell sorted on an Aria Fusion. Clones were screened for *Phf15* deletion using PCR (primers Forward: agcacacttgtaaccctcct and Reverse: gaccaatgtctgttgttgttcg) followed by restriction digest with BtgI (New England Biolabs, Ipswich, MA). Percent decrease in *Phf15* mRNA transcript expression was determined via RT-qPCR (primer sequences are listed in Supplementary Table 2.1).

Immune stimulation

For all immune stimulation time course experiments, cells (knockdown, knockout, overexpression and respective controls) were subcultured in 24-well plates at a density of 10^5 cells/well (in triplicate) and stimulated with LPS (final concentration of 100 ng/ml; Sigma Aldrich, St. Louis, MO), CpG ODN (final concentration of 2.5 uM; InvivoGen, San Diego, CA) or Poly(I:C) (final concentration of 25 uM; Sigma Aldrich, St. Louis, MO) for 1, 6, 12 or 24 hrs. No stimulation controls received an equivalent volume of sterile 1xPBS (Invitrogen, Carlsbad, CA).

RNA extraction

Mice were sacrificed according to the approved protocol. Brains were quickly isolated and frontal cortical areas were dissected, flash frozen and stored at – 80 °C. RNA was extracted using a bead homogenizer (30 seconds, setting '5''; Bead Mill, VWR) in Trizol reagent (ThermoFisher, Waltham, MA). Total RNA was extracted using the Direct-zol RNA miniprep kit (Zymo Research, Irvine, CA) according to the manufacturer's instructions. For cell lines, after immune stimulation, media was aspirated and wells were washed 2x with ice-cold 1xPBS (Invitrogen, Carlsbad, CA). RNA was extracted using the Direct-zol RNA miniprep kit (Zymo Research, Irvine, CA).

Real-Time Quantitative PCR (RT-qPCR)

cDNA was reversed transcribed from total RNA using the SuperScript™ III First-Strand Synthesis System kit (ThermoFisher, Waltham, MA) following the manufacturer's instructions. RT-qPCR was run using SYBR green (Roche, Pleasanton, CA) on a QuantStudio 6 (ThermoFisher, Waltham, MA) real-time PCR machine. All RT-qPCR primers were specific to the desired template, spanned exon-exon junctions and captured all transcript variants for the specific gene under study. Ct values were normalized to the housekeeping gene *Hprt*. Primer sequences used in this study are listed in Supplementary Table 2.1.

RNA-seq library preparation and analysis

RNA was extracted from a total of n= 3 replicates per condition (*Phf15* KO or control) and was used to prepare libraries for RNA sequencing using the KAPA mRNA HyperPrep Kit according to the manufacturer's instructions (KAPA Biosystems, Wilmington, MA). Libraries were quality control checked via Qubit (ThermoFisher, Waltham, MA) and via RT-qPCR with a next generation sequencing (NGS) library quantification kit (Zymo Research, Irvine, CA). RNA sequencing (1 lane) was performed on a HiSeq4000 sequencing system (Illumina Inc., San Diego, CA; UC Berkeley Genomics Sequencing Laboratory). Sequencing reads were aligned to the *Mus musculus* reference genome assembly GRCm38 (mm10) using Spliced Transcripts Alignment to a Reference (STAR) aligner [163]. Count data was analyzed with Hypergeometric Optimization of Motif EnRichment (HOMER) software for next-generation sequencing analysis (http://homer.ucsd.edu/homer/ngs/index.html) which uses the R/Bioconductor package DESeq2 [164] to perform differential gene expression analysis. To adjust for multiple comparisons, DESeq2 uses the Benjamini-Hochberg procedure to control the false discovery rate (FDR) and returned FDR adjusted *p* values and log2fold expression changes between *Phf15* KO and control conditions for each gene. Genes were filtered by adjusted *p* value (adjusted $p < 0.01$ for upregulated genes or 0.05 for downregulated genes) and log2 fold change in expression (greater than 1.5 log2fold change for upregulated genes and less than -1.5 for downregulated genes). Too few downregulated genes (< 200) passed the more stringent adjusted $p < 0.01$

cutoff for robust downstream biological function analysis, so the adjusted *p* value threshold was lowered to *p adj* < 0.05. Results were visualized using the R package EnhancedVolcano [165]. Lists of upregulated and downregulated genes were input into Metascape [136], a gene annotation and analysis tool, to determine enriched biological themes within the gene lists.

Motif enrichment

Transcription factor binding sites (motifs) were analyzed using HOMER (http://homer.ucsd.edu/homer/ngs/index.html).

Statistical Analysis

Relative mRNA expression of *Phf15* in mouse frontal cortical areas was analyzed using ordinary one-way ANOVA with post hoc Tukey's multiple comparisons to compare expression levels across age. Percent knockdown and time course experiments measuring expression levels of inflammatory markers (*Tnfα, Nos2, Il-1β)* between control and *Phf15* shRNAs sh*Phf15*-1 and sh*Phf15*-2 after immune stimulation (with LPS, CpG-ODN or Poly(I:C)) were analyzed via Unpaired t-tests between each shRNA versus control shRNA within timepoint. Fold overexpression or percent reduction and time course experiments for *Phf15* overexpression and knockout cell lines were analyzed using Unpaired t-tests (overexpression or knockout vs. respective control) within each time point. $P < 0.05$ was considered significant in all experiments.

Section 2.6: Supplementary Materials

Supplementary Figures 2.1-2.9 and Supplementary Table 2.1.

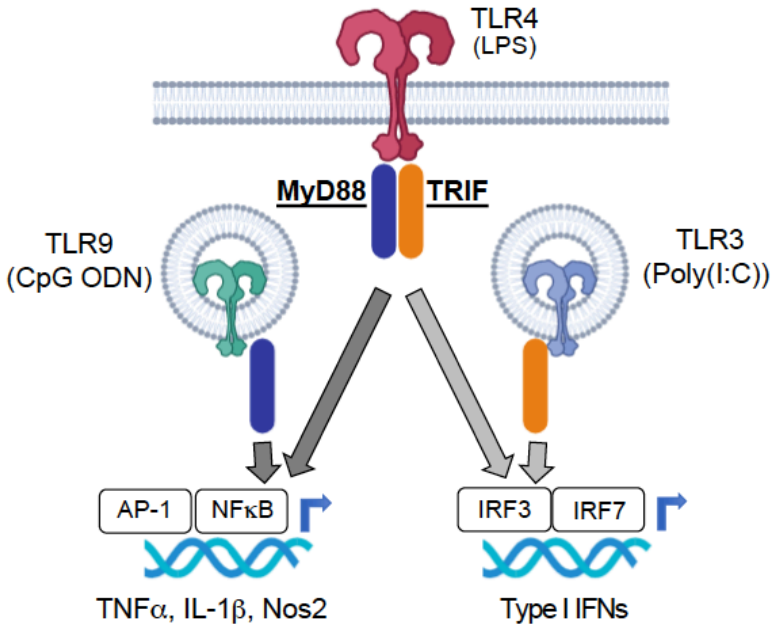

Supplementary Figure 2.1. Schematic of TLR4, TLR9 and TLR3 signal transduction pathways. TLR4, activated by LPS, uses *both* the MyD88 and TRIF downstream adapters to transduce its signaling cascade, leading to transcription of canonical proinflammatory factors like *TNFα*, *IL-1β* and *Nos2* as well as, the type I interferons (*IFNs*). TLR9, activated by CpG ODN, uses the MyD88 adapter, while TLR3, stimulated here by Poly(I:C), uses TRIF.

TLR4, Toll-like receptor 4; LPS, lipopolysaccharide; MyD88, Myeloid differentiation primary response 88; TRIF, TIR-domain-containing adapter-inducing interferon-β; TLR9, Toll-like receptor 9; CpG ODN, CpG Oligodeoxynucleotide; TLR3, Toll-like receptor 3; Poly(I:C), Polyinosinic:polycytidylic acid; AP-1, Activator protein 1; NF-κB, Nuclear factor kappa-light-chain-enhancer of activated B cells; *TNFα*, tumor necrosis factor alpha*; IL-1β*, Interleukin 1 beta*; Nos2*, Nitric oxide synthase, inducible; IRF3, Interferon regulatory factor 3; IRF7, Interferon regulatory factor 7; IFNs, interferons.

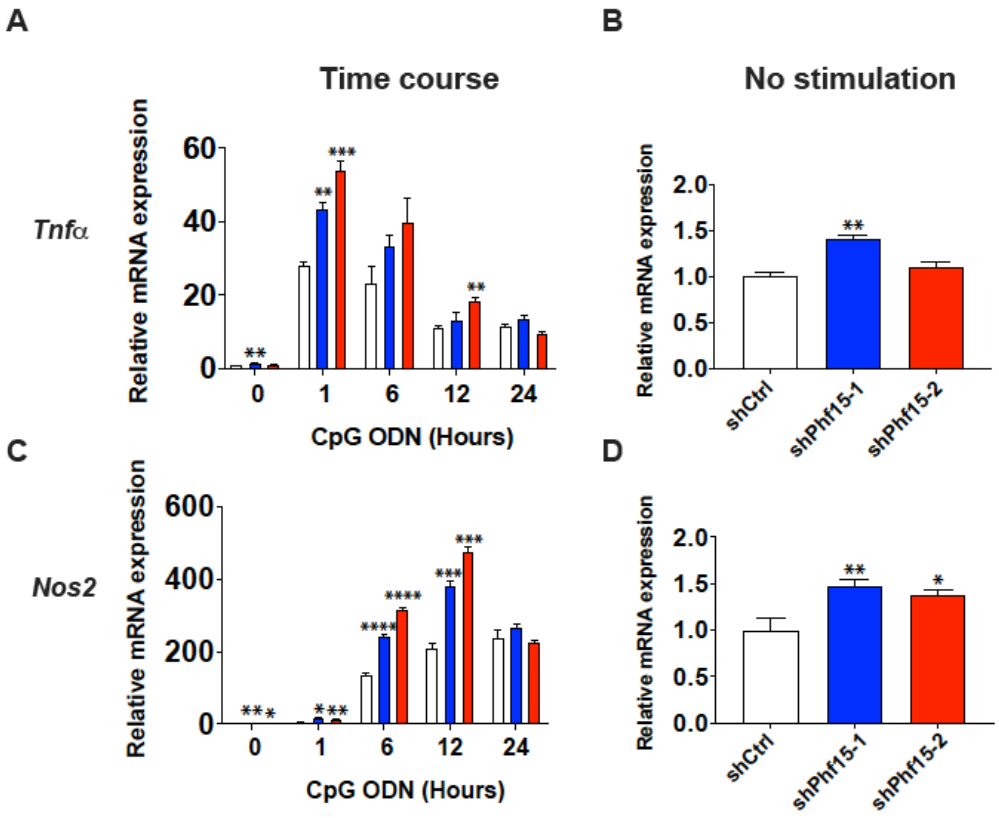

Supplementary Figure 2.2. Knockdown of *Phf15* increases the magnitude of the microglial inflammatory response after TLR9 stimulation. Time course experiments showing relative mRNA expression levels of *Tnfa* (**A**) and *Nos2* (**C**) after CpG ODN stimulation of *Phf15* knockdown microglial SIM-A9 cells compared to shCtrl (control scrambled shRNA). *Tnfa* and *Nos2* expression at time point 0 from the time course experiments are displayed separately in (**B**) and (**D**), respectively. Data are mean ± SEM (n = 3 per condition). Unpaired t-tests for *shPhf15-1* or *shPhf15-2* and shCtrl cells for individual timepoints: asterisks indicate *p<0.05, **p<0.01, ***p<0.001,****p<0.0001. Knockdown efficiency for cell lines shPhf15-1 and shPhf15-2 compared to shCtrl is shown in Figure 2.2a. CpG ODN, CpG Oligodeoxynucleotide; *Tnfa*, Tumor necrosis factor alpha; *Nos2*, Nitric oxide synthase, inducible.

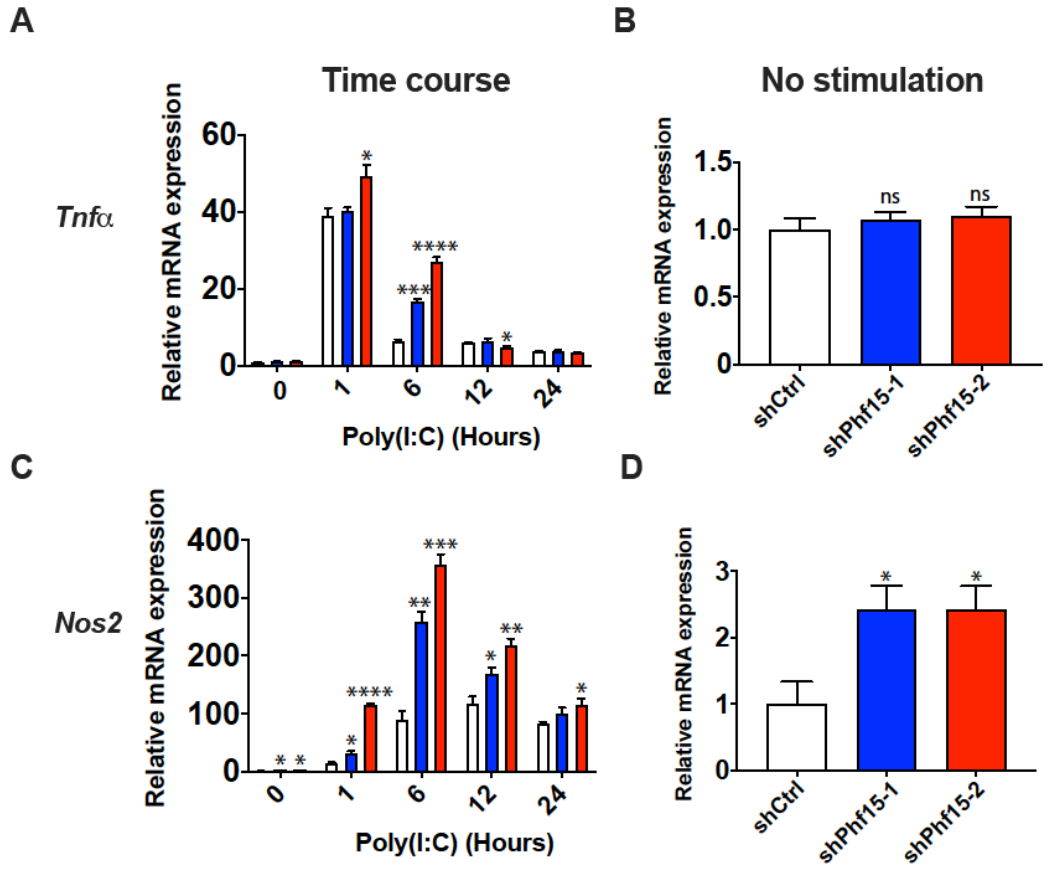

Supplementary Figure 2.3. Knockdown of *Phf15* increases the magnitude of the microglial inflammatory response after TLR3 activation. 24-hour time course experiments showing relative mRNA expression levels of *Tnfa* (**A**) and *Nos2* (**C**) after Poly(I:C) stimulation of *Phf15* knockdown microglial SIM-A9 cells compared to shCtrl (control scrambled shRNA). *Tnfa* and *Nos2* expression at time point 0 from the time course experiments are displayed separately in (**B**) and (**D**), respectively. Data are mean ± SEM (n = 3 per condition). Unpaired t-tests for *shPhf15-1* or *shPhf15-2* and shCtrl cells for individual timepoints: asterisks indicate *p<0.05, **p<0.01, ***p<0.001,****p<0.0001. Knockdown efficiency for cell lines sh*Phf15*-1 and sh*Phf15*-2 compared to shCtrl is shown in Figure 2.2a.
Poly(I:C), Polyinosinic:polycytidylic acid; *Tnfa*, Tumor necrosis factor alpha; *Nos2*, Nitric oxide synthase, inducible.

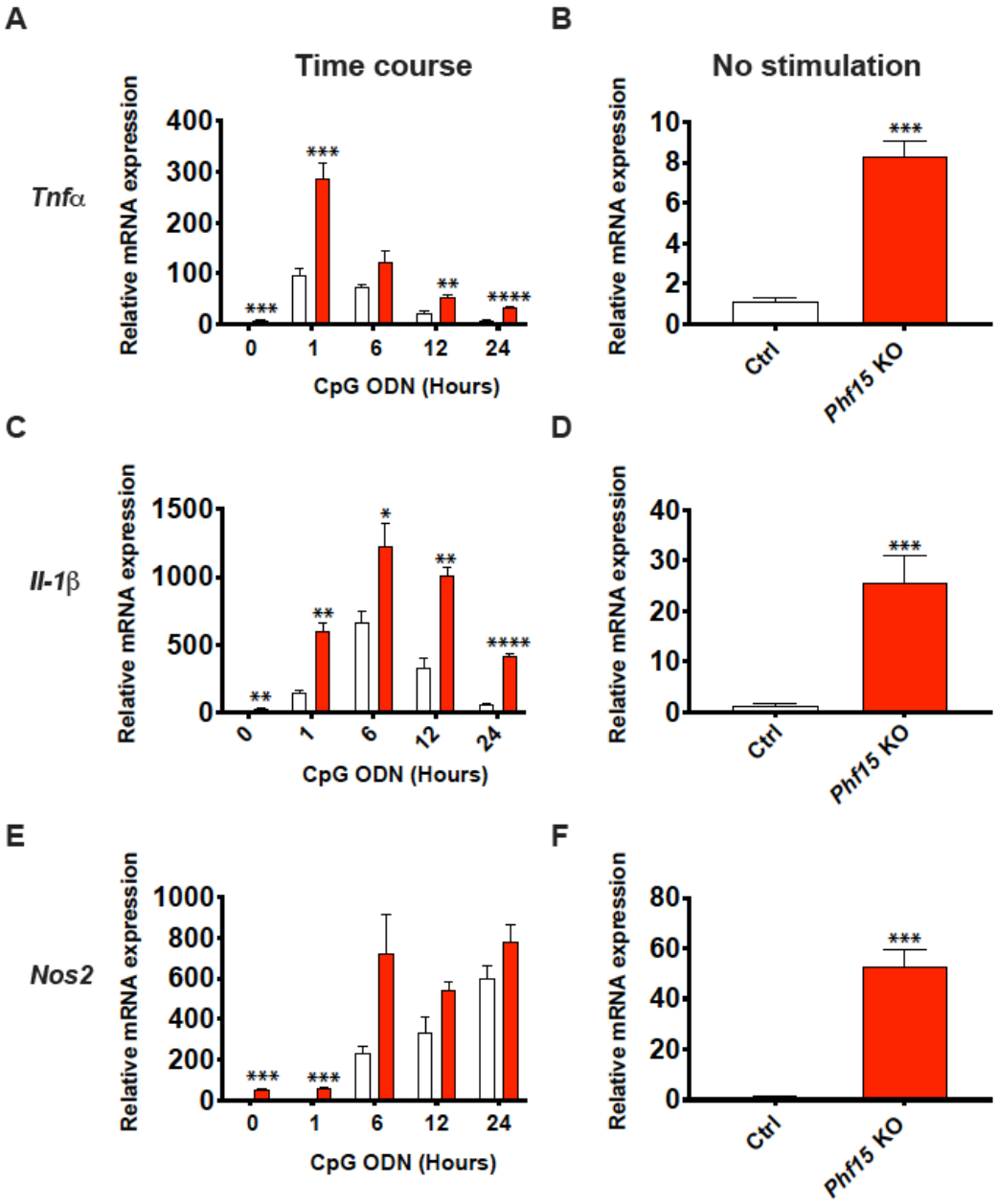

Supplementary Figure 2.4. Knockout of *Phf15* followed by TLR9 stimulation increases the magnitude and duration of inflammatory gene expression. 24-hour time course experiments showing relative mRNA expression levels of proinflammatory factors, *Tnfa* (**A**), *Il-1β* (**C**), and *Nos2* (**E**) after CpG ODN stimulation. *Tnfa, Il-1β* and *Nos2* expression at time point 0 from the time course experiments are displayed separately in (**B**), (**D**) and (**F**), respectively. All data are mean ± SEM (n = 3 per condition). Unpaired t-tests between *Phf15* KO and control cells for percent reduction and for individual timepoints: asterisks indicate *p<0.05, **p<0.01, ***p<0.001,****p<0.0001. Percent reduction in *Phf15* transcript expression in *Phf15* knockout SIM-A9 microglia compared to control is shown in Figure 2.3a.

CpG ODN, CpG Oligodeoxynucleotide; *Tnfα*, Tumor necrosis factor alpha; *Il-1β*, Interleukin 1 beta; *Nos2*, Nitric oxide synthase, inducible.

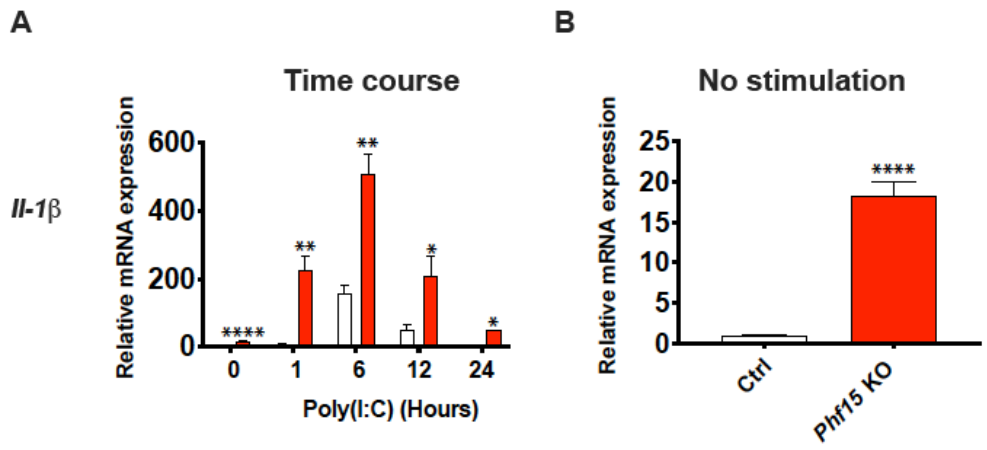

Supplementary Figure 2.5. Knockout of *Phf15* followed by TLR3 activation increases expression of *Il-1β*. (**A**) 24-hour time course experiment showing relative mRNA expression levels of *Il-1β* after Poly(I:C) stimulation. *Il-1β* expression at time point 0 from the time course experiments is displayed separately in (**B**). All data are mean ± SEM (n = 3 per condition). Unpaired t-tests between *Phf15* knockout and control cells for individual timepoints: asterisks indicate *p<0.05, **p<0.01, ****p<0.0001.
Percent reduction in *Phf15* transcript expression in *Phf15* knockout SIM-A9 microglia compared to control is shown in Figure 2.3a.
CpG ODN, CpG Oligodeoxynucleotide; *Il-1β*, Interleukin 1 beta.

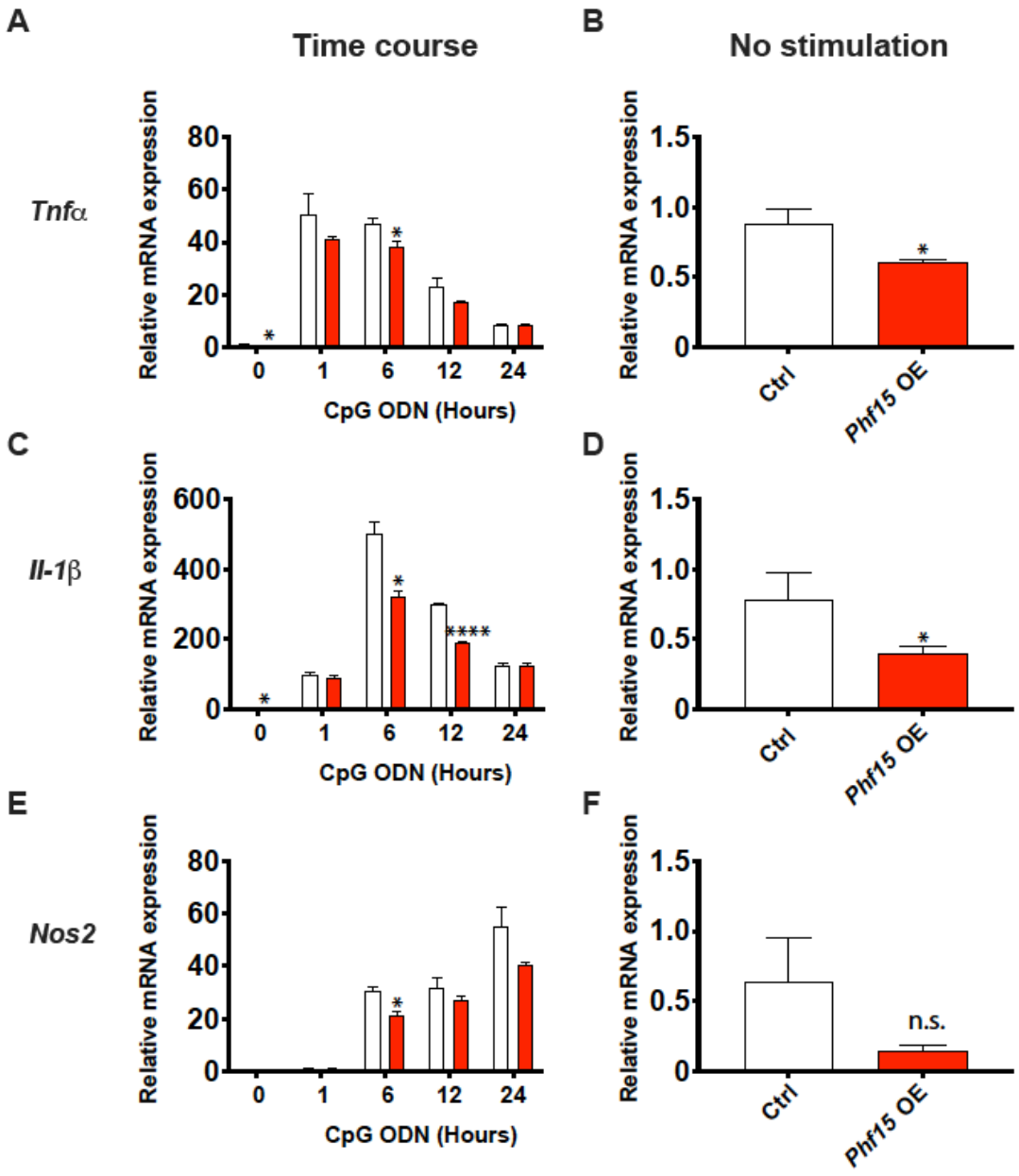

Supplementary Figure 2.6. *Phf15* overexpression dampens the microglial inflammatory response after TLR9 stimulation.
24-hour time course experiments showing relative mRNA expression levels of *Tnfa* (**A**), *Il-1β* (**C**), and *Nos2* (**E**) after CpG ODN stimulation. *Tnfa, Il-1β* and *Nos2* expression at time point 0 from the time course experiments are displayed separately in (**B**), (**D**) and (**F**), respectively. All data are mean ± SEM (n = 3 per condition). Unpaired t-tests between *Phf15* OE and control cells for fold-overexpression and for individual timepoints: asterisks indicate *p<0.05, ****p<0.0001.
Fold overexpression (OE) of *Phf15* in SIM-A9 microglia compared to control cells is shown in Figure 2.4a.

CpG ODN, CpG Oligodeoxynucleotide; *Tnfα*, Tumor necrosis factor alpha; *Il-1β*, Interleukin 1 beta; *Nos2*, Nitric oxide synthase, inducible.

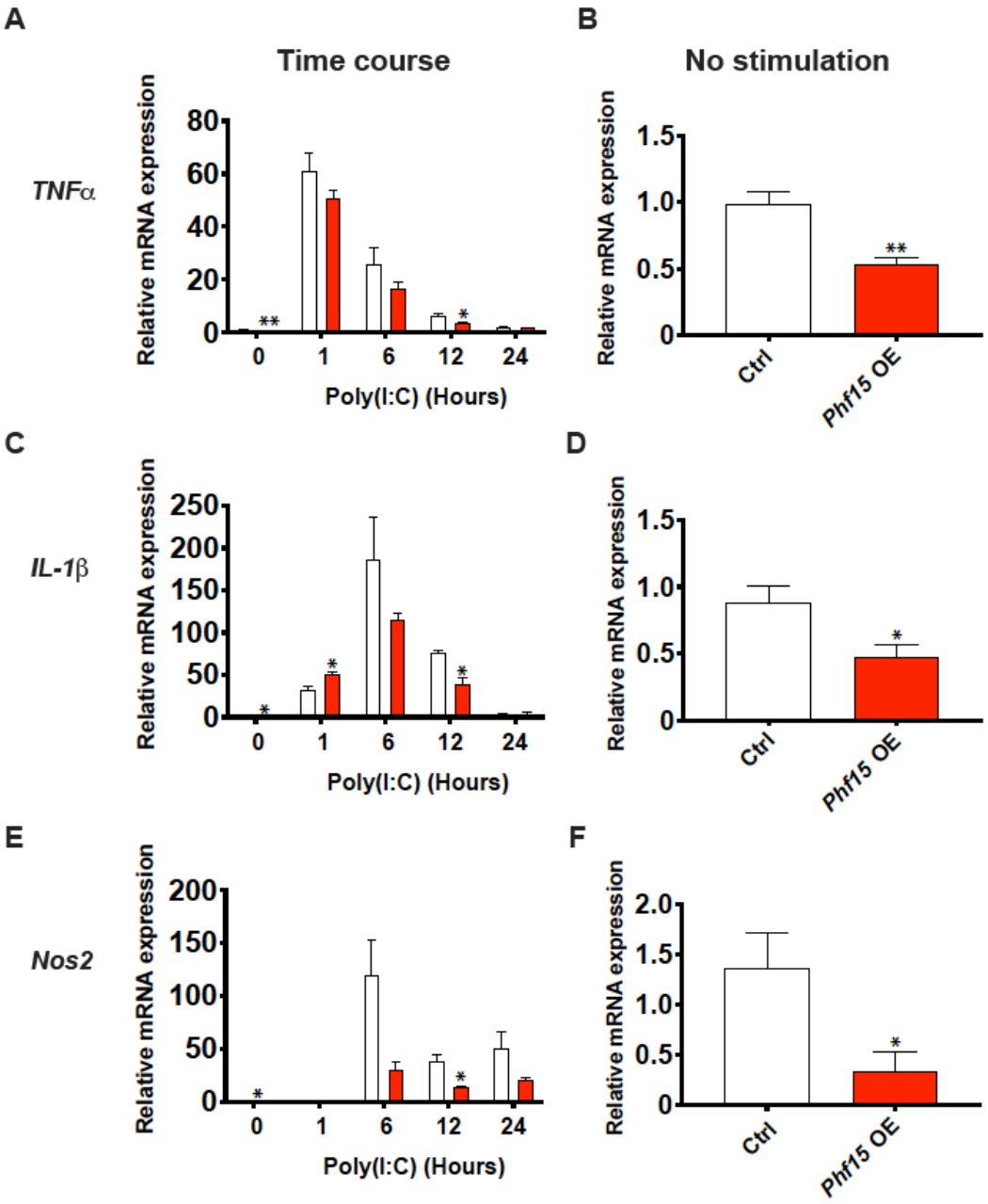

Supplementary Figure 2.7. *Phf15* overexpression dampens the microglial inflammatory response after TLR3 activation.
24-hour time course experiments showing relative mRNA expression levels *Tnfa* (**A**), *Il-1β* (**C**), and *Nos2* (**E**) after Poly(I:C) stimulation. *Tnfa, Il-1β* and *Nos2* expression at time point 0 from the time course experiments are displayed separately in (**B**), (**D**) and (**F**), respectively. All data are mean ± SEM (n = 3 per condition). Unpaired t-tests between

Phf15 OE and control cells for fold-overexpression and for individual timepoints: asterisks indicate *$p<0.05$, **$p<0.01$.
Fold overexpression of *Phf15* in SIM-A9 microglia compared to control cells is shown in 2. 4a.
Poly(I:C), Polyinosinic:polycytidylic acid; *Tnfα*, Tumor necrosis factor alpha; *Il-1β*, Interleukin 1 beta; *Nos2*, Nitric oxide synthase, inducible.

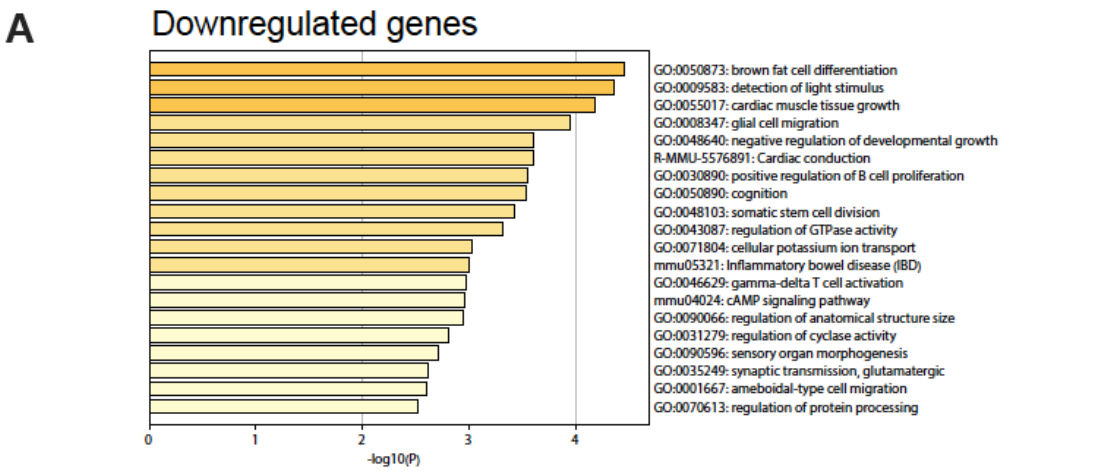

B

Motif	Name	P-value
	Twist2	1e-4
	BHLHA15	1e-4

Supplementary Figure 2.8. Loss of *Phf15* leads to downregulation of genes involved in growth, differentiation and glial cell migration processes under baseline conditions. RNA-seq was performed on *Phf15* knockout SIM-A9 microglia under No stimulation conditions shown in Figure 2.5. (**A**) GO analysis for biological process categories for the set of significantly downregulated genes in *Phf15* knockout SIM-A9 microglia is shown. Biological categories center around various cell growth and differentiation processes and glial cell migration. (**B**) Enriched transcription factor binding motifs for the set of downregulated genes in the No stimulation (baseline) condition include Twist2 and MIST1/BHLHA15.
Twist2, Twist-related protein 2; MIST1/BHLHA15, basic helix–loop–helix 15.

A

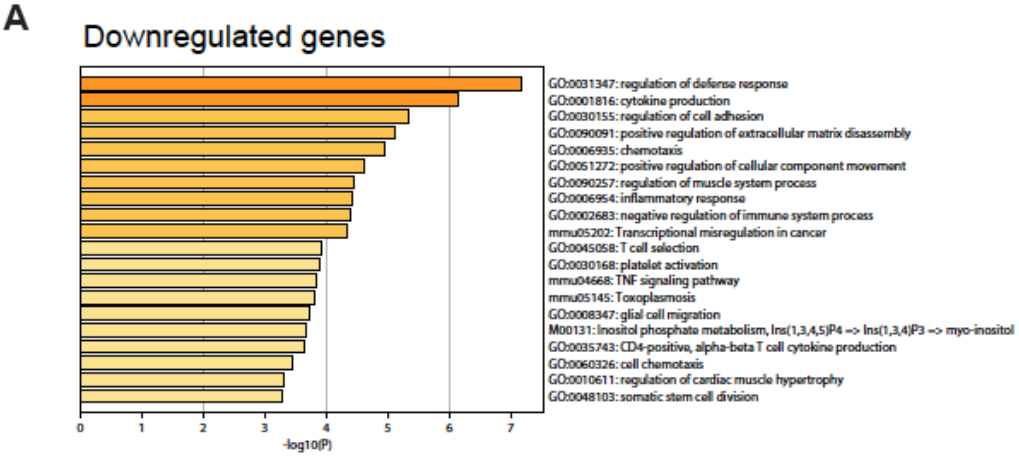

B

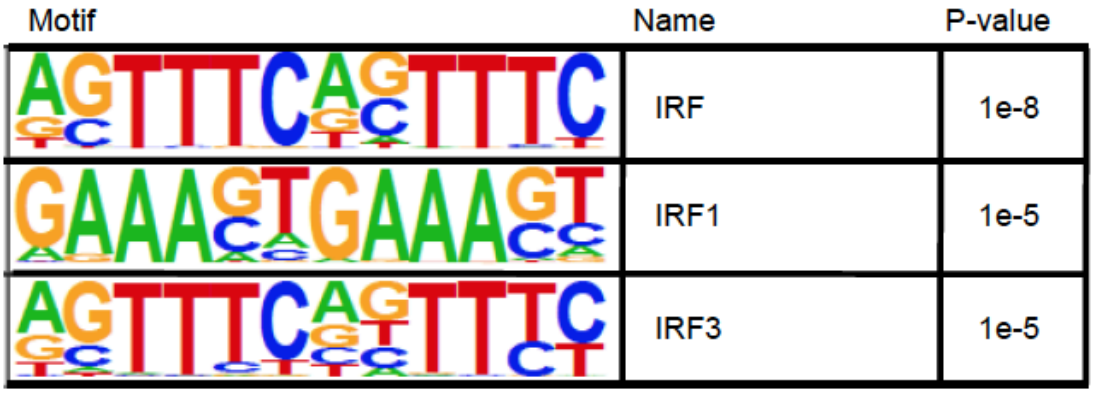

Supplementary Figure 2.9. Knockout of *Phf15* leads to downregulation of genes involved in regulation of defense response and cytokine production 6 hours after LPS stimulation. RNA-seq was performed on *Phf15* knockout SIM-A9 microglia after LPS stimulation shown in Figure 2.6. (**A**) GO analysis for biological process categories for the set of significantly downregulated genes in *Phf15* knockout SIM-A9 microglia is shown. (**B**) Enriched transcription factor binding motifs for the set of downregulated genes after LPS stimulation include ISRE (IRF binding motif), IRF1 and IRF3 binding motifs.

ISRE, Interferon (IFN) stimulated response element; IRF1, IFN response factor 1; IRF3, IFN response factor 3.

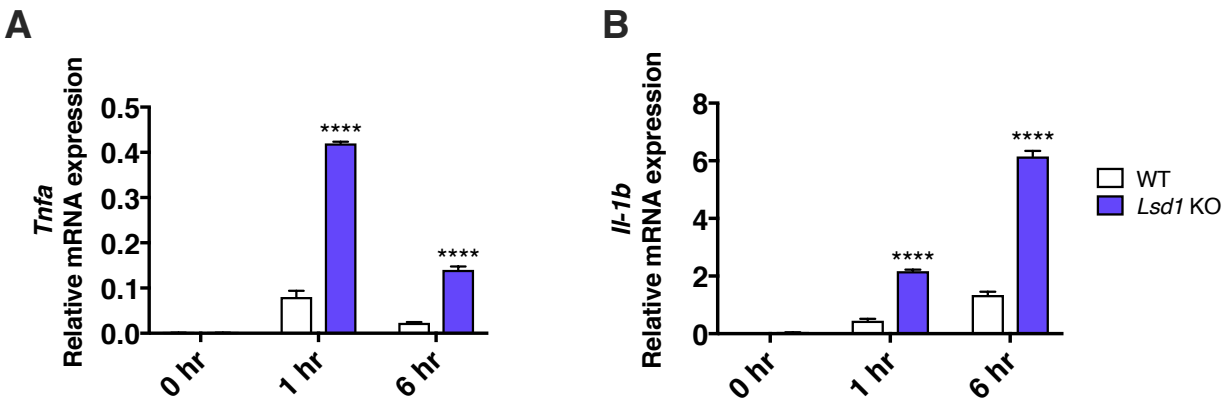

Supplementary Figure 2.10. Knockout of *Lsd1* increases expression of proinflammatory factors in microglia. Relative mRNA expression levels of *Tnfα* (**A**) and *Il-1b* (**B**) were increased in microglia of *Lsd1* KO mice compared to WT after immune stimulation. Data are mean ± SEM (n = 3 mice per condition). Two-way ANOVA with post hoc Sidak's comparisons within timepoint between groups: asterisks denote ****$p<0.0001$. *Tnfα*, tumor necrosis factor alpha; *Il-1β*, Interleukin 1 beta; *Lsd1*, Lysine specific demethylase 1.

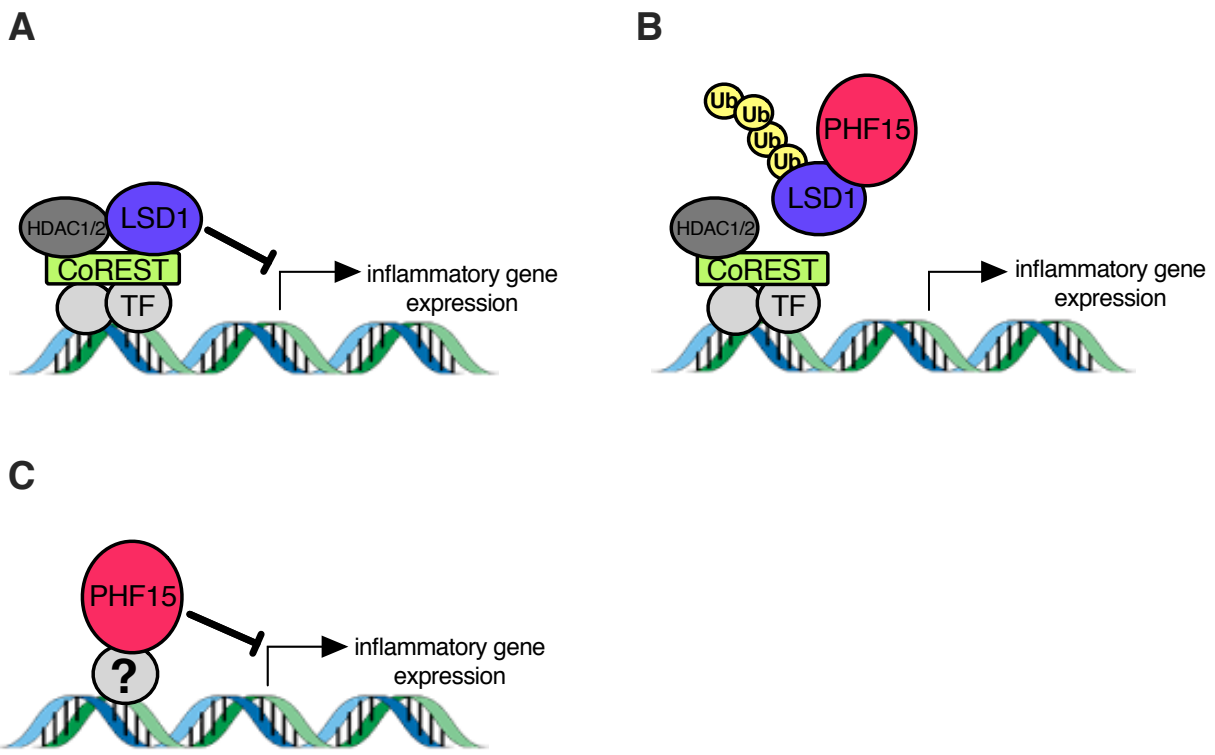

Supplementary Figure 2.11. PHF15 does not inhibit proinflammatory gene expression via degradation of LSD1 in mouse microglia.
(**A**) LSD1 is associated with the CoRest co-repressor complex which inhibits inflammatory gene expression. (**B**) Ubiquitylation of LSD1 by PHF15 targets it for degradation, releasing inhibition of inflammatory gene expression. (**C**) In our model, PHF15 interacts with an unknown transcription factor(s) that putatively bind(s) to ISRE or IRF, AP-1 or other transcription factor binding motifs to inhibit inflammatory gene expression.
Lsd1, Lysine specific demethylase 1; CoREST, REST corepressor 1 (also RCOR1); HDAC1/2, Histone deacetylase complex 1/2; TF, transcription factor; ISRE, Interferon-stimulated response element; IRF, Interferon regulatory factor; AP-1, Activator protein 1.

Supplementary Table 2.1. List of qPCR primers

Gene	Direction	Sequence
Phf15	+	TCAGCATCAAGATGTTCCAAACT
	-	TGAGCTGGTATGAATCTGGGA

Tnfα	+	CCCTCACACTCAGATCATCTTCT
	-	GCTACGACGTGGGCTACAG
Nos2	+	GTTCTCAGCCCAACAATACAAGA
	-	GTGGACGGGTCGATGTCAC
Il-1β	+	CGTGGACCTTCCAGGATGAG
	-	CGTCACACACCAGCAGGTTA
Hprt	+	TCAGTCAACGGGGGACATAAA
	-	GGGGCTGTACTGCTTAACCAG

Phf15, PHD finger protein 15; *Tnfα*, Tumor necrosis factor alpha; *Nos2*, Nitric oxide synthase, inducible; *Il-1β*, Interleukin 1 beta; *Hprt*, Hypoxanthine Phosphoribosyltransferase.

Chapter 3: Loss of STING function inhibits age-related increase in *Il-6* expression but does not improve motor and memory function in aged mice

Section 3.1: Rationale

Given its role in mediating production of the senescence-associated secretory phenotype (SASP) [56] and the role of cellular senescence in inflammaging and associated age-related dysfunction [2], I wanted to test in collaboration with the Raulet laboratory whether mice lacking a functional Cyclic GMP-AMP (cGAMP) synthase (cGAS)-Stimulator of interferon genes (STING) (cGAS-STING) pathway would be protected from increased aging-related inflammation and associated deficits in brain function. I used p16-3MR GT mice, a cross between the senescent cell-labeling p16-3MR mouse strain [166] and *Goldenticket* (GT) mice which lack functional STING and are impaired in Type I interferon (IFN-I) production [167]. Additionally, I wished to determine whether, at the molecular level, STING might lead to inhibition of *Phf15* in order to increase brain inflammation. I recently described *Phf15* as a negative regulator of microglia inflammatory function that regulates both classical and antiviral inflammatory responses [168]. Inhibition of *Phf15* via cGAS-STING would result in increased expression of IFN-I-dependent antiviral mediators and proinflammatory chemokines leading to increased inflammation.

Section 3.2: Results

Loss of STING does not improve motor coordination in old or middle-aged mice

To determine whether loss of STING might protect mice from aging-related deficits in motor coordination that are typically seen in both humans [169] and mice [170], I tested male and female p16-3MR GT mice and sex and age-matched controls (CON p16-3MR) on the rotarod at 10 and 26 months of age. The rotarod is an apparatus which consists of a horizontal, rotating bar. Mice are placed on the bar and the latency to fall, that is how long they are able to remain on the bar, is measured as a proxy for motor coordination and balance with longer latencies correlating to better performance [171,172]. Male and female mice were tested separately due to reported sex differences in rotarod performance [173].

There was no significant difference for the time mice remained on the bar between p16-3MR GT and control mice at 26 months of age for either gender (Figure 3.1A, B) for any of the testing days. Mice also did not improve, i.e., increase the length of time they remained on the bar between any two testing days (Figure 3.1C, D). Previous studies have indicated that rotarod performance is negatively correlated with

body weight [170,173], but I found no differences in body weight between 26-month old p16-3MR GT and control mice for either gender (Figure 3.1E, F), thus body weight was not a confound for this experimental group.

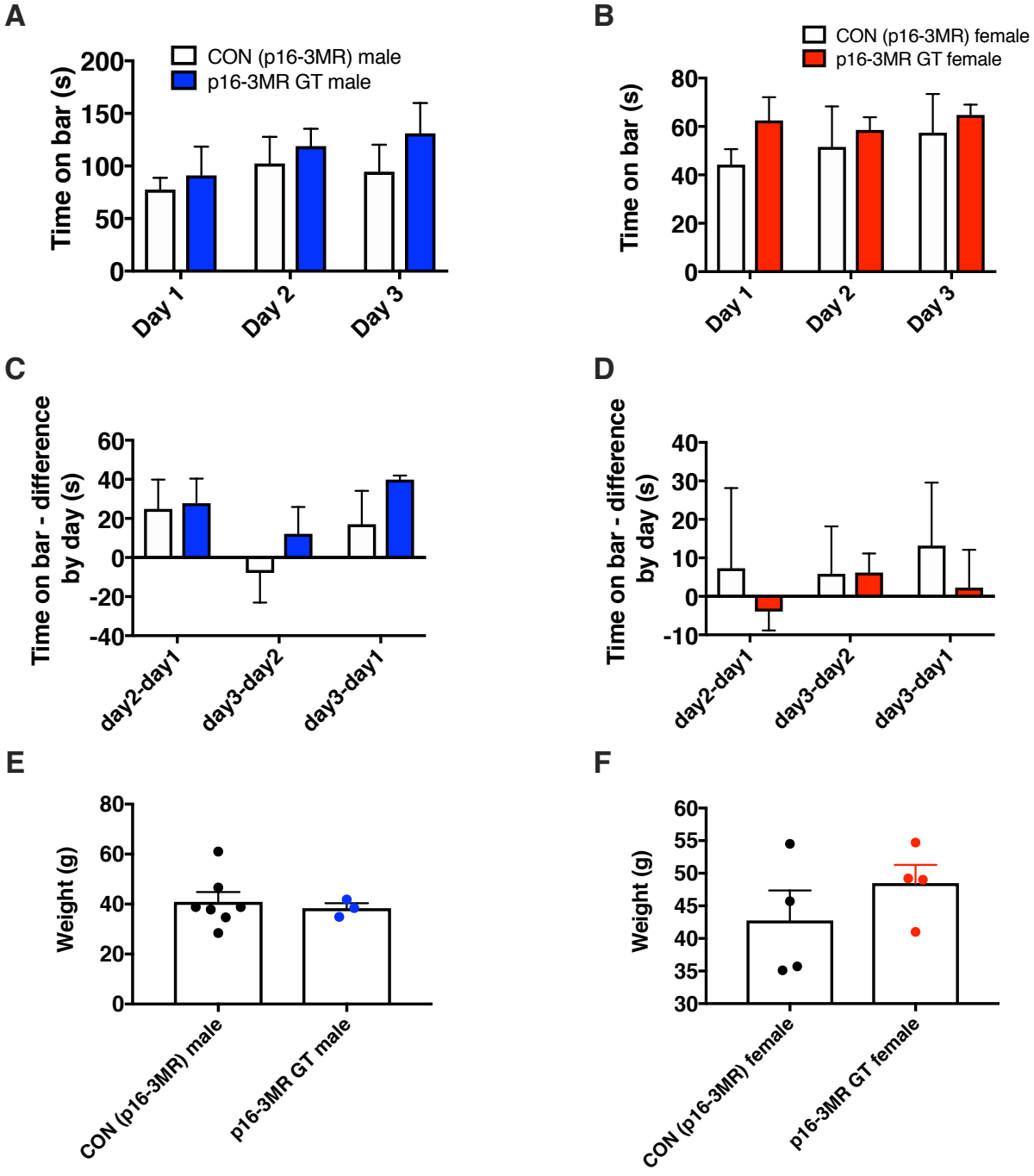

Figure 3.1. Loss of STING does not improve motor coordination in old (26 month-old) mice. (A) There was no significant difference in time on bar between 26 month-old STING-deficient (p16-3MR GT, blue bars) and control (CON (p16-3MR), open bars) male mice on the rotarod for any of the testing days. Data are mean ± SEM (n = 7 CON (p16-3MR), n = 3

p16-3MR GT).
(**B**) There was no significant difference in time on bar between 26 month-old STING-deficient (p16-3MR GT, red bars) and control (CON (p16-3MR), open bars) female mice on the rotarod over 3 days of testing. Data are mean ± SEM (n = 4 CON (p16-3MR), n = 4 p16-3MR GT).
(**C**) There was no significant difference in latency to fall between testing days (i.e., difference in the day-to-day time that mice spent on the bar) for male mice between STING knockout (p16-3MR GT, blue bars) and control mice (CON (p16-3MR), open bars). Data are mean ± SEM (n = 7 CON (p16-3MR), n = 3 p16-3MR GT).
(**D**) Same as (**C**) but for female mice (p16-3MR GT, red bars; CON (p16-3MR), open bars). Data are mean ± SEM (n = 4 CON (p16-3MR), n = 4 p16-3MR GT). (**A-D**) RM 2-way ANOVA with Sidak's multiple comparisons between genotype by day.
(**E**) There was no significant difference in body weight between STING knockout male (p16-3MR GT, blue dots) and control mice (CON (p16-3MR), black dots). Data are mean ± SEM (n = 7 CON (p16-3MR), n = 3 p16-3MR GT). Unpaired t-test.
(**F**) Same as (**C**) but for female mice. Data are mean ± SEM (n = 4 CON (p16-3MR), n = 4 p16-3MR GT). Unpaired t-test.

There was also no significant difference for time on bar between p16-3MR GT and control mice at 10 months of age for males and females (Figure 3.2A, C and 3.2B, D, respectively), although control males showed significant improvement between days 1 and 2, as well as, days 1 and 3 of testing (Figure 3.2A). There was a significant increase in body weight between 10-month old male p16-3MR GT and controls (Figure 3.2E), which did not translate into decreased time on bar for the heavier, p16-3MR GT group. However, this may possibly account for why control mice improved between days 1 and 2 and days 1 and 3 and p16-3MR GT mice did not. There was no significant difference in body weight between 10-month old p16-3MR GT and control female mice (Figure 3.2F). Overall, I found no differences in rotarod performance between p16-3MR GT mice and age-matched controls for either gender in old and middle age, indicating that loss of STING is not protective for age-related deficits in motor coordination.

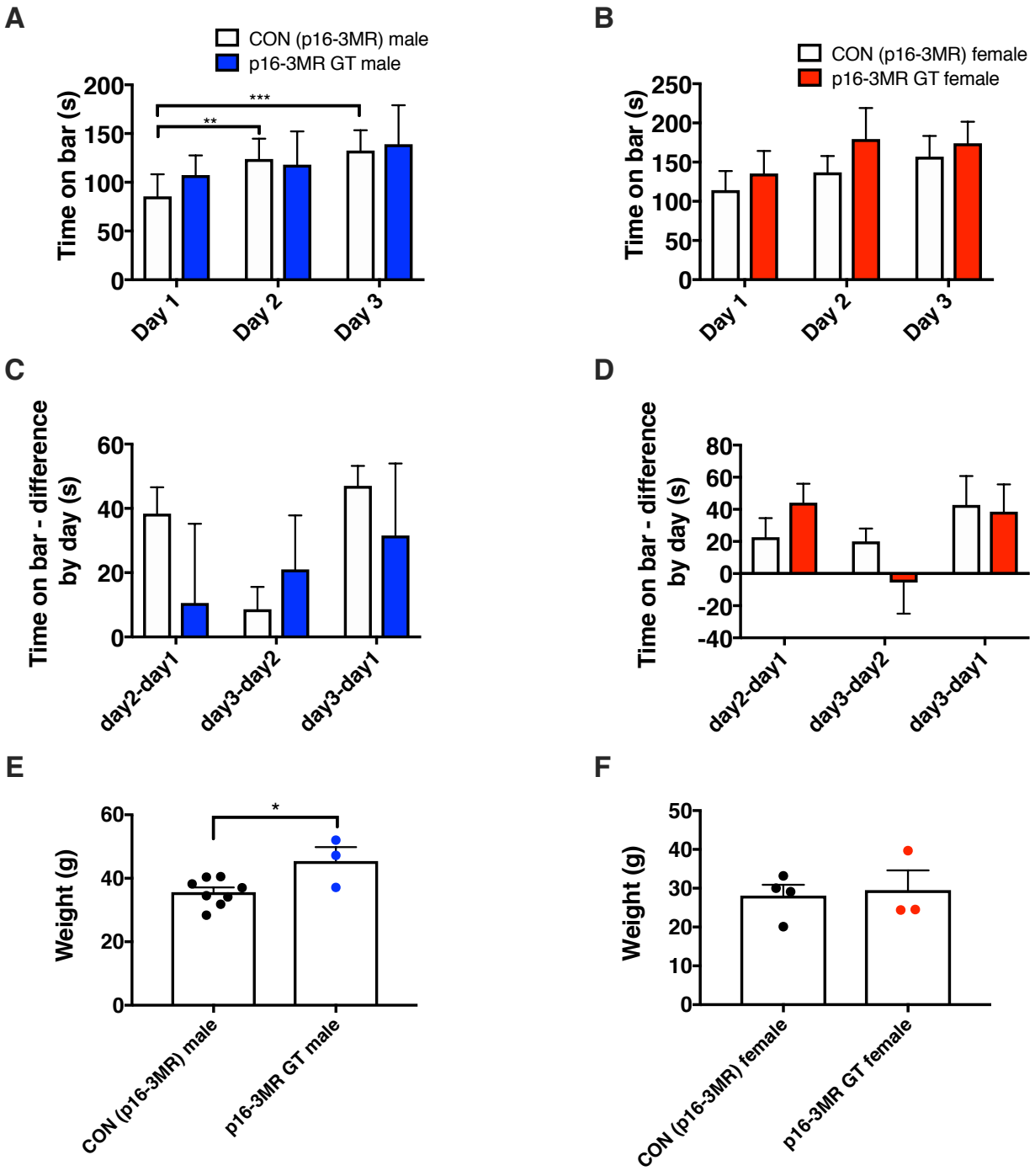

Figure 3.2. Loss of STING does not improve motor coordination in middle-aged (10 month-old) mice

(**A**) There was a significant main effect of day ($F_{1.813}$, 16.32 = 10.91, $p = 0.0012$) for 10 month-old CON (p16-3MR) male mice (open bars) for time on bar between day 1 and day 2, as well as, day 1 and day 3 compared to p16-3MR GT (STING-deficient) mice (blue bars). There was no interaction between testing day and genotype. Data are mean ± SEM

(n = 8 CON (p16-3MR), n = 3 p16-3MR GT).
(**B**) There was no significant difference in time on bar between 10 month-old STING-deficient female mice (p16-3MR GT, red bars) versus control (CON (p16-3MR), open bars) on the rotarod over the 3 testing days. Data are mean ± SEM (n = 4 CON (p16-3MR), n = 3 p16-3MR GT).
(**C**) There was no significant difference in latency to fall between testing days (i.e., difference in the day-to-day time that mice spent on the bar) for male mice between STING knockout (p16-3MR GT, blue bars) and control mice (CON (p16-3MR), open bars). Data are mean ± SEM (n = 8 CON (p16-3MR), n = 3 p16-3MR GT).
(**D**) Same as (A) but for female mice (p16-3MR GT, red bars; CON (p16-3MR), open bars). Data are mean ± SEM (n = 4 CON (p16-3MR), n = 3 p16-3MR GT). (A-D) RM 2-way ANOVA with Sidak's multiple comparisons between genotype by day.
(**E**) There was a significant increase in body weight in STING knockout male (p16-3MR GT, blue dots) compared to control mice (CON (p16-3MR), black dots). Data are mean ± SEM (n = 8 CON (p16-3MR), n = 3 p16-3MR GT). Unpaired t-test: *$p<0.05$.
(**F**) There was no significant difference in body weight between STING knockout female (p16-3MR GT, red dots) and control mice (CON (p16-3MR), black dots). Data are mean ± SEM (n = 4 CON (p16-3MR), n = 3 p16-3MR GT). Unpaired t-test.

Loss of STING does not decrease proinflammatory cytokine or chemokine expression in cerebellum in old mice

Inflammatory changes in the brain can precede the onset of behavioral deficits, thus I tested whether STING deficiency might prevent proinflammatory cytokine and chemokine expression in cerebellum, which mediates motor coordination and aspects of locomotor behavior. I found no significant difference in mRNA expression levels of Interleukin-6 (*Il-6)* or C-C motif chemokine ligand 20 (*Ccl20)* in the cerebellum of old, 27 month-old mice (Figure 3.3A, B, respectively), although there was a significant decrease in young (4.5 month-old) STING knockout mice compared to age-matched controls (Figure 3.3A). Overall, loss of STING does not significantly decrease expression of proinflammatory factors in the cerebellum in old mice.

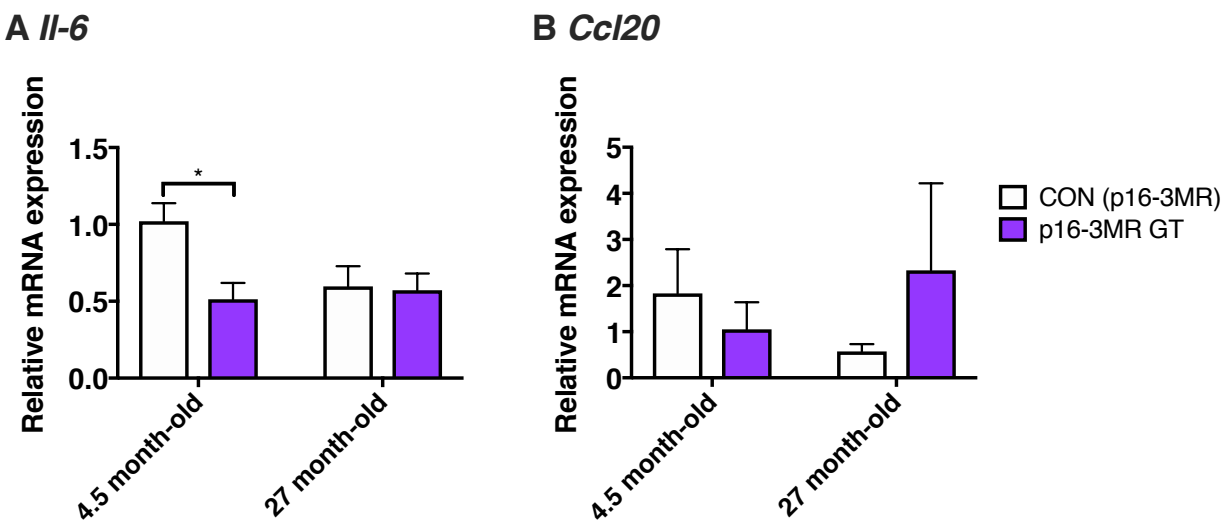

Figure 3.3. STING deficiency does not decrease expression of proinflammatory mediators in the cerebellum of aged mice
(**A**) There was a significant difference in mRNA expression of *Il-6* in cerebellum between p16-3MR GT (purple bars) and control mice (CON (p16-3MR), open bars) in young, 4.5 month-old mice but no difference in old, 27 month-old mice.
(**B**) There were no significant differences in *Ccl20* mRNA levels in cerebellum between p16-3MR GT (purple bars) and control mice (CON (p16-3MR), open bars) in young, 4.5 month-old mice nor old, 27 month-old mice.
All data are mean ± SEM (n = 4-6 young 4.5 month-old mice per genotype, n = 5-7 old 27 month-old mice per genotype). Unpaired t-test between genotype for each age group: **p*<0.05.
Il-6, interleukin 6; *Ccl20*, C-C motif chemokine ligand 20.

Loss of STING does not improve working memory in old or middle-aged mice

In order to assess whether loss of STING might improve cognitive function in old and middle aged mice, I tested p16-3MR GT and control mice on the Y maze–a test for working memory at 10 and 26 months of age (Figure 3.4A). Working memory is one of the first cognitive functions to show age-related impairment in humans with an onset of about 60 years of age or roughly late middle age. Similarly, working memory deficits have been noted in mice at 10 and 24-26 months of age [174]. The Y maze is used to assess working memory by measuring spontaneous alternation [175]. The apparatus consists of three identical plastic arms set at 120° from each other. The number of 3 consecutive entries in different arms is considered an alternation triplet (e.g. ABC or BCA or CAB) with the percent alternation triplet calculated as: (Number of alternation triplets x 100)/(Max Alternation Triplet) where the Max Alternation Triplet = Total Arm Entries –2. Greater percent alternation triplet indicates better working memory performance.

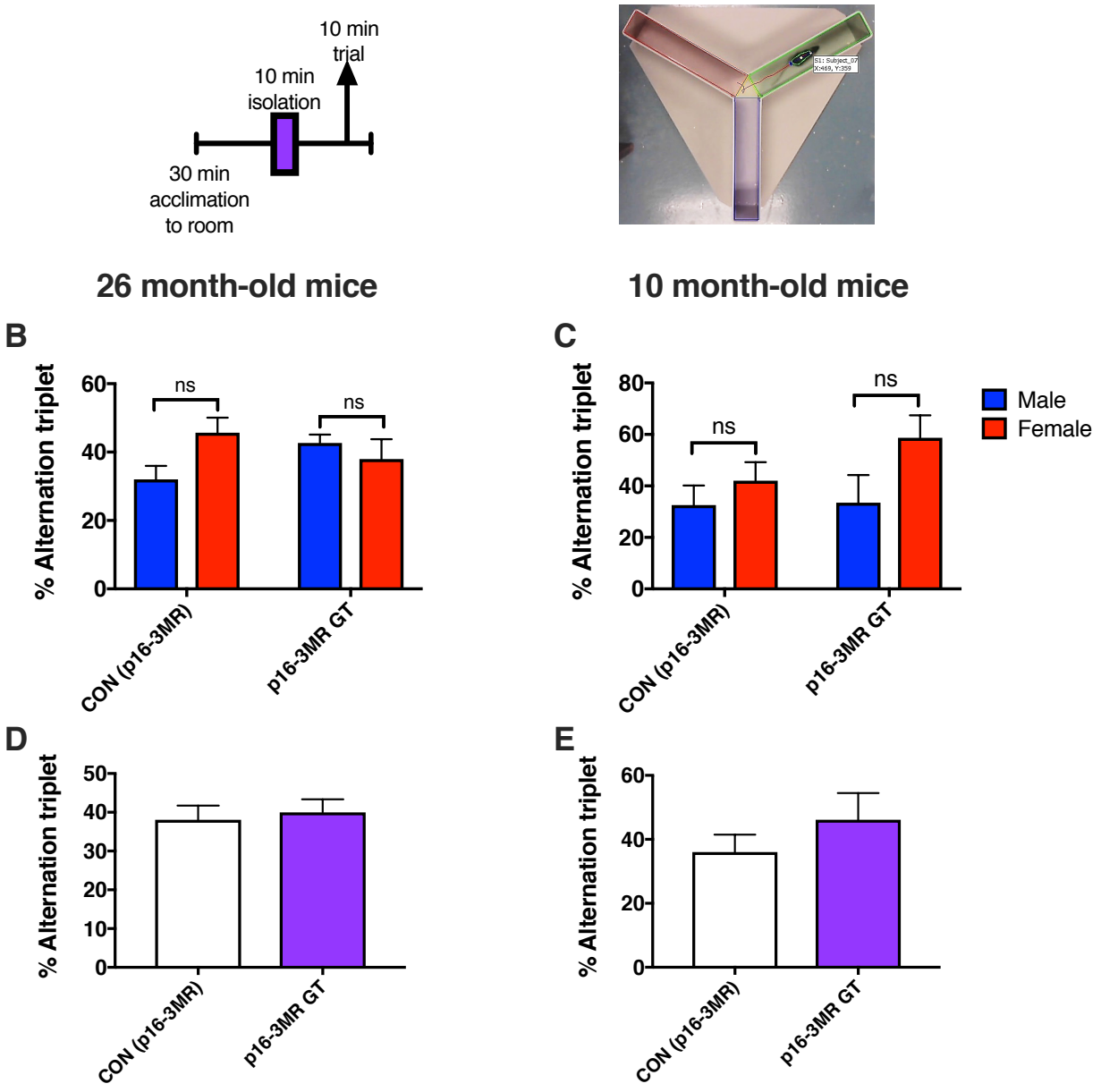

Figure 3.4. Loss of STING does not improve working memory in old nor middle-aged mice.
(**A**) Timeline for Y maze testing.
(**B**) There was no significant difference in % Alternation triplet between male (blue bars) and female mice (red bars) within genotype at 26 months of age. Data are mean ± SEM (n = 5 male, n = 4 female CON (p16-3MR); n = 3 male, n = 4 female p16-3MR GT).
(**C**) There was no significant difference in % Alternation triplet between male (blue bars) and female mice (red bars) within genotype at 10 months of age. Data are mean ± SEM (n = 7 male, n = 4 female CON (p16-3MR); n = 3 male, n = 3 female p16-3MR GT).
(**B** and **C**) Unpaired t-test within genotype between males and females for each age group.
(**D**) There was no significant difference in % Alternation triplet between 26 month-old

STING-deficient (p16-3MR GT, purple bars) and control mice (CON(p16-3MR), open bars). Data are mean ± SEM (n = 10 CON (p16-3MR), n = 7 p16-3MR GT)
(**E**) There was no significant difference in % Alternation triplet between 10 month-old STING-deficient (p16-3MR GT, purple bars) and control mice (CON(p16-3MR), open bars). Data are mean ± SEM (n = 12 CON (p16-3MR), n = 6 p16-3MR GT).
(**D** and **E**) Unpaired t-test between genotype for each age group.

There were no differences in % alternation triplet between male and female mice within genotype (Figure 3.4B, C) so males and females were pooled for statistical analysis. I found no significant difference in % alternation triplet indicating no differences in working memory performance between p16-3MR GT and control animals at 26 and 10 months of age (Figure 3.4D, E, respectively). Overall, my results indicate that loss of STING does not improve working memory performance in old (26 months) and middle (10 months) of age.

Loss of STING significantly decreases levels of proinflammatory cytokine *Il-6* in the hippocampus of old mice

To test whether loss of STING might suppress proinflammatory cytokine and chemokine expression in brain areas mediating working memory function, I tested mRNA expression levels of *Il-6*, *Ccl5*, *Ccl20* and C-X-C motif chemokine 10 (*Cxcl10)* in the hippocampus of old (27 month-old) and young (4.5 month-old) p16-3MR GT and age-matched control (CON (p16-3MR)) mice.

I found significantly reduced mRNA expression of *Il-6*, a proinflammatory cytokine and a key mediator of the SASP in the hippocampus of old (27-month old) p16-3MR GT mice compared to controls (Figure 3.5A). Importantly, there was a significant effect of age and genotype, as well as, an age x genotype interaction, indicating that the age-related *Il-6* increase is less pronounced in STING knockout mice. *Il-6* has been shown to promote the production of new astrocytes [176] and oligodendrocytes [177] (both types of glial cells in the brain) diverting neural stem cells into making new glia at the expense of generating new neurons. Thus, I hypothesized that decreased *Il-6* expression in p16-3MR GT mice might prevent production of new glia while preserving neurogenesis–the generation of new neurons. I measured mRNA expression of Glutamate aspartate transporter 1 (*Glast*), an astrocytic marker, in the hippocampus of young and old p16-3MR GT and control mice. Although there was a significant difference in *Glast* levels in young (4.5 month-old) mice this difference was not present in the old (27 month-old) mice (Figure 3.5B). There were also no significant differences in mRNA expression levels of other proinflammatory factors, the chemokines *Ccl5* (Figure 3.5C), *Ccl20* (Figure 3.5D) and *Cxcl10* (Figure 3.5E). Overall, loss of STING led to significantly decreased levels of *Il-6* in the hippocampus of old mice but I found no difference in expression of other inflammatory factors.

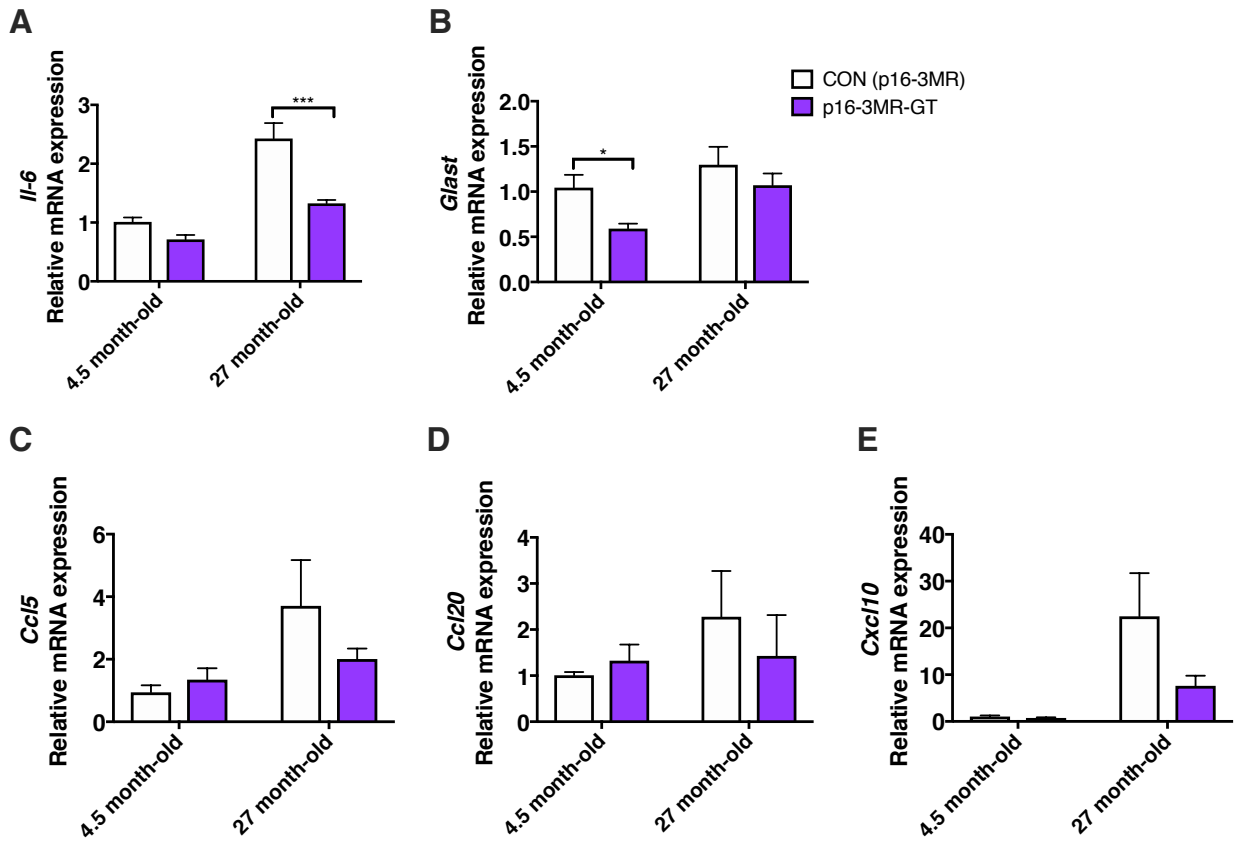

Figure 3.5. Loss of STING decreases proinflammatory cytokine *Il-6* expression in hippocampus of old mice

(**A**) mRNA expression levels of *Il-6* were significantly reduced in hippocampus of old, 27 month-old STING knockout mice (p16-3MR GT, purple bars) compared to control (CON (p16-3MR), open bars). There was a significant main effect of age ($F_{1,8} = 49.79$, $p = 0.001$) and genotype ($F_{1,10} = 17.31$, $p = 0.0019$), as well as, a significant age x genotype interaction ($F_{1,8} = 7.772$, $p = 0.0236$). 2-way ANOVA followed by Sidak's post hoc comparisons: *** $p<0.001$.

(**B**) There was a significant decrease in mRNA expression levels of *Glast* in hippocampus of 4.5 month-old STING knockout mice (p16-3MR GT, purple bars) compared to control (CON (p16-3MR), open bars). There was no significant difference at 27 months of age. Unpaired t-test between control and p16-3MR GT within age group: *$p<0.05$.

(**C**) There was no significant difference in *Ccl5* mRNA expression in hippocampus of 4.5 or 27 month-old STING knockout mice (p16-3MR GT, purple bars) compared to control (CON (p16-3MR), open bars). Unpaired t-test between control and p16-3MR GT within age group.

(**D**) There was no significant difference between p16-3MR GT (purple bars) and control mice (CON (p16-3MR), open bars) in *Ccl20* mRNA expression in hippocampus at 4.5 or 27 months of age. Unpaired t-test between control and p16-3MR GT within age group

(**E**) There was no significant difference in *Cxcl10* mRNA expression in hippocampus of 4.5 or 27 month-old STING knockout mice (p16-3MR GT, purple bars) compared to control (CON (p16-3MR), open bars). Unpaired t-test between control and p16-3MR GT within age

group.
All data are mean ± SEM (n = 4-6 young, 4.5 month-old mice per genotype; n = 5-7 old, 27 month-old mice per genotype).
Il-6, interleukin 6; *Glast*, Glutamate aspartate transporter 1; *Ccl5*, C-C motif chemokine ligand 5; *Ccl20*, C-C motif chemokine ligand 20; *Cxcl10*, C-X-C motif chemokine 10.

Loss of STING does not affect expression of *Phf15* in the brain

Because the cGAS-STING pathway is an important positive regulator of IFN-I gene expression [178] and it has been observed that IFN-Is facilitate senescence [179], I wondered whether STING might regulate age-induced proinflammatory gene expression via inhibition of *Phf15*, a negative regulator of microglia inflammatory function and specifically, the microglial antiviral response [168]. I hypothesized that *Phf15* expression might be significantly increased in p16-3MR GT mice compared to age-matched controls. I tested mRNA levels of *Phf15* in hippocampus, cerebellum and frontal cortical areas (which mediate memory, motor coordination and executive function, respectively) in 4.5 and 27 month-old p16-3MR GT mice compared to controls. I found no significant differences in *Phf15* expression in any of the brain regions examined or for any age group (Figure 3.6A-C).

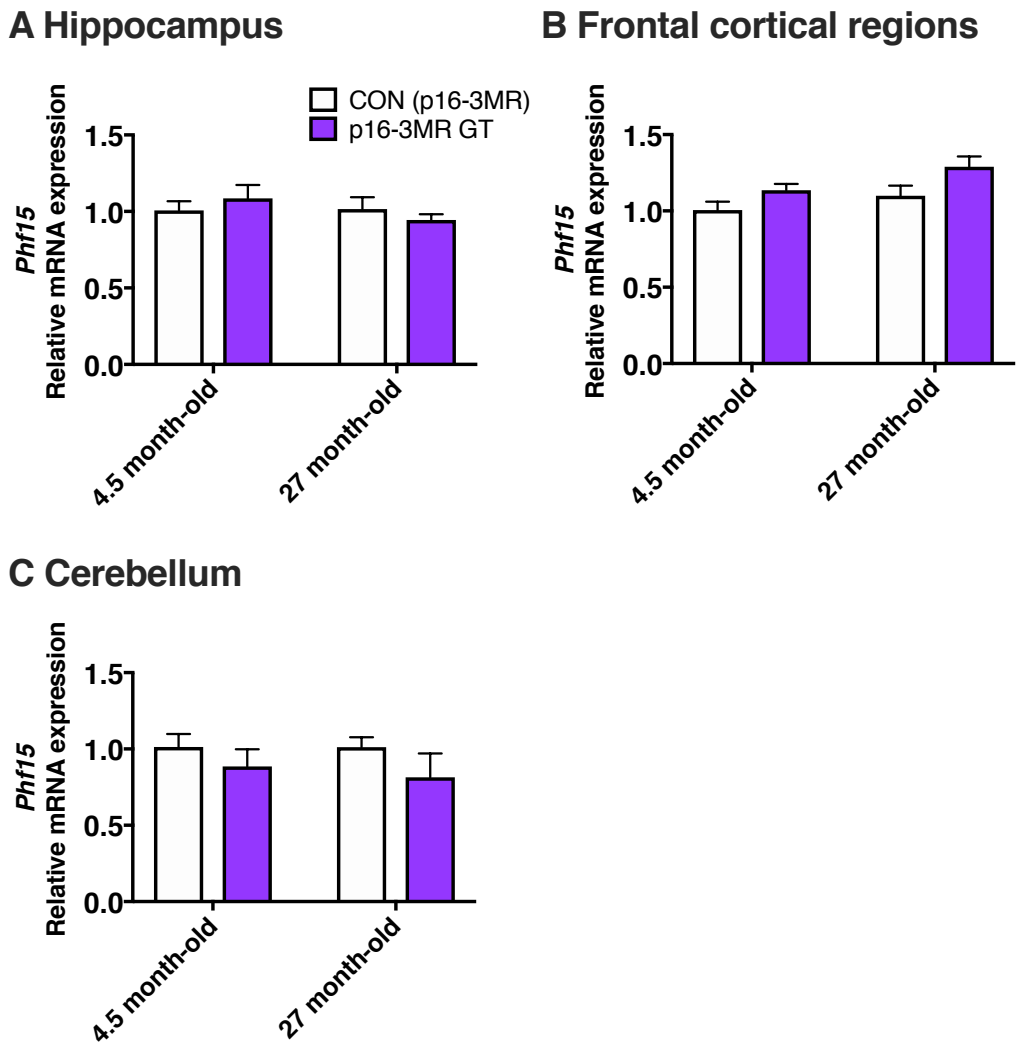

Figure 3.6. Loss of STING does not affect *Phf15* mRNA expression levels in the brain
There was no significant difference in *Phf15* mRNA expression in:
(**A**) hippocampus,
(**B**) frontal cortical regions or
(**C**) cerebellum of 4.5 or 27 month-old STING knockout mice (p16-3MR GT, purple bars) compared to control (CON (p16-3MR), open bars).
All data are mean ± SEM (n = 4-6 young, 4.5 month-old mice per genotype; n = 5-7 old, 27 month-old mice per genotype). Unpaired t-test between control and p16-3MR GT within age group.

For frontal cortical regions, there was also no significant difference in mRNA expression levels of proinflammatory factors *Il-6* or *Ccl20* (Figure 3.7A, B). Overall, my data suggest that STING-mediated production of the SASP in the aged brain likely does not occur via decreased levels of *Phf15*.

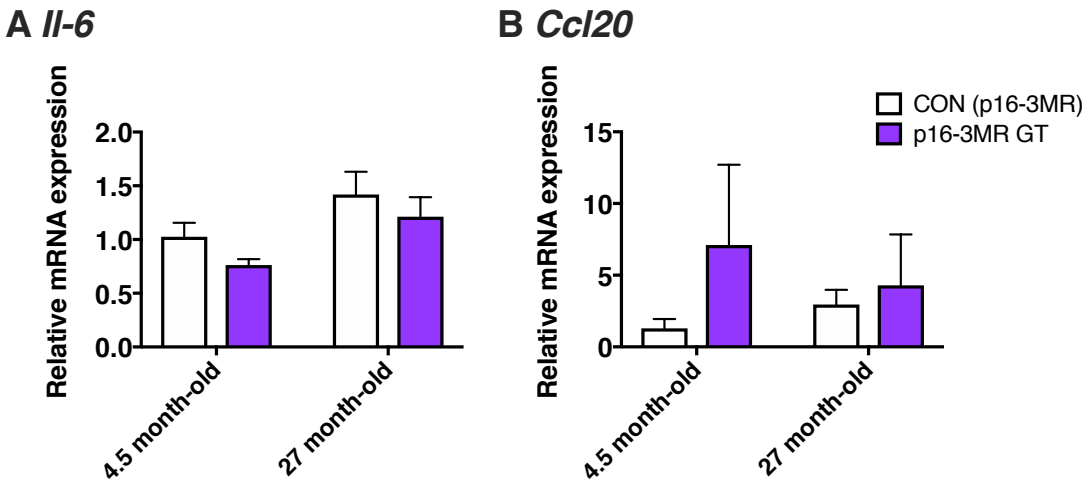

Figure 3.7. Loss of STING does not decrease proinflammatory cytokine/chemokine expression in frontal cortical regions
(**A**) and (**B**) There were no significant differences in *Il-6* (**A**) or *Ccl20* (**B**) mRNA expression between p16-3MR GT (purple bars) and control mice (CON (p16-3MR), open bars) in frontal cortical areas at 4.5 or 27 months of age.
All data are mean ± SEM (n = 4-6 young 4.5 month-old mice per genotype, n = 5-7 old 27 month-old mice per genotype). Unpaired t-tests between genotype for each age group.
Il-6, interleukin 6; *Ccl20*, C-C motif chemokine ligand 20.

Section 3.3: Discussion

Overall, I found that STING deficiency leads to decreased expression of proinflammatory cytokine *Il-6* in the hippocampus of old, 27 month-old mice compared to controls. The hippocampus which mediates various memory-related processes including working memory, is particularly sensitive to aging-related dysfunction [180]. Previous studies have found that *Il-6* can skew neural stem cell differentiation towards the generation of new astrocytes (astrogliogenesis) [176] at the expense of generating new neurons. However, I did not find decreased mRNA expression of *Glast*, a marker of astrocytes and proxy for astrocyte numbers, in the hippocampus of 27 month-old STING-deficient mice compared to controls. Additionally, I did not find decreased expression of other cytokines or chemokines characteristic of the SASP in hippocampus nor related functional improvements in working memory in STING-deficient mice compared to age-matched controls. Taken together, my results suggest that although loss of STING decreased *Il-6* in hippocampus, this decrease did not translate into improved working memory function. It is possible that the spontaneous alternation protocol used with the Y maze is not sensitive enough to detect more subtle deficits in working memory function and a larger battery of working memory assays might have

been beneficial in order to discriminate between normal and impaired function. Similarly, I found no difference in performance on a motor coordination task or significant differences in inflammatory cytokine/chemokine expression in the cerebellum (the area of the brain responsible for regulating voluntary movement, including motor coordination and balance) between aged STING knockout and control animals.

The cGAS-STING pathway is an important regulator of SASP gene expression at the molecular level, mediating the production of inflammatory chemokines (CXCL10 and various CCL's including CCL5 and SP CCL20) and IFN-I responses via activation of the transcription factors Interferon regulatory factor 3 IRF3 [181,182] and Signal transducer and activator of transcription 6 (STAT6) [183]. I have previously shown that *Phf15* is a repressor of microglial inflammatory function, which regulates the antiviral response as well as proinflammatory cytokine expression [168]. Due to the similarity of the inflammatory response resulting from the cGAS-STING pathway and that mediated by *Phf15*, i.e., the activation of IRF3 to mediate IFN-I responses, I hypothesized that during aging, cells undergoing senescence might lead to expression of the SASP via downregulation of *Phf15*. Thus, I might observe decreased *Phf15* mRNA levels in the brains of control mice but not STING-deficient mice. Although I used a bulk tissue approach to measure *Phf15* expression levels, in the brain *Phf15* is almost exclusively expressed in microglia (Figure 3.8) [184]. Thus, bulk tissue *Phf15* mRNA expression mostly reflects microglial *Phf15*. I did not find significant differences in *Phf15* mRNA levels between STING knockout and age-matched controls in any of the brain regions tested (hippocampus, cerebellum, frontal cortical regions) indicating that positive regulation of antiviral IFN-I-related gene expression via cGAS-STING might not act through inhibition of *Phf15*. Putatively, *Phf15* may work to repress pathogen-associated molecular patterns (PAMPs)/Toll-like receptor (TLR)-mediated inflammatory responses, as opposed to, cytosolic DNA-sensing by cGAS-STING. For example, the TLR4 and TLR3 signaling pathways which can activate classic proinflammatory and IFN-I responses via Nuclear factor kappa-light-chain-enhancer of activated B cells (NF-κB) and IRF3.

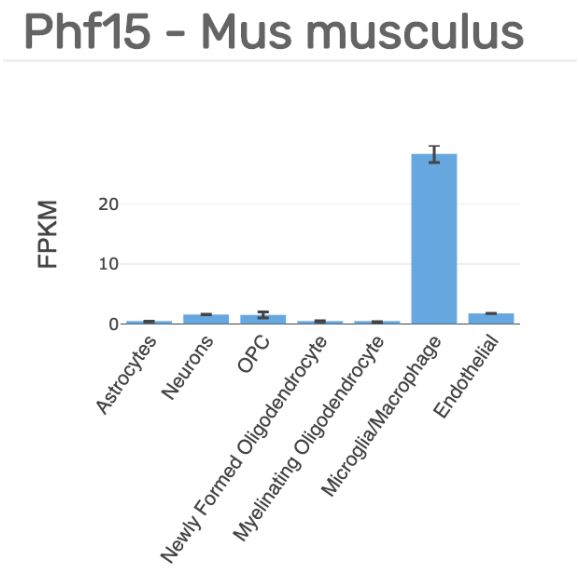

Figure 3.8. *Phf15* is almost exclusively expressed in microglia in the brain. Histogram obtained from Brain RNA-seq, RNA-seq of cell types isolated from mouse brain (http://www.brainrnaseq.org/)

In summary, although the cGAS-STING pathway is involved in regulation of the SASP during aging-related cellular senescence, I found only slight decreases in proinflammatory cytokine expression in hippocampus and no improvement in memory or motor function during old age in STING knockout mice. Additionally, my results suggest that expression of SASP-related inflammatory factors by the cGAS-STING pathway might not proceed via inhibition of *Phf15*.

Section 3.4: Materials and Methods

3.4.1: Ethics Statement

This study was carried out in accordance with the recommendations in the Guide for the Care and Use of Laboratory Animals of the National Institutes of Health. The Animal Use Protocol (AUP-2017-02-9539) was approved by the Animal Care and Use Committee of the University of California, Berkeley.

3.4.2: Animals

p16-3MR BL/6 mice were obtained from the laboratory of Judith Campisi (Buck Institute for Research on Aging, Novato, CA). C57BL/6J-Sting1^{gt}/J mice (*Goldenticket*, GT) were purchased from the Jackson Laboratory. GT mice were genotyped via amplification and sequencing of exon 6 of *Sting* which contains the T596A mutation using the following primers: Exon 6-For, 5′-TCACACTGAGAAGGCTAACGAGC-3′; Exon 6-Rev, 5′-CACCATAGAACAGGGATCACGC-3'. p16-3MR BL/6 mice were crossed to homozygous GT mice and the p16-3MR genotype was confirmed via PCR using the following primers: For GACGTGCCTCCACAGGTAG; Rev CGAGAACGCCGTGATTTT. Mice were maintained on a 12:12-h light–dark cycle (lights on at 0700 hours) with *ad libitum* access to food and water. All animal care and procedures were approved by the University of California, Berkeley Animal Care and Use Committee.

3.4.3: Behavioral Studies

Rotarod. The rotarod tests motor coordination and balance [171,172]. Mice were placed on on a horizontal, accelerating rotating cylinder (Rota-rod 47650, Ugo Basile, Italy) and the latency to fall–a measure of the mouse's balance, coordination and general physical condition–was noted. Mice were tested over 3 consecutive days. Each daily session included a training run of 300 seconds at 5 rpm followed by 1 hour of rest and 3

consecutive accelerating (5-40 rpm for 300 seconds) trials with an inter-trial interval of ~30 minutes. All trials were video recorded and latency to fall was scored by 2 blind observers. Male and female animals were tested separately.

Y maze. The Y maze was used to assess working memory by measuring spontaneous alternation [175]. The apparatus consisted of three identical plastic arms set at 120° from each other. Individual subject mice were placed in the center portion of the maze and were allowed to freely explore for 10 minutes. Movement in the Y maze was tracked, recorded and analyzed using the SMART 3.0 Video Tracking Software (Panlab; Harvard Apparatus, Holliston, MA). Three consecutive entries into three different arms was considered an alternation triplet (e.g. ABC or BCA or CAB). Percent alternation triplet was calculated as: (Number of alternation triplets x 100)/(Max Alternation Triplet) where the Max Alternation Triplet = Total Arm Entries –2. Males and females were tested separately but results for all animals were pooled by age group for statistical analysis.

3.4.4: RNA extraction

Mice were quickly sacrificed according to the approved protocol. Brains were isolated and frontal cortical areas, hippocampus and cerebellum were dissected, flash frozen and stored at – 80 °C. RNA was extracted using a bead homogenizer (30 seconds, setting '5''; Bead Mill, VWR) in Trizol reagent (ThermoFisher, Waltham, MA). After homogenization, tubes were incubated at room temperature for 5 min and spun down at 12,000 g for 5 min at 4C. The supernatant was transferred to a fresh RNase/DNase free eppendorf and total RNA was extracted using the Direct-zol RNA miniprep kit (Zymo Research, Irvine, CA) according to the manufacturer's instructions.

3.4.5: Real-time quantitative PCR (RT-qPCR)

cDNA was reversed transcribed from total RNA using the SuperScript™ III First-Strand Synthesis System kit (ThermoFisher, Waltham, MA) following the manufacturer's instructions. RT-qPCR was run using SYBR green (Roche, Pleasanton, CA) on a QuantiStudio 6 (ThermoFisher, Waltham, MA) real-time PCR machine. All RT-qCPR primers were specific to the desired template, spanned exon-exon junctions and captured all transcript variants for the specific gene under study. Primers were designed using SnapGene and NCBI Primer BLAST software. Specificity of primer pairs was confirmed using melt curve analysis. Ct values were normalized to the housekeeping gene *Hprt* and fold-change differences were determined using the delta-delta Ct ($2^{-\Delta\Delta Ct}$) method. Primer sequences used in this study are listed in Table 3.1.

Table 3.1. List of RT-qPCR primers

Gene	Direction	Sequence
Phf15	+	TCAGCATCAAGATGTTCCAAACT

	-	TGAGCTGGTATGAATCTGGGA
Il-6	+	GCTACCAAACTGGATATAATCAGGA
	-	CCAGGTAGCTATGGTACTCCAGAA
Ccl20	+	ACTGTTGCCTCTCGTACATACA
	-	GAGGAGGTTCACAGCCCTTTT
Hprt	+	TCAGTCAACGGGGGACATAAA
	-	GGGGCTGTACTGCTTAACCAG

Phf15, PHD finger protein 15; *Il-6*, Interleukin 6; *Ccl20*, C-C motif chemokine ligand 20; *Hprt*, Hypoxanthine Phosphoribosyltransferase.

3.4.6: Statistical Analysis

Prism 8 software (GraphPad, San Diego, CA) was used for statistical analysis. P values were calculated using Unpaired t-tests, repeated measures (RM) 2-way ANOVA or ordinary 2-way ANOVA as indicated.

Chapter 4: Prolonged high fat feeding and obesity do not affect working memory or levels of *Phf15* in the mouse brain

Section 4.1: Rationale

Although numerous studies have reported on the effects of high fat diet (HFD) treatment on inflammatory markers in the brain, as well as, detrimental effects on cognitive function, the length of HFD treatment, behavioral task employed as well as other physiological measures (i.e., the loss of synaptic markers, impaired long-term potentiation (LTP), etc.) correlated to impaired brain function, varied widely between studies [185–188] (for review see [189]). Thus, I sought to first determine the length of HFD treatment necessary to negatively impact working memory which is one of the earliest cognitive abilities to show impairment in humans during aging (alongside executive function and processing speed) with an onset of about 60 years of age–roughly late middle-age [150].

Additionally, because HFD increases brain inflammation, I wondered if it might do so via decreases in *Phf15* which I have previously shown is a repressor of microglial inflammatory function [168]. Microglia are the major mediators of inflammatory processes in the brain and increased numbers of microglia, as well as, increased microglial activation have been found after HFD treatment [40,190]. I had previously shown that *Phf15* mRNA levels increased in frontal cortical brain regions in 20-month old ('old mice')–but not 14-month old ('middle aged') mice–compared to young 2.5-month old mice during healthy aging [168]. I proposed that this increase might serve as a protective mechanism to counteract aging-induced inflammation and protect brain health. Frontal cortical regions mediate various aspects of cognitive function and are selectively affected in aging-related neurodegenerative conditions like Parkinson's disease (PD), Alzheimer's disease (AD) and frontotemporal dementia (FTD) [126,127]. I thus hypothesized that HFD-treated mice would have significantly decreased levels of *Phf15* in the brain compared to age-matched controls fed a normal chow (NC) diet.

Section 4.2: Results

Prolonged HFD treatment significantly increases weight but does not impair working memory in adult mice.

To determine the length of HFD treatment necessary to induce impairments in working memory, I tested several cohorts of adult mice on differing lengths of HFD treatment in a working memory task, the Y maze. I chose 3 and 5 months of HFD as these were standard treatment lengths found to correlate with different types of impaired memory function [186,187,189]. In addition, I tested an earlier time point, 1.5 months, as well as, a

much longer-term exposure, 11 months of HFD by 14 months of age, which is roughly equal to mouse 'middle age.'

I found that, compared to age-matched controls, HFD treatment significantly increased body weight when applied for 1.5, 3, 5 and 11 months (Figure 4.1A, C, E, respectively). However, I did not find any differences in percent alternation triplet for any length of HFD treatment (Figure 4.1B, D, F). There was also no significant difference in the total number of arm entries (Figure 4.2A, C, E) or total distance traveled in the Y maze for any of the treatment groups (Figure 4.2B, D, F).

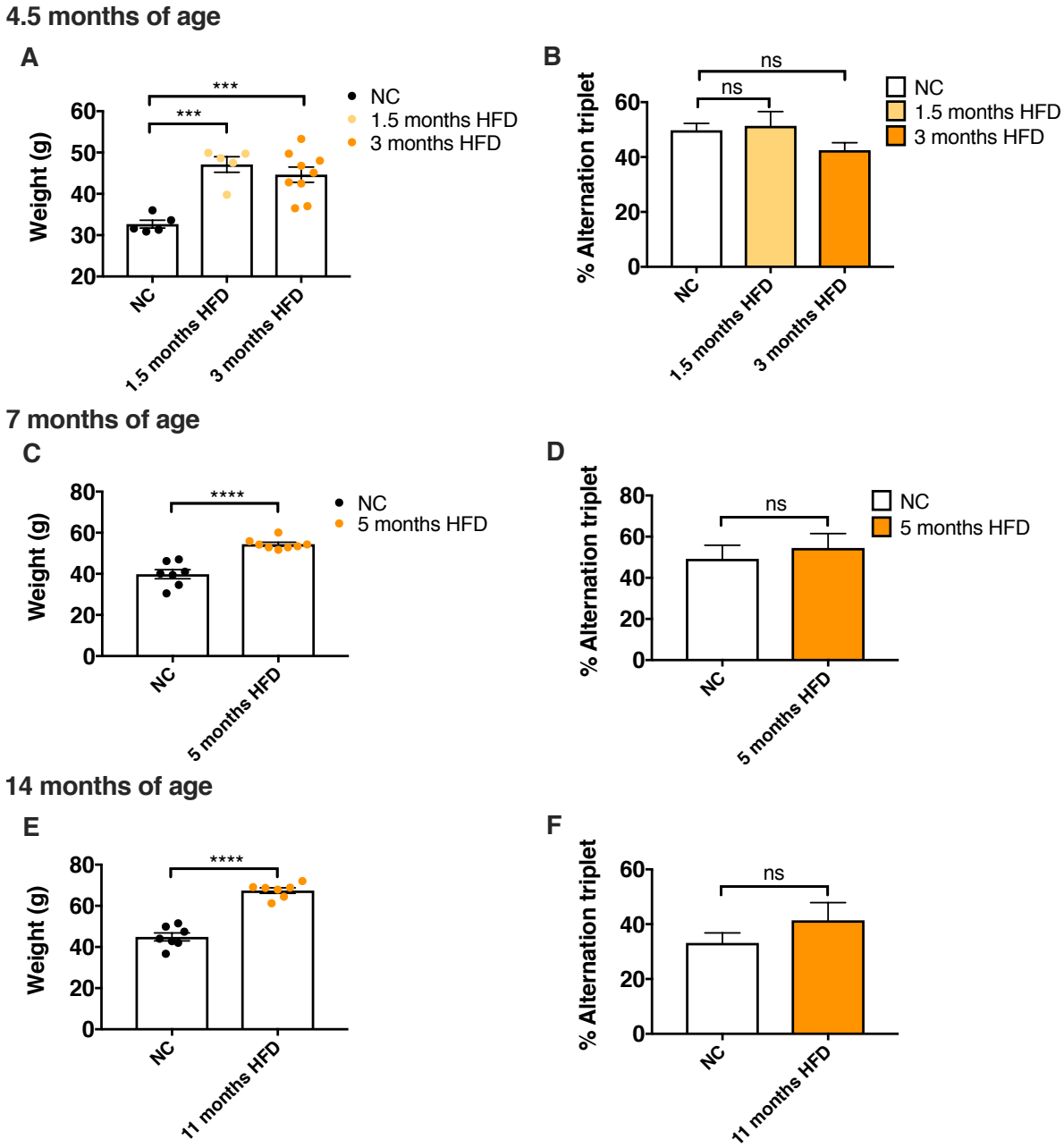

Figure 4.1. HFD treatment significantly increased body weight but did not negatively impact working memory.
(**A**) 1.5 and 3 months of HFD (light orange and dark orange dots, respectively) significantly increased body weight in 4.5 month-old mice compared to control mice fed normal chow (NC; black dots).
(**B**) There was no difference in percent alternation triplet between mice treated with HFD for 1.5 (light orange bar) nor 3 months (dark orange bar) compared to NC controls (open bar) at 4.5 months of age. (**A** and **B**) All data are mean ± SEM (n = 5 NC control, n = 5 HFD for 1.5 months, n = 10 HFD for 3 months). One-way ANOVA with Tukey's post hoc tests between groups: ***$p<0.001$.
(**C**) 7 month-old mice fed a HFD for 5 months (dark orange dots) weighed significantly more than age-matched controls fed NC (black dots).
(**D**) There was no difference in percent alternation triplet between 7 month-old mice fed a HFD for 5 months (dark orange bar) and aged-matched controls on NC (open bar). (**C** and **D)** All data are mean ± SEM (n = 7 NC control, n = 8 HFD for 5 months). Unpaired t-tests: ****$p<0.0001$.
(**E**) 14 month-old mice fed a HFD for 11 months (dark orange dots) had significantly increased body weight compared to aged-matched controls fed NC (black dots).
(**F**) There was no significant difference in percent alternation triplet between 14 month-old mice fed a HFD fro 11 months and age-matched, NC-fed controls. (**E** and **F**) All data are mean ± SEM (n = 7 NC control, n = 7 HFD for 11 months). Unpaired t-tests: ****$p<0.0001$.

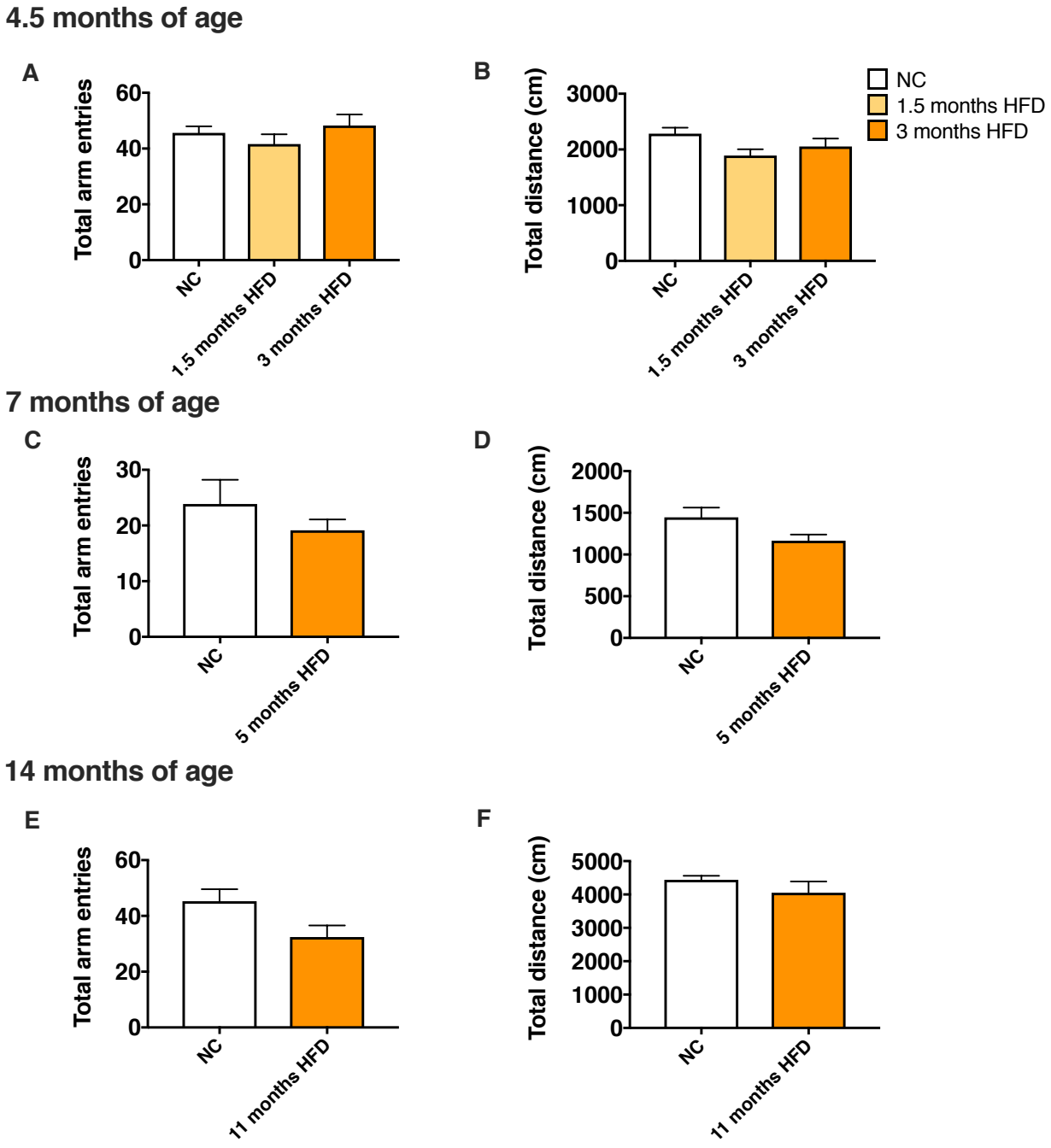

Figure 4.2. Additional information for Y maze testing.
(**A**) There was no difference in the total number of arm entries nor total distance traveled (**B**) in the Y maze between mice treated with HFD for 1.5 (light orange bar) nor 3 months (dark orange bar) compared to normal chow (NC) controls (open bar) at 4.5 months of age. Data are mean ± SEM (n = 5 NC control, n = 5 HFD for 1.5 months, n = 10 HFD for 3 months). One-way ANOVA with Tukey's post hoc tests.
(**C**) There was no difference in the total number of arm entries nor total distance traveled (**D**) in the Y maze between mice treated with HFD for 5 months (dark orange bar)

compared to normal chow (NC) controls (open bar) at 7 months of age. Data are mean ± SEM (n = 7 NC control, n = 8 HFD for 5 months). Unpaired t-test.
(**E**) There was no difference in the total number of arm entries or total distance traveled (**F**) in the Y maze between mice treated with HFD for 11 months (dark orange bar) compared to normal chow (NC) controls (open bar) at 14 months of age. Data are mean ± SEM (n = 7 NC control, n = 7 HFD for 11 months). Unpaired t-test.

Prolonged HFD treatment does not significantly affect *Phf15* mRNA expression in frontal cortical regions

I found no difference in *Phf15* mRNA levels in frontal cortical regions (Figure 4.3A) between middle-aged (14-month old) mice fed a HFD for 12 months and NC-fed, age-matched controls. Although there was a significant difference in body weight (Figure 4.3B), fasted blood glucose levels also did not differ (Figure 4.3C).

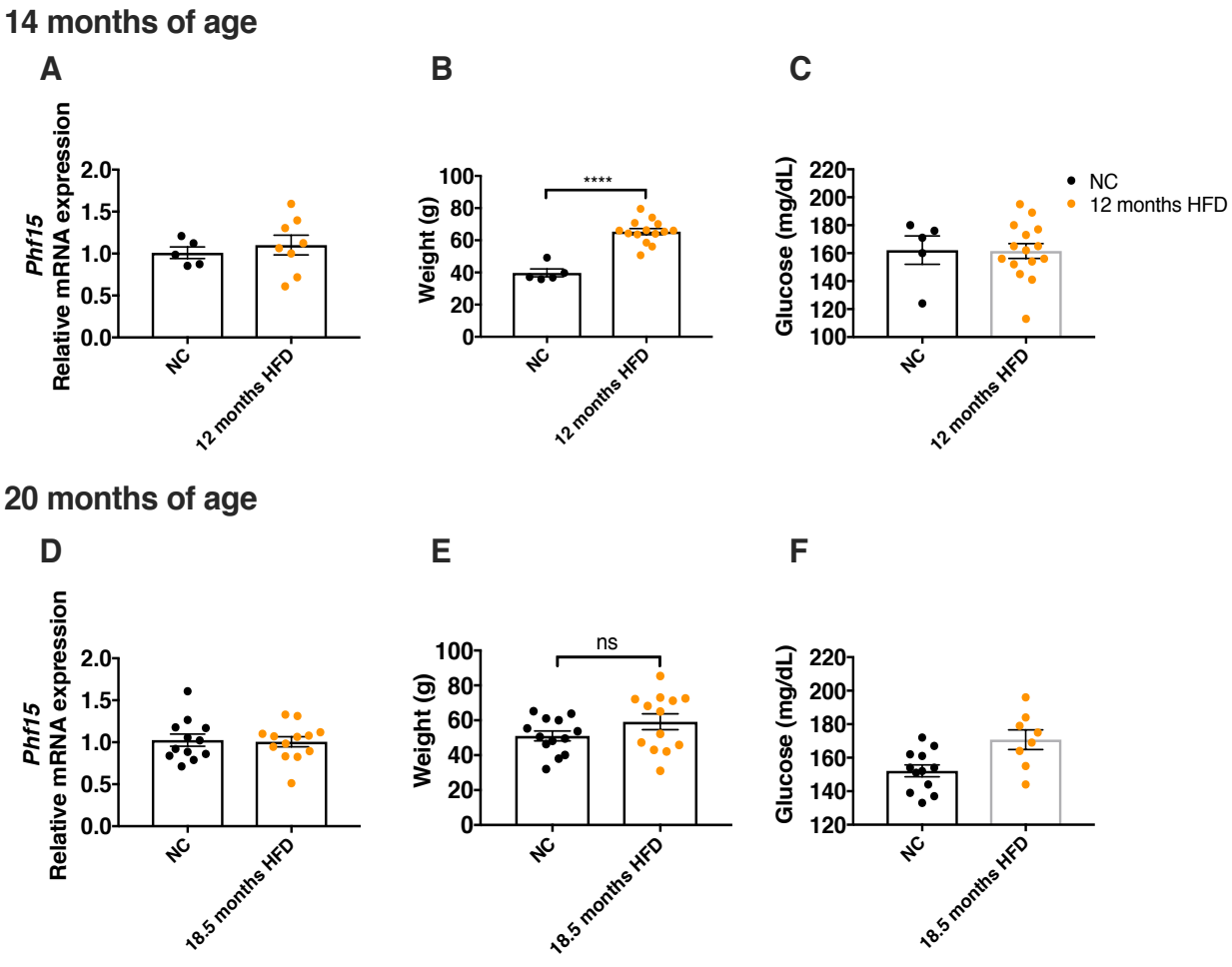

Figure 4.3. *Phf15* mRNA levels in frontal cortical areas did not differ between HFD and NC-fed mice during middle or old age.

(**A**) There was no difference in *Phf15* mRNA expression in frontal cortical regions of 14-month old ('middle-aged') mice fed a HFD for 12 months (orange dots) and age-matched NC-fed control mice (black dots). Data are mean ± SEM (n = 5 NC control, n = 8 HFD). Unpaired t-tests.
(**B**) There was a significant difference in body weight between 14-month old mice fed a HFD for 12 months and age-matched NC-fed control animals. Data are mean ± SEM (n = 5 NC control, n = 14 HFD). Unpaired t-test: *****p<0.0001*.
(**C**) There was no difference in blood glucose levels between 14-month old (middle-aged) mice fed a HFD for 12 months (orange dots) and age-matched NC-fed control mice (black dots). Data are mean ± SEM (n = 5 NC control, n = 15 HFD). Unpaired t-test.
(**D**) There was no difference in *Phf15* mRNA expression in frontal cortical regions of 20-month old ('old') mice fed a HFD for 18.5 months (orange dots) and age-matched NC-fed control mice (black dots). Data are mean ± SEM (n = 12 NC control, n = 13 HFD). Unpaired t-tests.
(**E**) There was no significant difference in body weight between 20-month old mice fed a HFD for 18.5 months and age-matched NC-fed control animals. Data are mean ± SEM (n = 13 NC control, n = 13 HFD). Unpaired t-test.
(**F**) There was no difference in blood glucose levels between 20-month old ('old') mice fed a HFD for 18.5 months (orange dots) and age-matched NC-fed control mice (black dots). Data are mean ± SEM (n = 12 NC control, n = 8 HFD). Unpaired t-test.

There was also no significant difference in *Phf15* mRNA expression between old (20-month old) mice fed a HFD for 18.5 months and age-matched controls (Figure 4.3D). As I had previously shown that *Phf15* mRNA levels increased significantly by 20 months of age compared to young controls [168], perhaps the HFD intervention lowered this increase to control levels. There was no difference in blood glucose levels after a 5-6 hour fast between mice fed a HFD for 18.5 months compared to age-matched controls (Figure 4.3F) or any differences in body weight (Figure 4.3E).

Section 4.3: Discussion

Although previous studies have reported memory-related cognitive deficits resulting from HFD treatment [186,187,189], I did not find any changes in percent alternation triplet in the Y maze, a measure of working memory, for any length of HFD treatment tested in this study. As expected, there was a significant increase in body weight for mice at different ages and increasing length of HFD, the latter compared to age-matched controls, except for the 20-months of age/18.5 months of HFD treatment group.

I also found no difference in fasted blood glucose at 20 months of age/18.5 months of HFD nor 14 months of age ('middle-age')/12 months of HFD. Although, HFD treatment is a widely applied protocol for inducing metabolic dysfunction in mice, studies have found divergent responses between increased body weight and fasting blood

glucose levels, with some studies finding positive correlations [191] and others finding no correlation for similar lengths of HFD treatment [192]. In general, the period of HFD treatment in these studies (~12 to 20 weeks) tended to be shorter than in the present study.

Prolonged HFD treatment also did not significantly reduce *Phf15* mRNA expression levels in frontal cortical regions compared to NC-fed, age-matched controls. I had previously found increased *Phf15* mRNA expression in frontal cortical regions in 20-month old mice [168] and it is possible that 18.5 months HFD might have reduced this aging-related increase to control levels. Overall, although HFD significantly increased body weight in mice, I was unable to find any indication of metabolic dysfunction, working memory deficits or differences in *Phf15* levels in the brain.

Section 4.4: Materials and Methods

4.4.1: Ethics Statement

This study was carried out in accordance with the recommendations in the Guide for the Care and Use of Laboratory Animals of the National Institutes of Health. The Animal Use Protocol (AUP-2017-02-9539) was approved by the Animal Care and Use Committee of the University of California, Berkeley.

4.4.2: Animals and Diets

C57BL/6J male mice were purchased from the Jackson Laboratory and randomly assigned to NC or HFD (D12492 Rodent Diet with 60 kcal% fat, Research Diets Inc., New Brunswick, NJ). HFD supplemented 60% calories from fat, 20% calories from carbohydrates and 20% calories from protein. Mice were maintained on a 12:12-h light–dark cycle (lights on at 0700 hours) with *ad libitum* access to food and water. All animal care and procedures were approved by the University of California, Berkeley Animal Care and Use Committee.

4.4.4: Behavioral Studies

Y maze. The Y maze was used to assess working memory by measuring spontaneous alternation [175]**.** The apparatus consisted of three identical plastic arms set at 120° from each other. Individual subject mice were placed in the center portion of the maze and were allowed to freely explore for 10 minutes. Movement in the Y maze was tracked, recorded and analyzed using the SMART 3.0 Video Tracking Software (Panlab; Harvard Apparatus, Holliston, MA).). Three consecutive entries into three different arms was considered an alternation triplet (e.g. ABC or BCA or CAB). Percent alternation triplet was calculated as: (Number of alternation triplets x 100)/(Max Alternation Triplet) where the Max Alternation Triplet = Total Arm Entries –2.

4.4.5: Blood glucose measurement

Mice were fasted for 5-6 hours and blood glucose was measured via tail nick using an Accu-Chek Performa glucose meter and Accu-Chek Performa test strips (Accu-Chek, Roche, Indianapolis, IN).

4.4.6: RNA extraction

At the indicated ages (14 or 20 months of age), mice were quickly sacrificed according to the approved protocol. Brains were isolated and frontal cortical areas were dissected, flash frozen and stored at – 80°C. RNA was extracted using a bead homogenizer (30 seconds, setting '5''; Bead Mill, VWR) in Trizol reagent (ThermoFisher, Waltham, MA). After homogenization, tubes were incubated at room temperature for 5 min and spun down at 12,000 g for 5 min at 4C. The supernatant was transferred to a fresh RNase/DNase free eppendorf and total RNA was extracted using the Direct-zol RNA miniprep kit (Zymo Research, Irvine, CA) according to the manufacturer's instructions.

4.4.7: Real-time quantitative PCR (RT-qPCR)

cDNA was reversed transcribed from total RNA using the SuperScript™ III First-Strand Synthesis System kit (ThermoFisher, Waltham, MA) following the manufacturer's instructions. RT-qPCR was run using SYBR green (Roche, Pleasanton, CA) on a QuantiStudio 6 (ThermoFisher, Waltham, MA) real-time PCR machine. All RT-qPCR primers were specific to the desired template, spanned exon-exon junctions and captured all transcript variants for the specific gene under study. Primers were designed using SnapGene and NCBI Primer BLAST software. Specificity of primer pairs was confirmed using melt curve analysis. Ct values were normalized to the housekeeping gene *Hprt* and fold-change differences were determined using the delta-delta Ct ($2^{-\Delta\Delta Ct}$) method. Primer sequences used in this study are listed in Table 4.1.

Table 4.1. List of RT-qPCR primers

Genes	Direction	Sequence
Phf15	+	TCAGCATCAAGATGTTCCAAACT
	-	TGAGCTGGTATGAATCTGGGA
Hprt	+	TCAGTCAACGGGGGACATAAA
	-	GGGGCTGTACTGCTTAACCAG

Phf15, PHD finger protein 15; *Hprt*, Hypoxanthine Phosphoribosyltransferase.

4.4.8: Statistical Analysis

Prism 8 software (GraphPad, San Diego, CA) was used for statistical analysis. P values were calculated using Unpaired t-tests or 1-way ANOVA as indicated.

Chapter 5: Closing Remarks

My work [168] describes the function of a completely novel repressor of microglial inflammatory function—PHD finger protein 15 (*Phf15*)—that may be especially relevant in regulating the age-induced microglial proinflammatory phenotype. Using a murine microglial cell line (SIM-A9), I showed that *Phf15*, one of the top 25 microglial genes upregulated during healthy aging in humans [100] and a putative epigenetic gene regulator, inhibits expression of various proinflammatory mediators (Tumor necrosis factor α (*Tnfα*), Interleukin 1β (*Il-1β*), Nitric oxide synthase, inducible (*Nos2*)) under basal (no immune stimulation) and signal-dependent activation, i.e., after induction with Toll-like receptor (TLR) 4, TLR3 and TLR9 ligands. Importantly, *Phf15* also regulates the magnitude *and* duration of the microglial inflammatory response. Because excessive and unresolved microglial-mediated inflammation is a key contributor to the pathophysiology of many age-dependent neurodegenerative diseases like Parkinson's and Alzheimer's disease [92–96] finding repressors that can strongly regulate the microglial inflammatory response is crucial for possible future therapeutic interventions.

Importantly, a critical point in the control of inflammation occurs at the level of gene transcription with distinct molecular mechanisms regulating different aspects of the response. Basal state repression, for example, involves recruitment of co-repressor complexes that prevent initiation of inflammatory gene transcription. After immune stimulation, additional mechanisms can restrain active transcription and maintain quiescence. Finally, numerous mechanisms mediate the resolution of the inflammatory response, including mechanisms that remove transcription factors from inflammatory gene promoters (termed transrepression) (for review see [97–99]). It is noteworthy that *Phf15* is involved in the regulation of several of these.

Perhaps most interestingly, global transcriptional changes after deletion of *Phf15* in mouse microglia closely mimicked recently published aged microglial inflammatory phenotypes [153–155]. Specifically, microglia of aged mice (18-24 months of age) increase expression of type I interferon (IFN-I) responsive genes, upregulating a very similar set of genes to our *Phf15* knockout microglia under basal conditions. This suggests that *Phf15* could function as a regulatory checkpoint, restraining the transition from homeostatic towards the chronic, proinflammatory, IFN-I responsive state seen in microglia during aging.

Additionally, my work also explored whether factors that are known contributors to aging-induced inflammation (inflammaging), for example a high fat diet (HFD) and resulting obesity or cellular senescence might contribute to brain inflammation and cognitive dysfunction via inhibition of microglial *Phf15*. Although I found that expression of Interleukin-6 *(Il-6*), a classic marker of the senescence-associated secretory phenotype (SASP) [51,52] was decreased in hippocampus—an area that mediates various memory-related processes—of aged (27 month old) of STING-deficient mice, this did not translate into improved working memory function nor differences in *Phf15* levels in the brain. Thus, expression of SASP-related inflammatory factors by the cGAS-STING pathway might not proceed via inhibition of *Phf15*. Similarly, prolonged HFD treatment and obesity did not affect working memory or levels of *Phf15* in the mouse brain,

suggesting that brain inflammation resulting from a HFD or obesity is not a result of decreased levels of *Phf15*.

References

1. Ferrucci, L. *et al.* The origins of age-related proinflammatory state. *Blood* **105**, 2294–2299 (2005).
2. Ferrucci, L. & Fabbri, E. Inflammageing: chronic inflammation in ageing, cardiovascular disease, and frailty. *Nat. Rev. Cardiol.* 1–18 (2018) doi:10.1038/s41569-018-0064-2.
3. Franceschi, C. *et al.* Inflamm-aging: An Evolutionary Perspective on Immunosenescence. *Ann. N. Y. Acad. Sci.* **908**, 244–254 (2006).
4. Fulop, T. *et al.* Immunosenescence and Inflamm-Aging As Two Sides of the Same Coin: Friends or Foes? *Front. Immunol.* **8**, 1960 (2018).
5. Ruparelia, N., Chai, J. T., Fisher, E. A. & Choudhury, R. P. Inflammatory processes in cardiovascular disease: a route to targeted therapies. *Nat. Rev. Cardiol.* **14**, 133–144 (2017).
6. Leonardi, G. C., Accardi, G., Monastero, R., Nicoletti, F. & Libra, M. Ageing: from inflammation to cancer. *Immun. Ageing* **15**, 1 (2018).
7. Miller, A. H. & Raison, C. L. The role of inflammation in depression: from evolutionary imperative to modern treatment target. *Nat. Rev. Immunol.* **16**, 22–34 (2016).
8. Mosher, K. I. & Wyss-Coray, T. Microglial dysfunction in brain aging and Alzheimer's disease. *Biochem. Pharmacol.* **88**, 594–604 (2014).
9. Gorelick, P. B. Role of inflammation in cognitive impairment: results of observational epidemiological studies and clinical trials: Gorelick. *Ann. N. Y. Acad. Sci.* **1207**, 155–162 (2010).
10. Calabrese, V. *et al.* Aging and Parkinson's Disease: Inflammaging, neuroinflammation and biological remodeling as key factors in pathogenesis. *Free Radic. Biol. Med.* **115**, 80–91 (2018).
11. Baylis, D., Bartlett, D. B., Patel, H. P. & Roberts, H. C. Understanding how we age: insights into inflammaging. *Longev. Heal.* **2**, 8 (2013).
12. Fabbri, E. *et al.* Aging and the Burden of Multimorbidity: Associations With Inflammatory and Anabolic Hormonal Biomarkers. *J. Gerontol. Ser. A* **70**, 63–70 (2015).
13. Soysal, P. *et al.* Inflammation and frailty in the elderly: A systematic review and meta-analysis. *Ageing Res. Rev.* **31**, 1–8 (2016).
14. Di Cesare, M. Trends in adult body-mass index in 200 countries from 1975 to 2014: a pooled analysis of 1698 population-based measurement studies with 19·2 million participants. *The Lancet* **387**, 1377–1396 (2016).
15. Kanoski, S. E. & Davidson, T. L. Western diet consumption and cognitive impairment: Links to hippocampal dysfunction and obesity. *Physiol. Behav.* **103**, 59–68 (2011).
16. Gregor, M. F. & Hotamisligil, G. S. Inflammatory mechanisms in obesity. *Annu. Rev. Immunol.* **29**, 415–445 (2011).
17. Hotamisligil, G. S. Inflammation, metaflammation and immunometabolic disorders. *Nature* **542**, 177–185 (2017).

18. Lumeng, C. N. & Saltiel, A. R. Inflammatory links between obesity and metabolic disease. *J. Clin. Invest.* **121**, 2111–2117 (2011).
19. Elias, M. F., Elias, P. K., Sullivan, L. M., Wolf, P. A. & D'Agostino, R. B. Lower cognitive function in the presence of obesity and hypertension: the Framingham heart study. *Int. J. Obes.* **27**, 260–268 (2003).
20. Elias, M. F., Elias, P. K., Sullivan, L. M., Wolf, P. A. & D'Agostino, R. B. Obesity, diabetes and cognitive deficit: The Framingham Heart Study. *Neurobiol. Aging* **26**, 11–16 (2005).
21. Valdearcos, M. *et al.* Microglial Inflammatory Signaling Orchestrates the Hypothalamic Immune Response to Dietary Excess and Mediates Obesity Susceptibility. *Cell Metab.* **26**, 185-197.e3 (2017).
22. Kopp, A. *et al.* Toll-like receptor ligands cause proinflammatory and prodiabetic activation of adipocytes via phosphorylation of extracellular signal-regulated kinase and c-Jun N-terminal kinase but not interferon regulatory factor-3. *Endocrinology* **151**, 1097–1108 (2010).
23. Huang, S. *et al.* Saturated fatty acids activate TLR-mediated proinflammatory signaling pathways. *J. Lipid Res.* **53**, 2002–2013 (2012).
24. Erridge, C., Attina, T., Spickett, C. M. & Webb, D. J. A high-fat meal induces low-grade endotoxemia: evidence of a novel mechanism of postprandial inflammation. *Am. J. Clin. Nutr.* **86**, 1286–1292 (2007).
25. Laugerette, F. *et al.* Emulsified lipids increase endotoxemia: possible role in early postprandial low-grade inflammation. *J. Nutr. Biochem.* **22**, 53–59 (2011).
26. Ghoshal, S., Witta, J., Zhong, J., de Villiers, W. & Eckhardt, E. Chylomicrons promote intestinal absorption of lipopolysaccharides. *J. Lipid Res.* **50**, 90–97 (2009).
27. Shapiro, H., Thaiss, C. A., Levy, M. & Elinav, E. The cross talk between microbiota and the immune system: metabolites take center stage. *Curr. Opin. Immunol.* **30**, 54–62 (2014).
28. Mariat, D. *et al.* The Firmicutes/Bacteroidetes ratio of the human microbiota changes with age. *BMC Microbiol.* **9**, 123 (2009).
29. Moreira, A. P. B., Texeira, T. F. S., Ferreira, A. B., Peluzio, M. do C. G. & Alfenas, R. de C. G. Influence of a high-fat diet on gut microbiota, intestinal permeability and metabolic endotoxaemia. *Br. J. Nutr.* **108**, 801–809 (2012).
30. Pepping, J. K., Freeman, L. R., Gupta, S., Keller, J. N. & Bruce-Keller, A. J. NOX2 deficiency attenuates markers of adiposopathy and brain injury induced by high-fat diet. *Am. J. Physiol. - Endocrinol. Metab.* **304**, E392–E404 (2013).
31. Nerurkar, P. V. *et al.* Momordica charantia (bitter melon) attenuates high-fat diet-associated oxidative stress and neuroinflammation. *J. Neuroinflammation* **8**, 64 (2011).
32. Bocarsly, M. E. *et al.* Obesity diminishes synaptic markers, alters microglial morphology, and impairs cognitive function. *Proc. Natl. Acad. Sci.* **112**, 15731–15736 (2015).
33. Debette, S. *et al.* Abdominal obesity and lower gray matter volume: a Mendelian randomization study. *Neurobiol. Aging* **35**, 378–386 (2014).

34. Raji, C. A. *et al.* Brain structure and obesity. *Hum. Brain Mapp.* **31**, 353–364 (2010).
35. Janowitz, D. *et al.* Association between waist circumference and gray matter volume in 2344 individuals from two adult community-based samples. *NeuroImage* **122**, 149–157 (2015).
36. Karlsson, H. K. *et al.* Obesity is associated with white matter atrophy: a combined diffusion tensor imaging and voxel-based morphometric study. *Obes. Silver Spring Md* **21**, 2530–2537 (2013).
37. Marsland, A. L. *et al.* Brain morphology links systemic inflammation to cognitive function in midlife adults. *Brain. Behav. Immun.* **48**, 195–204 (2015).
38. Hao, S., Dey, A., Yu, X. & Stranahan, A. M. Dietary obesity reversibly induces synaptic stripping by microglia and impairs hippocampal plasticity. *Brain. Behav. Immun.* **51**, 230–239 (2016).
39. Lu, J. *et al.* Ursolic acid improves high fat diet-induced cognitive impairments by blocking endoplasmic reticulum stress and IκB kinase β/nuclear factor-κB-mediated inflammatory pathways in mice. *Brain. Behav. Immun.* **25**, 1658–1667 (2011).
40. Jeon, B. T. *et al.* Resveratrol Attenuates Obesity-Associated Peripheral and Central Inflammation and Improves Memory Deficit in Mice Fed a High-Fat Diet. *Diabetes* **61**, 1444–1454 (2012).
41. Pistell, P. J. *et al.* Cognitive impairment following high fat diet consumption is associated with brain inflammation. *J. Neuroimmunol.* **219**, 25–32 (2010).
42. Donath, M. Y. & Shoelson, S. E. Type 2 diabetes as an inflammatory disease. *Nat. Publ. Group* **11**, 98–107 (2011).
43. Mallorquí-Bagué, N. *et al.* Type 2 diabetes and cognitive impairment in an older population with overweight or obesity and metabolic syndrome: baseline cross-sectional analysis of the PREDIMED-plus study. *Sci. Rep.* **8**, 16128–9 (2018).
44. Munshi, M. N. Cognitive Dysfunction in Older Adults With Diabetes: What a Clinician Needs to Know. *Diabetes Care* **40**, 461–467 (2017).
45. Barnes, D. E. & Yaffe, K. The projected effect of risk factor reduction on Alzheimer's disease prevalence. *Lancet Neurol.* **10**, 819–828 (2011).
46. Spangenberg, E. E. & Green, K. N. Inflammation in Alzheimer's disease: Lessons learned from microglia-depletion models. *Brain. Behav. Immun.* **61**, 1–11 (2017).
47. Akiyama, H. *et al.* Inflammation and Alzheimer's disease. *Neurobiol. Aging* **21**, 383–421 (2000).
48. Austad, S. N. *Inflammation and Aging*. (2019).
49. Campisi, J. & Fagagna, F. d'Adda di. Cellular senescence: when bad things happen to good cells. *Nat. Rev. Mol. Cell Biol.* **8**, 729–740 (2007).
50. Collado, M., Blasco, M. A. & Serrano, M. Cellular Senescence in Cancer and Aging. *Cell* **130**, 223–233 (2007).
51. Glück, S. *et al.* Innate immune sensing of cytosolic chromatin fragments through cGAS promotes senescence. *Nat. Cell Biol.* **19**, 1061–1070 (2017).
52. Coppé, J.-P., Desprez, P.-Y., Krtolica, A. & Campisi, J. The Senescence-Associated Secretory Phenotype: The Dark Side of Tumor Suppression. *Annu. Rev. Pathol. Mech. Dis.* **5**, 99–118 (2010).

53. Tchkonia, T., Zhu, Y., Deursen, J. van, Campisi, J. & Kirkland, J. L. Cellular senescence and the senescent secretory phenotype: therapeutic opportunities. *J. Clin. Invest.* **123**, 966–972 (2013).
54. Acosta, J. C. *et al.* A complex secretory program orchestrated by the inflammasome controls paracrine senescence. *Nat. Cell Biol.* **15**, 978–990 (2013).
55. Nelson, G. *et al.* A senescent cell bystander effect: senescence-induced senescence. *Aging Cell* **11**, 345–349 (2012).
56. Yang, H., Wang, H., Ren, J., Chen, Q. & Chen, Z. J. cGAS is essential for cellular senescence. *Proc. Natl. Acad. Sci.* **114**, E4612–E4620 (2017).
57. Diner, E. J. *et al.* The innate immune DNA sensor cGAS produces a noncanonical cyclic dinucleotide that activates human STING. *Cell Rep.* **3**, 1355–1361 (2013).
58. Ablasser, A. & Gulen, M. F. The role of cGAS in innate immunity and beyond. *J. Mol. Med.* **94**, 1085–1093 (2016).
59. Baker, D. J. & Petersen, R. C. Cellular senescence in brain aging and neurodegenerative diseases: evidence and perspectives. *J. Clin. Invest.* **128**, 1208–1216 (2018).
60. Zhang, P. *et al.* Senolytic therapy alleviates Aβ-associated oligodendrocyte progenitor cell senescence and cognitive deficits in an Alzheimer's disease model. *Nat. Neurosci.* **22**, 719–728 (2019).
61. Chinta, S. J. *et al.* Cellular senescence and the aging brain. *Exp. Gerontol.* **68**, 3–7 (2015).
62. Benarroch, E. E. Neuron-Astrocyte Interactions: Partnership for Normal Function and Disease in the Central Nervous System. *Mayo Clin. Proc.* **80**, 1326–1338 (2005).
63. Magistretti, P. J. Neuron–glia metabolic coupling and plasticity. *J. Exp. Biol.* **209**, 2304–2311 (2006).
64. Yankner, B. A., Lu, T. & Loerch, P. The Aging Brain. *Annu. Rev. Pathol. Mech. Dis.* **3**, 41–66 (2008).
65. Nimmerjahn, A., Kirchhoff, F. & Helmchen, F. Resting microglial cells are highly dynamic surveillants of brain parenchyma in vivo. *Science* **308**, 1314–1318 (2005).
66. Neumann, H., Kotter, M. R. & Franklin, R. J. M. Debris clearance by microglia: an essential link between degeneration and regeneration. *Brain J. Neurol.* **132**, 288–295 (2009).
67. Parkhurst, C. N. & Gan, W.-B. Microglia dynamics and function in the CNS. *Curr. Opin. Neurobiol.* **20**, 595–600 (2010).
68. Parkhurst, C. N. *et al.* Microglia Promote Learning-Dependent Synapse Formation through Brain-Derived Neurotrophic Factor. *Cell* **155**, 1596–1609 (2013).
69. Schafer, D. P. *et al.* Microglia Sculpt Postnatal Neural Circuits in an Activity and Complement-Dependent Manner. *Neuron* **74**, 691–705 (2012).
70. Wake, H., Moorhouse, A. J., Miyamoto, A. & Nabekura, J. Microglia: actively surveying and shaping neuronal circuit structure and function. *Trends Neurosci.* **36**, 209–217 (2013).
71. Kettenmann, H., Hanisch, U.-K., Noda, M. & Verkhratsky, A. Physiology of microglia. *Physiol. Rev.* **91**, 461–553 (2011).

72. Ransohoff, R. M. & Perry, V. H. Microglial physiology: unique stimuli, specialized responses. *Annu. Rev. Immunol.* **27**, 119–145 (2009).
73. Saijo, K. & Glass, C. K. Microglial cell origin and phenotypes in health and disease. *Nat. Publ. Group* **11**, 775–787 (2011).
74. Hanisch, U.-K. & Kettenmann, H. Microglia: active sensor and versatile effector cells in the normal and pathologic brain. *Nat. Neurosci.* **10**, 1387–1394 (2007).
75. Wang, Z. *et al.* Saturated fatty acids activate microglia via Toll-like receptor 4/NF-κB signalling. *Br. J. Nutr.* **107**, 229–241 (2012).
76. Valdearcos, M. *et al.* Microglia Dictate the Impact of Saturated Fat Consumption on Hypothalamic Inflammation and Neuronal Function. *Cell Rep.* **9**, 2124–2138 (2014).
77. Button, E. B. *et al.* Microglial Cell Activation Increases Saturated and Decreases Monounsaturated Fatty Acid Content, but Both Lipid Species are Proinflammatory. *Lipids* **49**, 305–316 (2014).
78. Baden, P., De Cicco, S., Yu, C. & Deleidi, M. Immune Senescence and Inflammaging in Neurological Diseases. in *Handbook of Immunosenescence* (eds. Fulop, T., Franceschi, C., Hirokawa, K. & Pawelec, G.) 1–21 (Springer International Publishing, 2018). doi:10.1007/978-3-319-64597-1_143-1.
79. Bernhardi, R. V., Tichauer, J. E. & Eugenín, J. Aging-dependent changes of microglial cells and their relevance for neurodegenerative disorders. *J. Neurochem.* **112**, 1099–1114 (2010).
80. Nakanishi, H. & Wu, Z. Microglia-aging: Roles of microglial lysosome- and mitochondria-derived reactive oxygen species in brain aging. *Behav. Brain Res.* **201**, 1–7 (2009).
81. Itagaki, S., McGeer, P. L., Akiyama, H., Zhu, S. & Selkoe, D. Relationship of microglia and astrocytes to amyloid deposits of Alzheimer disease. *J. Neuroimmunol.* **24**, 173–182 (1989).
82. Styren, S. D., Civin, W. H. & Rogers, J. Molecular, cellular, and pathologic characterization of HLA-DR immunoreactivity in normal elderly and Alzheimer's disease brain. *Exp. Neurol.* **110**, 93–104 (1990).
83. Arends, Y. M., Duyckaerts, C., Rozemuller, J. M., Eikelenboom, P. & Hauw, J.-J. Microglia, amyloid and dementia in Alzheimer disease: A correlative study. *Neurobiol. Aging* **21**, 39–47 (2000).
84. Di Patre, P. L. *et al.* Progression of clinical deterioration and pathological changes in patients with Alzheimer disease evaluated at biopsy and autopsy. *Arch. Neurol.* **56**, 1254–1261 (1999).
85. Landreth, G. E. & Reed-Geaghan, E. G. Toll-Like Receptors in Alzheimer's Disease. in *Toll-like Receptors: Roles in Infection and Neuropathology* (ed. Kielian, T.) 137–153 (Springer, 2009). doi:10.1007/978-3-642-00549-7_8.
86. Ye, S.-M. & Johnson, R. W. Increased interleukin-6 expression by microglia from brain of aged mice. *J. Neuroimmunol.* **93**, 139–148 (1999).
87. Njie, eMalick G. *et al.* Ex vivo cultures of microglia from young and aged rodent brain reveal age-related changes in microglial function. *Neurobiol. Aging* **33**, 195.e1-195.e12 (2012).

88. Lai, A. Y., Dibal, C. D., Armitage, G. A., Winship, I. R. & Todd, K. G. Distinct activation profiles in microglia of different ages: A systematic study in isolated embryonic to aged microglial cultures. *Neuroscience* **254**, 185–195 (2013).
89. Yu, W. H. *et al.* Phenotypic and functional changes in glial cells as a function of age. *Neurobiol. Aging* **23**, 105–115 (2002).
90. Conde, J. R. & Streit, W. J. Effect of aging on the microglial response to peripheral nerve injury. *Neurobiol. Aging* **27**, 1451–1461 (2006).
91. Sawada, M., Sawada, H. & Nagatsu, T. Effects of Aging on Neuroprotective and Neurotoxic Properties of Microglia in Neurodegenerative Diseases. *Neurodegener. Dis.* **5**, 254–256 (2008).
92. Orre, M. *et al.* Reactive glia show increased immunoproteasome activity in Alzheimer's disease. *Brain J. Neurol.* **136**, 1415–1431 (2013).
93. Cribbs, D. H. *et al.* Extensive innate immune gene activation accompanies brain aging, increasing vulnerability to cognitive decline and neurodegeneration: a microarray study. *J. Neuroinflammation* **9**, 179 (2012).
94. Frank, S. *et al.* TREM2 is upregulated in amyloid plaque-associated microglia in aged APP23 transgenic mice. *Glia* **56**, 1438–1447 (2008).
95. Frank-Cannon, T. C., Alto, L. T., McAlpine, F. E. & Tansey, M. G. Does neuroinflammation fan the flame in neurodegenerative diseases? *Mol. Neurodegener.* **4**, 47 (2009).
96. Sugama, S. Stress-induced microglial activation may facilitate the progression of neurodegenerative disorders. *Med. Hypotheses* **73**, 1031–1034 (2009).
97. Medzhitov, R. & Horng, T. Transcriptional control of the inflammatory response. *Nat. Rev. Immunol.* **9**, 692–703 (2009).
98. Glass, C. K. & Ogawa, S. Combinatorial roles of nuclear receptors in inflammation and immunity. *Nat. Rev. Immunol.* **6**, 44–55 (2005).
99. Glass, C. K. & Saijo, K. Nuclear receptor transrepression pathways that regulate inflammation in macrophages and T cells. *Nat. Publ. Group* **10**, 365–376 (2010).
100. Soreq, L. *et al.* Major Shifts in Glial Regional Identity Are a Transcriptional Hallmark of Human Brain Aging. *Cell Rep.* **18**, 557–570 (2017).
101. Panchenko, M. V. Structure, function and regulation of jade family PHD finger 1 (JADE1). *Gene* **589**, 1–11 (2016).
102. Musselman, C. A. & Kutateladze, T. G. PHD Fingers: Epigenetic Effectors and Potential Drug Targets. *Mol. Interv.* **9**, 314–323 (2009).
103. Kalkhoven, E., Teunissen, H., Houweling, A., Verrijzer, C. P. & Zantema, A. The PHD Type Zinc Finger Is an Integral Part of the CBP Acetyltransferase Domain. *Mol. Cell. Biol.* **22**, 1961–1970 (2002).
104. Rack, J. G. M. *et al.* The PHD finger of p300 Influences Its Ability to Acetylate Histone and Non-Histone Targets. *J. Mol. Biol.* **426**, 3960–3972 (2014).
105. O'Connell, S. *et al.* Polycomblike PHD Fingers Mediate Conserved Interaction with Enhancer of Zeste Protein. *J. Biol. Chem.* **276**, 43065–43073 (2001).
106. Han, X. *et al.* Destabilizing LSD1 by Jade-2 promotes neurogenesis: an antibraking system in neural development. *Mol. Cell* **55**, 482–494 (2014).

107. Shi, Y. *et al.* Histone demethylation mediated by the nuclear amine oxidase homolog LSD1. *Cell* **119**, 941–953 (2004).
108. Foster, C. T. *et al.* Lysine-specific demethylase 1 regulates the embryonic transcriptome and CoREST stability. *Mol. Cell. Biol.* **30**, 4851–4863 (2010).
109. You, A., Tong, J. K., Grozinger, C. M. & Schreiber, S. L. CoREST is an integral component of the CoREST- human histone deacetylase complex. *Proc. Natl. Acad. Sci. U. S. A.* **98**, 1454–1458 (2001).
110. Saijo, K. *et al.* A Nurr1/CoREST pathway in microglia and astrocytes protects dopaminergic neurons from inflammation-induced death. *Cell* **137**, 47–59 (2009).
111. Foy, R. L. *et al.* Role of Jade-1 in the Histone Acetyltransferase (HAT) HBO1 Complex. *J. Biol. Chem.* **283**, 28817–28826 (2008).
112. Lalonde, M.-E. *et al.* Exchange of associated factors directs a switch in HBO1 acetyltransferase histone tail specificity. *Genes Dev.* **27**, 2009–2024 (2013).
113. Coles, A. H., Gannon, H., Cerny, A., Kurt-Jones, E. & Jones, S. N. Inhibitor of growth-4 promotes I B promoter activation to suppress NF- B signaling and innate immunity. *Proc. Natl. Acad. Sci.* **107**, 11423–11428 (2010).
114. Hickman, S., Izzy, S., Sen, P., Morsett, L. & El Khoury, J. Microglia in neurodegeneration. *Nat. Publ. Group* **21**, 1359–1369 (2018).
115. Salter, M. W. & Stevens, B. Microglia emerge as central players in brain disease. *Nat. Publ. Group* **23**, 1018–1027 (2017).
116. Glass, C. K., Saijo, K., Winner, B., Marchetto, M. C. & Gage, F. H. Mechanisms Underlying Inflammation in Neurodegeneration. *Cell* **140**, 918–934 (2010).
117. McCoy, M. K. Blocking Soluble Tumor Necrosis Factor Signaling with Dominant-Negative Tumor Necrosis Factor Inhibitor Attenuates Loss of Dopaminergic Neurons in Models of Parkinson's Disease. *J. Neurosci. Off. J. Soc. Neurosci.* **26**, 9365–9375 (2006).
118. Sriram, K. *et al.* Mice deficient in TNF receptors are protected against dopaminergic neurotoxicity: implications for Parkinson's disease. *FASEB J.* **16**, 1474–1476 (2002).
119. Smale, S. T. & Natoli, G. Transcriptional Control of Inflammatory Responses. *Cold Spring Harb. Perspect. Biol.* **6**, a016261–a016261 (2014).
120. Bernstein, B. E., Meissner, A. & Lander, E. S. The Mammalian Epigenome. *Cell* **128**, 669–681 (2007).
121. Smale, S. T., Tarakhovsky, A. & Natoli, G. Chromatin Contributions to the Regulation of Innate Immunity. *Annu. Rev. Immunol.* **32**, 489–511 (2014).
122. Baruch, K. *et al.* Aging. Aging-induced type I interferon response at the choroid plexus negatively affects brain function. *Science* **346**, 89–93 (2014).
123. Gabuzda, D. & Yankner, B. A. Physiology: Inflammation links ageing to the brain. *Nature* **497**, 197–198 (2013).
124. Godbout, J. P. *et al.* Exaggerated neuroinflammation and sickness behavior in aged mice following activation of the peripheral innate immune system. *FASEB J.* **19**, 1329–1331 (2005).

125. Sparkman, N. L. & Johnson, R. W. Neuroinflammation Associated with Aging Sensitizes the Brain to the Effects of Infection or Stress. *Neuroimmunomodulation* **15**, 323–330 (2008).
126. Craik, F. I. M. & Salthouse, T. A. *The Handbook of Aging and Cognition*. (Psychology Press, 2011). doi:10.4324/9780203837665.
127. Simen, A. A., Bordner, K. A., Martin, M. P., Moy, L. A. & Barry, L. C. Cognitive dysfunction with aging and the role of inflammation. *Ther. Adv. Chronic Dis.* **2**, 175–195 (2011).
128. Zhao, J. *et al.* Neuroinflammation induced by lipopolysaccharide causes cognitive impairment in mice. *Sci. Rep.* 1–12 (2019) doi:10.1038/s41598-019-42286-8.
129. Glaros, T. G. *et al.* Causes and consequences of low grade endotoxemia and inflammatory diseases. *Front. Biosci. J. Virtual Libr.* 754–765 (2013).
130. Sandiego, C. M. *et al.* Imaging robust microglial activation after lipopolysaccharide administration in humans with PET. *Proc. Natl. Acad. Sci. U. S. A.* **112**, 12468–12473 (2015).
131. Brown, G. C. The endotoxin hypothesis of neurodegeneration. 1–10 (2019) doi:10.1186/s12974-019-1564-7.
132. Chen, Y.-C. *et al.* Sequence variants of toll like receptor 4 and late-onset Alzheimer's disease. *PLoS ONE* **7**, e50771 (2012).
133. Perez-Pardo, P. *et al.* Role of TLR4 in the gut-brain axis in Parkinson's disease: a translational study from men to mice. *Gut* **68**, 829–843 (2019).
134. Akira, S. & Takeda, K. Toll-like receptor signalling. *Nat. Rev. Immunol.* **4**, 499–511 (2004).
135. Takeda, K. & Akira, S. TLR signaling pathways. *Semin. Immunol.* **16**, 3–9 (2004).
136. Zhou, Y. *et al.* Metascape provides a biologist-oriented resource for the analysis of systems-level datasets. *Nat. Commun.* 1–10 (2019) doi:10.1038/s41467-019-09234-6.
137. Chen, L.-F. & Greene, W. C. Shaping the nuclear action of NF-κB. *Nat. Rev. Mol. Cell Biol.* **5**, 392–401 (2004).
138. McDonald, P. P. Transcriptional regulation in neutrophils: teaching old cells new tricks. *Adv. Immunol.* **82**, 1–48 (2004).
139. Zheng, S., Hedl, M. & Abraham, C. Twist1 and Twist2 Contribute to Cytokine Downregulation following Chronic NOD2 Stimulation of Human Macrophages through the Coordinated Regulation of Transcriptional Repressors and Activators. *J. Immunol. Baltim. Md 1950* **195**, 217–226 (2015).
140. Lo, H.-Y. G. *et al.* A single transcription factor is sufficient to induce and maintain secretory cell architecture. *Genes Dev.* **31**, 154–171 (2017).
141. Kaminska, B., Mota, M. & Pizzi, M. Signal transduction and epigenetic mechanisms in the control of microglia activation during neuroinflammation. 1–13 (2016) doi:10.1016/j.bbadis.2015.10.026.
142. Nagatsu, T. & Sawada, M. Inflammatory process in Parkinson's disease: role for cytokines. *Curr. Pharm. Des.* **11**, 999–1016 (2005).
143. Boka, G. *et al.* Immunocytochemical analysis of tumor necrosis factor and its receptors in Parkinson's disease. *Neurosci. Lett.* **172**, 151–154 (1994).

144. Mogi, M. *et al.* Tumor necrosis factor-alpha (TNF-alpha) increases both in the brain and in the cerebrospinal fluid from parkinsonian patients. *Neurosci. Lett.* **165**, 208–210 (1994).
145. Qin, X.-Y., Zhang, S.-P., Cao, C., Loh, Y. P. & Cheng, Y. Aberrations in Peripheral Inflammatory Cytokine Levels in Parkinson Disease. *JAMA Neurol.* **73**, 1316–9 (2016).
146. Rizzo, F. R. *et al.* Tumor Necrosis Factor and Interleukin-1 βModulate Synaptic Plasticity during Neuroinflammation. *Neural Plast.* **2018**, 1–12 (2018).
147. Stellwagen, D. & Malenka, R. C. Synaptic scaling mediated by glial TNF-α. *Nature* **440**, 1054–1059 (2006).
148. Takeuchi, H. *et al.* Tumor necrosis factor-alpha induces neurotoxicity via glutamate release from hemichannels of activated microglia in an autocrine manner. *J. Biol. Chem.* **281**, 21362–21368 (2006).
149. Ye, L. *et al.* IL-1β and TNF-α induce neurotoxicity through glutamate production: a potential role for neuronal glutaminase. *J. Neurochem.* **125**, 897–908 (2013).
150. Denver, P. & McClean, P. Distinguishing normal brain aging from the development of Alzheimer's disease: inflammation, insulin signaling and cognition. *Neural Regen. Res.* **13**, 1719–12 (2018).
151. Lee, M. G., Wynder, C., Cooch, N. & Shiekhattar, R. An essential role for CoREST in nucleosomal histone 3 lysine 4 demethylation. *Nature* (2005).
152. Grabert, K. *et al.* Microglial brain region\textminusdependent diversity and selective regional sensitivities to aging. *Nat. Neurosci.* **19**, 504–516 (2016).
153. Hammond, T. R. *et al.* Single-Cell RNA Sequencing of Microglia throughout the Mouse Lifespan and in the Injured Brain Reveals Complex Cell-State Changes. *Immunity* **50**, 253–271.e6 (2019).
154. Deczkowska, A. *et al.* Mef2C restrains microglial inflammatory response and is lost in brain ageing in an IFN-I-dependent manner. *Nat. Commun.* 1–13 (2017) doi:10.1038/s41467-017-00769-0.
155. The Tabula Muris Consortium *et al. A Single Cell Transcriptomic Atlas Characterizes Aging Tissues in the Mouse*. http://biorxiv.org/lookup/doi/10.1101/661728 (2019) doi:10.1101/661728.
156. Deczkowska, A., Amit, I. & Schwartz, M. Microglial immune checkpoint mechanisms. *Nat. Neurosci.* 1–8 (2018) doi:10.1038/s41593-018-0145-x.
157. Readhead, B. *et al.* Multiscale Analysis of Independent Alzheimer's Cohorts Finds Disruption of Molecular, Genetic, and Clinical Networks by Human Herpesvirus. *Neuron* **99**, 64-82.e7 (2018).
158. Makin, S. The amyloid hypothesis on trial. *Nature* **559**, S4–S7 (2018).
159. Vijaya Kumar, D. K. *et al.* Amyloid-β Peptide Protects Against Microbial Infection In Mouse and Worm Models of Alzheimer's Disease. *Sci. Transl. Med.* **8**, 340ra72 (2016).
160. Gosztyla, M. L., Brothers, H. M. & Robinson, S. R. Alzheimer's Amyloid-β is an Antimicrobial Peptide: A Review of the Evidence. *J. Alzheimers Dis.* **62**, 1495–1506 (2018).

161. STEWART, S. A. Lentivirus-delivered stable gene silencing by RNAi in primary cells. *RNA* **9**, 493–501 (2003).
162. Sena-Esteves, M., Tebbets, J. C., Steffens, S., Crombleholme, T. & Flake, A. W. Optimized large-scale production of high titer lentivirus vector pseudotypes. *J. Virol. Methods* **122**, 131–139 (2004).
163. Dobin, A. *et al.* STAR: ultrafast universal RNA-seq aligner. *Bioinformatics* **29**, 15–21 (2012).
164. Love, M. I., Huber, W. & Anders, S. Moderated estimation of fold change and dispersion for RNA-seq data with DESeq2. *Genome Biol.* **15**, 31–21 (2014).
165. Blighe, K., Rana, S. & Lewis, M. \emphEnhancedVolcano: Publication-ready volcano plots with enhanced colouring and labeling. doi:10.18129/B9.bioc.EnhancedVolcano.
166. Demaria, M. *et al.* An Essential Role for Senescent Cells in Optimal Wound Healing through Secretion of PDGF-AA. *Dev. Cell* **31**, 722–733 (2014).
167. Sauer, J.-D. *et al.* The N-ethyl-N-nitrosourea-induced Goldenticket mouse mutant reveals an essential function of Sting in the in vivo interferon response to Listeria monocytogenes and cyclic dinucleotides. *Infect. Immun.* **79**, 688–694 (2011).
168. Muroy, S. E., Timblin, G. A., Preininger, M. K., Cedillo, P. & Saijo, K. Phf15—a novel transcriptional repressor regulating inflammation in mouse microglia. *bioRxiv* 2019.12.17.879940 (2019) doi:10.1101/2019.12.17.879940.
169. *Technology for adaptive aging*. (National Academies Press, 2004).
170. Shoji, H., Takao, K., Hattori, S. & Miyakawa, T. Age-related changes in behavior in C57BL/6J mice from young adulthood to middle age. *Mol. Brain* **9**, 11 (2016).
171. Dunham, N. W. & Miya, T. S. A note on a simple apparatus for detecting neurological deficit in rats and mice. *J. Am. Pharm. Assoc.* **46**, 208–209 (1957).
172. Bohlen, M., Cameron, A., Metten, P., Crabbe, J. C. & Wahlsten, D. Calibration of rotational acceleration for the rotarod test of rodent motor coordination. *J. Neurosci. Methods* **178**, 10–14 (2009).
173. McFadyen, M. P., Kusek, G., Bolivar, V. J. & Flaherty, L. Differences among eight inbred strains of mice in motor ability and motor learning on a rotorod. *Genes Brain Behav.* **2**, 214–219 (2003).
174. Magnusson, K. R. *et al.* Age-related deficits in mice performing working memory tasks in a water maze. *Behav. Neurosci.* **117**, 485–495 (2003).
175. Buccafusco, J. J. Methods of Behavior Analysis in Neuroscience. (2009).
176. Van Wagoner, N. J. & Benveniste, E. N. Interleukin-6 expression and regulation in astrocytes. *J. Neuroimmunol.* **100**, 124–139 (1999).
177. Valerio, A. Soluble Interleukin-6 (IL-6) Receptor/IL-6 Fusion Protein Enhances in Vitro Differentiation of Purified Rat Oligodendroglial Lineage Cells. *Mol. Cell. Neurosci.* **21**, 602–615 (2002).
178. Chen, Q., Sun, L. & Chen, Z. J. Regulation and function of the cGAS–STING pathway of cytosolic DNA sensing. *Nat. Immunol.* **17**, 1142–1149 (2016).
179. Yu, Q. *et al.* DNA-Damage-Induced Type I Interferon Promotes Senescence and Inhibits Stem Cell Function. *Cell Rep.* **11**, 785–797 (2015).

180. Fan, X., Wheatley, E. G. & Villeda, S. A. Mechanisms of Hippocampal Aging and the Potential for Rejuvenation. *Annu. Rev. Neurosci.* **40**, 251–272 (2017).
181. Reinert, L. S. *et al.* Sensing of HSV-1 by the cGAS–STING pathway in microglia orchestrates antiviral defence in the CNS. *Nat. Commun.* **7**, 1–12 (2016).
182. Stetson, D. B. & Medzhitov, R. Recognition of Cytosolic DNA Activates an IRF3-Dependent Innate Immune Response. *Immunity* **24**, 93–103 (2006).
183. Chen, H. *et al.* Activation of STAT6 by STING Is Critical for Antiviral Innate Immunity. *Cell* **147**, 436–446 (2011).
184. Zhang, Y. *et al.* An RNA-Sequencing Transcriptome and Splicing Database of Glia, Neurons, and Vascular Cells of the Cerebral Cortex. *J. Neurosci.* **34**, 11929–11947 (2014).
185. Liu, Z., Patil, I., Sancheti, H., Yin, F. & Cadenas, E. Effects of Lipoic Acid on High-Fat Diet-Induced Alteration of Synaptic Plasticity and Brain Glucose Metabolism: A PET/CT and 13C-NMR Study. *Sci. Rep.* 1–13 (2017) doi:10.1038/s41598-017-05217-z.
186. Stranahan, A. M. *et al.* Diet-induced insulin resistance impairs hippocampal synaptic plasticity and cognition in middle-aged rats. *Hippocampus* **18**, 1085–1088 (2008).
187. Knight, E. M., Martins, I. V. A., Gümüsgöz, S., Allan, S. M. & Lawrence, C. B. High-fat diet-induced memory impairment in triple-transgenic Alzheimer's disease (3xTgAD) mice is independent of changes in amyloid and tau pathology. *Neurobiol. Aging* **35**, 1821–1832 (2014).
188. McLean, F. H. *et al.* Rapid and reversible impairment of episodic memory by a high-fat diet in mice. *Sci. Rep.* **8**, 1–9 (2018).
189. Guillemot-Legris, O. & Muccioli, G. G. Obesity-Induced Neuroinflammation: Beyond the Hypothalamus. *Trends Neurosci.* **40**, 237–253 (2017).
190. Rivera, P. *et al.* Pharmacological Administration of the Isoflavone Daidzein Enhances Cell Proliferation and Reduces High Fat Diet-Induced Apoptosis and Gliosis in the Rat Hippocampus. *PLoS ONE* **8**, e64750 (2013).
191. Atamni, H. J. A.-T., Mott, R., Soller, M. & Iraqi, F. A. High-fat-diet induced development of increased fasting glucose levels and impaired response to intraperitoneal glucose challenge in the collaborative cross mouse genetic reference population. *BMC Genet.* **17**, 10 (2016).
192. Wu, Y. *et al.* Chronic inflammation exacerbates glucose metabolism disorders in C57BL/6J mice fed with high-fat diet. *J. Endocrinol.* **219**, 195–204 (2013).